EARTHQUAKES AT STRESSED RAMPS EMPLACE INJECTITES

Timothy J. Sherry

Master of Science

Earth and Planetary Science

McGill University

Montreal,Quebec

2014-08-14

A thesis submitted to the Faculty of Graduate Studies and Research in partial fulfillment of the requirements of the degree of Masters of Science

DEDICATION

This thesis is dedicated to my younger sister, Jana Sherry, whose courage and strength inspires those around her and helps others cope with dystonia. Additionally, I would like to dedicate this thesis to Ronnie James Dio, Jeff Hanneman, and Dave Brockie whose guiding wisdom and fearsome riffs shown through the shadows of the night like a rainbow in the dark.

ACKNOWLEDGEMENTS

I thank my family, John, Dena, and Jana Sherry for their support and love through the years, and for coping with me living so far away from home. I thank Ben Melosh and Clint Isaacs for their assistance in the field. I thank Ben Mapani for his assistance in procuring Namibian research permits and for his assistance exporting samples from the country. Without him, this research would not have been possible. I thank the park rangers of Tsams Ost and Naukluft - Zebra Parks for their advice and for allowing us to charge our GPS units on their generator. Without them the GPS mapping would not have been possible. I thank Jodie Miller for her help at Stellenbosch University.

Most of all I would like to thank my advisor, Christie Rowe, who taught me the art and science of geologic mapping when I was an undergraduate student at University of California Santa Cruz. Her words of wisdom, advice, patience, and understanding made this thesis possible.

ABSTRACT

In this thesis I examine the influence of fault geometry on local static stress change fields and the development of fault rock structures. In the foreland of orogenic belts, the development of deformation structures such as faults, folds, and fractures is coupled with fluid flow. Fluids derived from underthrusting sediments enter actively deforming basins, and the feedback between deformation and fluid pressure controls the structures that form. In turn, major and minor structures determine permeability pathways for fluid migration. Thrust ramps are areas where low angle thrust faults locally increase in dip. Assuming elastic wall rock, the hanging wall must deform across the ramp to move past the asperity. This deformation influences the distribution of static stress along the fault and subsequent development of fault rock and damage structures. The Naukluft Thrust, a Cambrian basal décollement in central Namibia, hosts a granular carbonate fault rock called "Gritty Dolomite" which was a slurry of grains and supercritical CO_2. In proximity to a thrust ramp, gritty dolomite intruded upsection from the fault plane into the hanging wall, forming large (70 m) slurry-filled dikes called "injectites."

The thrust ramp on the Naukluft Thrust is a field analog for active fault-related deformation where we can apply static stress change models to relate fault slip to wall rock strain. The relationship between the thrust ramp and injectite structures was investigated by GPS mapping ∼20 km tortuous fault trace in the region of the thrust ramp and fitting a topographic model of the fault surface. Cross sections of the surface model, parallel to the southeast hanging wall transport direction, were input into the USGS Coulomb 3 software to model static stress changes caused by fault geometry. Model stress saturation was set equivalent to a dolomite wallrock tensile strength of 7 MPa to identify areas of potential tensile fracturing. An area of modeled fault dilation, corresponds to observed dilation of the fault zone.

Injectites tend to correlate with areas where high stress gradients in the wall rock develop between areas of compressional and tensile stress. The injectites are not well correlated with maximum static tensile stress in the wallrock. Static tensile stress change facilitated the emplacement of injectites, however it is likely that dynamic stresses during coseismic slip increased the fluid pressure of the gritty dolomite slurry and drove intrusion into fractured wall rock. I propose that at locations of increased compressional stress normal to the fault surface, injectite formation is favored along extreme wallrock stress gradients. Thus the combination of favorable wall rock conditions, and pressurization on the fault surface, best explains injectite formation.

I applied a novel approach to estimating paleoearthquake energy from injectite aperture, based on previous work which indicated that coseismically-produced CO_2 gas was the pressurizing fluid which drove slurry injection. The volume of gas available to fill injectites is related to the thickness and area of the earthquake slip patch which was frictionally heated to liberate CO_2. Injectite dimensions were used in a simplified volume calculation to model the earthquake slip patch required to generate the volume of material in the injectite. A simplified fluid of CO_2 - H_2O was used to elucidate the influence of water compressibility on the earthquake energy. Estimates of earthquake moment magnitude, M_w, were about 4.2. The compressibility of water's influence in the supercritical CO_2 slurry was negligible.

ABRÉGÉ

Dans la présente thèse, j'examine l'influence de la géométrie des failles sur les champs locaux de variations des contraintes statiques et le développement des structures dans les roches de faille. Dans l'avant-pays de ceintures orogéniques, la formation de structures de déformation telles que des failles, plis et fractures est jumelée à l'écoulement des fluides. Des fluides dérivés de sédiments chevauchés entrent dans des bassins en déformation active, et la rtroaction entre la dformation et la pression des fluides contrle les structures qui sy forment, les structures majeures et mineures déterminant en retour les voies de perméabilité pour la migration des fluides. Les rampes de chevauchement sont des zones où le pendage généralement faible de failles de chevauchement augmente localement. Si les roches bordant la faille sont élastiques, le toit doit se déformer le long d'une rampe pour permettre le franchissement de cette aspérité. Cette déformation influence la répartition des contraintes statiques le long de la faille et le développement subséquent des roches de faille et des structures d'endommagement. Le chevauchement de Naukluft, un décollement basal d'âge cambrien dans le centre de la Namibie, est l'hôte d'une roche de faille carbonatée granuleuse appelée Gritty Dolomite ou dolomie granuleuse, formèe à partir d'une boue de grains et de CO2 supercritique. À proximité d'une rampe de chevauchement, cette dolomie granuleuse a pénétré dans le toit à partir du plan de faille, formant de grands dykes (70 m) appelés injectites remplis par ces boues.

La rampe de chevauchement sur la faille de Naukluft est un analogue de terrain d'une déformation active associée à une faille auquel des modèles de variations des contraintes statiques peuvent être appliqués pour relier le glissement le long de la faille à la déformation dans les épontes. La relation entre la rampe de chevauchement et les structures d'injectite a été examinée en cartographiant par GPS sur environ 20 km la trace tortueuse de la faille

dans la région de la rampe de chevauchement et en calant sur ces observations un modèle topographique de la surface de la faille. Des coupes du modle de la surface parallèles à la direction sud-est de transport du toit ont été versées dans le logiciel Coulomb 3 de l'USGS pour modéliser les variations de contraintes statiques causées par la géométrie de la faille. La saturation des contraintes fixée dans le modèle équivalait à une résistance en tension de l'éponte dolomitique de 7 MPa, ceci afin de cerner les zones de possible fracturation en tension. Une zone de dilatation le long de la faille produite par le modèle correspond à la dilatation observée de la zone de faille. Les injectites ont tendance à être corrélées avec des zones où se forment de forts gradients de contraintes dans l'éponte, entre des zones de contraintes de compression et de tension. Les injectites ne sont pas bien corrélées avec des contraintes de tension statiques maximums dans l'éponte. Si des variations des contraintes de tension statiques ont facilité la mise en place d'injectites, il est probable que des contraintes dynamiques durant le glissement cosismique ont accru la pression des fluides dans la boue de dolomie granuleuse, en forant l'intrusion dans les roches fracturées bordant la faille. Je propose que, dans les sites de contraintes de compression accrues perpendiculaires à la surface de la faille, la formation d'injectites est favorisée le long de gradients extrêmes de contraintes dans l'ponte. Ainsi, une combinaison de conditions favorables dans l'éponte et de la pressurisation sur la surface de la faille est la meilleure explication de la formation d'injectites.

J'ai appliqué une approche novatrice à l'estimation de lénergie des paléoséismes à partir des dimensions de l'ouverture d'injectites, reposant sur des travaux antérieurs qui indiquent que du CO2 gazeux d'origine cosismique est le fluide pressurisant qui provoque l'injection de la boue. Le volume de gaz disponible pour remplir les injectites est relié à l'épaisseur et à la superficie de la parcelle de glissement sismique dont le chauffage par friction libére du CO2. Le calcul simplifié du volume d'une injectite à partir de ses dimensions permet de modéliser la parcelle de glissement sismique nécessaire pour produire le volume de matériau

observé dans cette injectite. Un fluide simplifié composé de CO2 et de H2O a été utilisé pour tenter d'expliquer l'influence de la compressibilité de l'eau sur l'énergie des séismes. Les valeurs estimées de la magnitude de moment de séismes, Mw, étaient de l'ordre de 4,2. La compressibilité de l'eau avait un effet négligeable sur la boue de CO2 supercritique.

TABLE OF CONTENTS

LIST OF FIGURES

CHAPTER 1
Introduction

Fold and thrust belts act as important settings for fluid generation, storage, and migration (Travé *et al.*, 2007; Fitz-Diaz *et al.*, 2011). These deformation belts are composed of many structures including a basal décollement, folds, duplexes, thrust ramps, and fractures. Structures and fluids are dynamically coupled where fluids influence structural formation and structures guide fluid migration (Moore *et al.*, 1990, 1991; Ge & Garven, 1994; Stockmal *et al.*, 2007; Travé *et al.*, 2007; Fitz-Diaz *et al.*, 2011).

The geometry of the fault surface can affect local stress conditions. In particular, the stress changes caused by motion on a fault can be modeled from first principles if the geometry of the fault is known. Thrust ramps are areas of increased dip on a thrust fault (Suppe, 1983; Kilsdonk & Fletcher, 1989). In a completely elastic model, the geometry of the thrust fault influences the distribution of normal stress change (forces pushing rock on either side of the fault together) during deformation (Srivastava & Engelder, 1990). Fault damage structures such as tensile fractures can influence the permeability structure of the surrounding rock (Cosgrove, 2001).

Injectites are bodies of granular rock (sediment or fault gouge) that intrude fractures in surrounding rock. They can have dramatic effects on the permeability structure, because they create high-porosity pathways through low-permeability sections. Under certain conditions fault-core material will intrude into wall rock fractures forming an injectite (Rowe *et al.*, 2012b) (Figure 1–2). At the Naukluft Thrust, central Namibia (Figure 1–1) a carbonate fault rock was created during coseismic slip and deformed through granular flow mechanisms (Rowe *et al.*, 2012a). Here I study the spatial distribution and orientation of

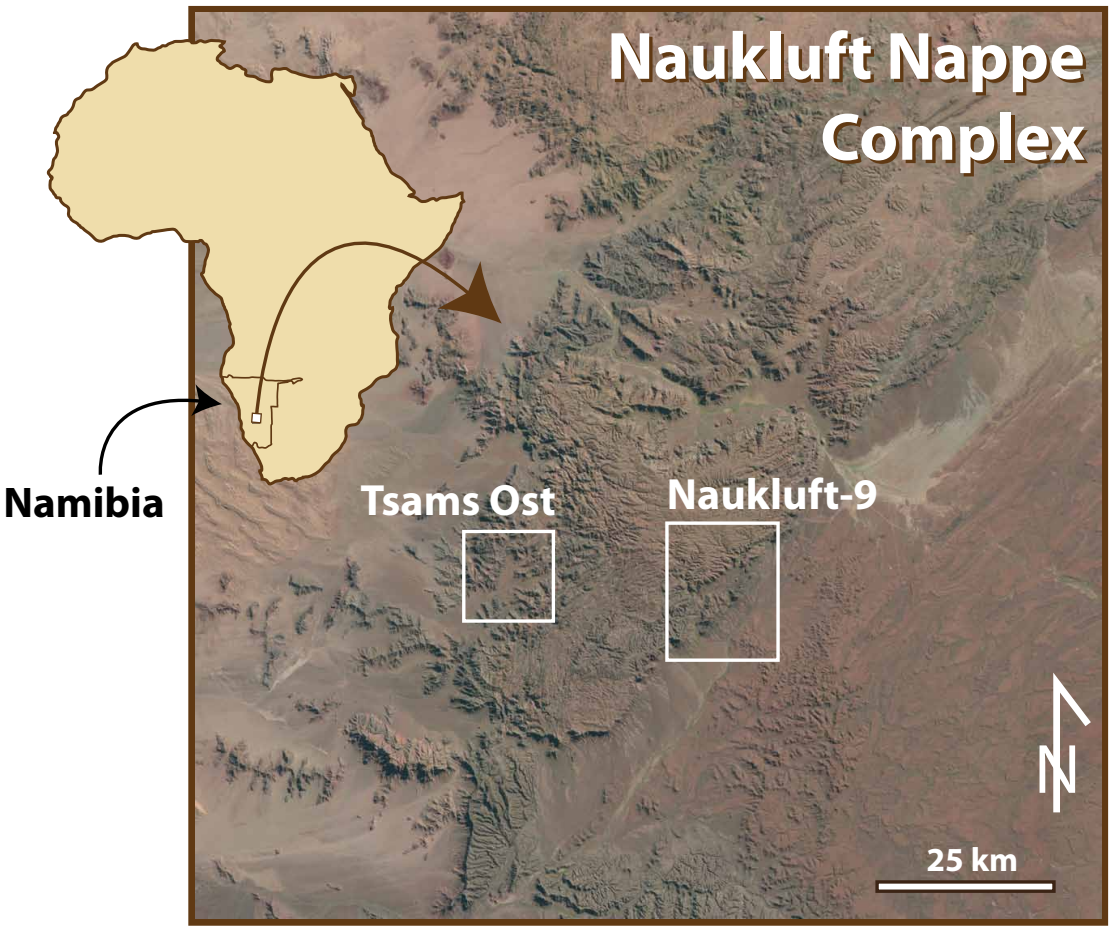

Figure 1–1: The Naukluft Nappe Complex in central Namibia is rimmed by the Naukluft Thrust. Two localities were investigated: Tsams Ost and Naukluft-9. Satellite photo from LandSat5. Naukluft-9 Park is located at Lat/Long: -24.262181°, 16.243830° (park ranger station), Tsams Ost is located at Lat/Long: -24.250565°, 16.082746° (camp site).

large (70 m) fault rock injectites near a thrust ramp to shed light on the formation conditions and local stress field during emplacement.

The spatial distribution and size of the injectites provides an opportunity to investigate the influence of thrust ramp geometry on the formation of the injectites. Using existing approaches to stress modeling, it is possible to estimate the stress changes in the surrounding rock due to motion on a fault. Stress changes are hypothesized to cause strain and deformation, including driving the formation of injectites. Injectites form when the static tensile

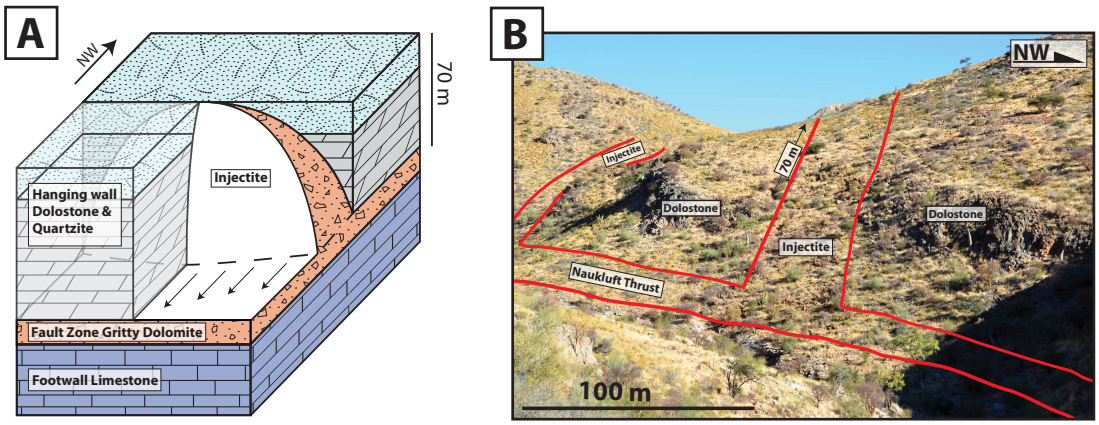

Figure 1–2: A. Schematic of idealized fault injectite geometry as an elastic opening mode crack with a volume equivalent to half an ellipsoid. B. Injectites at Zebra Hill cut hanging wall dolostone. Distance between injectites is ∼100 m.

stress and fluid pressure exceed the wall rock tensile strength. Previous studies have analyzed the orientations and cross cutting relationships between veins of quartz, dolomite, and calcite, and the injectites to investigate the history and orientation of hanging wall transport (Fagereng *et al.*, 2014). The large scale of the injectites compared with the mineral veins in the area raises the question: are static tensile stress changes from ramp geometry sufficient to fracture wall rock? In an oblique ramp setting, where is hanging wall failure most likely to occur? And, can we constrain the magnitude of earthquakes required to drive failure?

In order to model static tensile stress changes I first GPS mapped the thrust ramp. From this data I generated a topographic model of the fault surface. I constructed cross sections, parallel southeast transport direction of the hanging wall across the modeled fault surface. The cross section geometry was used to model static stress changes in the USGS Coulomb 3 software. I correlated the mapped injectite locations with the static stress change models. I used the dimensions of the injectites in a simplified CO_2-H_2O volume model of formation fluids generated during coseismic slip to estimate minimum paleoearthquake magnitude.

Background and Motivation

Foreland fold and thrust belts have long been regions of interest due to their complex relationship between fluids and structures. Fold and thrust belts are laterally extensive and host a wide array of structures (e.g. a basal décollement, folds, thrust ramps, multiple detachments, duplexes, and fractures). These structures are important for controlling largescale fluid flow (Travé *et al.*, 2007; Fitz-Diaz *et al.*, 2011) by acting as traps, conduits, and reservoirs for aqueous and hydrocarbon fluids freed during tectonic burial and accretion (Kirschner *et al.*, 1999). Structures and fluid pressure are dynamically coupled. Fluid pressure influences the formation of structures either by reducing the effective normal stress along fault (Hubbert & Rubey, 1959) or by hydrofracturing rock (Behrmann, 1991; Brown *et al.*, 1994; Ge & Garven, 1994). Anisotropies in the permeabilities of the formed structures influence fluid pressure gradients which drive and direct fluid flow in the system (Moore *et al.*, 1990, 1991; Ge & Garven, 1994; Stockmal *et al.*, 2007; Travé *et al.*, 2007; Fitz-Diaz *et al.*, 2011).

The geometry of a fault will influence the style of damage and deformation by focusing friction and stress at asperities, or rough patches (Sibson, 1986; Scholz, 1988). Asperities are microscopic topography on the fault (Rice, 2006) or large structures such as thrust ramps (Fagereng *et al.*, 2014). Thrust ramps develop when a décollement climbs up section and follows a higher stratigraphic plane or heterogeneous footwall geometry forces the hanging wall to bend (Suppe, 1983; Kilsdonk & Fletcher, 1989). Geometric models of thrust faults show that when the hanging wall encounters a ramp (a large asperity), the hanging wall must deform as it travels over the ramp either by bending or by "flexural flow" (Sanderson, 1982) to conserve either vertical or orthogonal thickness, respectively. Hanging wall beds bend upon entering the ramp, and again upon exiting the ramp (Srivastava & Engelder, 1990) with local stress magnitudes and orientation influenced by the geometry of inflection corners where sharper corners create focus stress magnitude changes (Kilsdonk & Fletcher, 1989).

The stress state is influenced by a number of factors including tectonic stress, overburden stress, non-tectonic horizontal stress, and pore fluid pressure (Twiss & Moores, 2006). The rheology of the material or rock affects how the material responds to stress either deforming via brittle or plastic processes (Twiss & Moores, 2006). Local geometries such as thrust faults and ramps will influence the stress stateas well. As the hanging wall moves over the ramp in a combination of dilation and hanging wall bending (Fagereng *et al.*, 2014), the normal stress is reduced (increase in tensile stress) at the fault ramp and tensile fractures are expected normal to the fault surface (Kilsdonk & Fletcher, 1989). In an idealized thrust ramp model the stress maps for both hanging wall and footwall are identical (Kilsdonk & Fletcher, 1989). Due to the stress concentrations, ramps are likely areas for earthquake nucleation as angle of the ramp dip may be oriented as a preferred plane of slip relative to a flat, horizontal décollement (Fagereng *et al.*, 2014). Oblique ramps occur when ramp strike is oriented at an angle other than perpendicular to the tectonic transport direction. Hanging wall and footwall material are deflected laterally out of the transport plane which results in convergence or divergence with material at frontal (transport perpendicular) ramps (Apotria, 1995). Previous studies have used stress modeling to predict the orientation and sense of motion on fractures around a slipping fault (Kirkpatrick *et al.*, 2008; Micklethwaite *et al.*, 2010). Here we explore a similar method to investigate the development of fluid controlling structures at pockets of tensile stress on a thrust ramp.

Investigating the relationship between thrust fault geometry, structures, and fluid pressure is useful in resolving the timing and history of fluid migration in foreland fold and thrust belts (Travé *et al.*, 2007; Fitz-Diaz *et al.*, 2011). As the Naukluft Basin closed, young sediment deformed and subducted under the frontal thrust, and older sediments deformed and stacked up behind the thrust forming duplexes and nappes (Korn & Martin, 1959). In accretionary prisms fluid-rich sediment is continually introduced through subduction and underthrusting of water rich sediments (Shipley *et al.*, 1990). Fluids are mobilized within the

wedge through tectonic burial and compaction dewatering of sediments (Shipley *et al.*, 1990; Kirschner *et al.*, 1999; Kirschner & Kennedy, 2001). These fluids play an important role on the bulk cohesive strength of the wedge, although, permeability differences in sedimentary layers lead to heterogeneous cohesion through the wedge (Platt, 1990). How fluid behaves and mobilizes in the system is tightly controlled by rock permeabilities.

Faults cut sedimentary layers and destroy the original wedge permeability structure by acting either as a transient enhanced permeability conduit for fluids (Cosgrove, 2001) or as a seal, blocking fluid flow (Billi *et al.*, 2003). Investigations on main thrusts of the Frontal Accretionary Prism, Oregon and Barbados Accretionary Prism found fault-parallel permeabilities up to 1000x to 10,000x more permeable than surrounding rocks. These faults acted as efficient conduits for channeling downthrust fluids (Moore *et al.*, 1990, 1991). Submarine surface seepages along traces of backthrusts connect to the mainthrust and drain fluids (Lallemant *et al.*, 1990; Moore *et al.*, 1990, 1991). Numerical modeling studies have found that high permeability fault zones focus fluid flow along the fault (Sheldon & Ord, 2005).

Brittle fault structures are especially influential on fluid transport in a fault. These faults have a fault core which may include discrete principle slip surfaces, gouges, cataclasites, breccias, and pseudotachylites. Fault cores can be surrounded by "damage zone" of rock deformed by tensile fractures, antithetic faults, and synthetic faults (Chester & Chester, 1998; Sibson, 2003; Kim *et al.*, 2004). The damage zone fractures exist over a large variety of length scales and the damage will extend into the footwall and hanging wall to distances proportional to wavelength irregularities in fault geometry (Dieterich & Smith, 2009). The fault rock style is influenced by a number of factors including fluid pressure, host rock and fault rock permeability, fault rheology, and fault geometry (Sibson, 1986; Chester & Chester, 1998; Rice & Dunham, 2009).

Possible mechanisms for fault parallel fluid migration may be explained by smeared sand layers, fluids following minimum tortuosity paths, and high fracture permeability at

faults (Moore *et al.*, 1990). Billi *et al.* (2003) showed that progressive fracturing increases fault zone permeability and works as a self-enhancing conduit for fluid transport. These high-permeability thrust faults are responsible for transporting fluids long distances (Travé *et al.*, 2007). However, faults may also act as seals where permeability is reduced with the development of particle rotation and cataclasis (Billi *et al.*, 2003). Fault gouge typically has a low permeability and may cause overpressured fluids to develop. Overpressured fluids can hydrofracture surrounding rock or facilitate slip (Ge & Garven, 1994). Kirschner & Kennedy (2001) proposed that if a fluid is adequately sealed a large volume is not required to generate transient and heterogeneously distributed high pore fluid pressures.

Faults are not the only large-scale permeability controlling structures. Although mostly documented in sedimentary environments as sandstone dikes, injectites are very important for controlling reservoir permeability (Cartwright, 2010). Sandstone injectites occur when an overpressured slurry of sand and fluid intrudes upsection into fractures in overlying low-permeability caprock. Injectites range in size from centimeter, meter, and 100s of meters at the outcrop scale (Boehm & Moore, 2002; Thompson *et al.*, 2007; Scott *et al.*, 2009; Sherry *et al.*, 2012; Ross *et al.*, 2014) to basin scale complexes (Cartwright, 2010; Huuse *et al.*, 2010). Basin scale injectites play a critical role in basin permeability structure by acting as possible reservoirs and as high-permeability conduits for fluids separated in the stratigraphic section by impermeable caprock layers (Cartwright, 2010; Huuse *et al.*, 2010). It is therefore important to consider injectites when characterizing the permeability structure of a geologic system. Although relatively rare in the geologic record, where present, injectites have dramatic effects on the permeability structure.

Fluid pressure plays an important role in fault and fracture development. Fluid pressure has traditionally been explored as a factor in facilitating fault motion by decreasing the effective normal stress on a fault (Hubbert & Rubey, 1959). Pore fluid is especially important in large detachment terranes if a weak unit, typically an evaporite or shale layer, is not present

to facilitate hanging wall transport (Briggs *et al.*, 2006). Faults regulate local fluid flow by influencing temporal stresses. Transient fluid pressures build and drop off in a cyclic fashion through a mechanism called "fault valving" (Sibson, 1992) where fault damage provides a local interconnected porosity and fluid pressure gradients controlled by a loading stress drive fluid movement. Permeability changes with lithology and is controlled by connected porosities and fluid pressure gradients which in turn are influenced by factors such as diagenesis, metamorphism, and structural evolution (Moore *et al.*, 1991). Thus, it is possible to have different permeabilities in different regions of the fault at different evolutionary stages of faulting (Billi *et al.*, 2003).

The movement of fluids through the fault system is achieved either through interseismic diffusion or coseismic transport. Rowe *et al.* (2012a) used Naukluft Thrust mineral grain shapes and injectite geometry to show the coseismic nature of injectite formation. Here we propose a method of estimating the earthquake magnitude that formed observed injectites. Traditionally, estimates of paleoseismic magnitude are made through a variety of methods such as using surface rupture to estimate area of slip (Kanamori, 1977), analyzing maximum displacements (Bonilla *et al.*, 1984; Wells & Coppersmith, 1994), empirically comparing the warping and folding of surfaces above faults with similar features on faults with a known earthquake magnitude event (McCalpin, 1996), using regional liquefaction (Seed *et al.*, 1983; Youd & Perkins, 1987; Law *et al.*, 1990; Bartlett & Youd, 1992), and using liquifaction-related sand dike widths as a measure of lateral surface spreading (Obermeier *et al.*, 1989; Bartlett & Youd, 1992; McCalpin, 1996). As far as we know our method of using earthquake fault injection dike width to estimate minimum seismic moment energy is novel.

In this paper, we present differential GPS mapping of an incised foreland thrust fault ramp on the Naukluft Thrust, central Namibia. The GPS data was used to fit a 3D model of fault surface topography. Static stress concentrations on cross sections of the modeled fault surface were spatially compared with field observations of large fault rock injectites.

Recognizing the fluid and stress conditions under which these large, permeability influencing structures occur may be used to predict their locations in seismic refraction profiles where the subtleties of fault rock style and damage are not easily recognized in the data (Neves *et al.*, 2004). Here we seek to test the geometric influence of a thrust ramp on the static tensile stress change with the development of large fault rock injectites. We then use observed injectite geometry and dimensions to make estimates of paleoearthquake magnitude.

Geologic Setting

The Naukluft Thrust is a $\sim$ 500 Ma basal foreland thrust fault in the Naukluft Nappe Complex (NNC) of central Namibia, Southwest Africa (Korn & Martin, 1959; Ahrendt *et al.*, 1978; Viola *et al.*, 2005; Rowe *et al.*, 2012a) (Figure 1–1). The NNC was first mapped in detail by the German geologists Hermann Korn and Henno Martin during 1935 - 36 where they documented the intense deformation of the metasediments in the Naukluft Mountains (Korn & Martin, 1959), which represents the southernmost basinal deformation resulted from collision between the Khalahari and Congo cratons (Korn & Martin, 1959; Ahrendt *et al.*, 1978; Hartnady, 1978; Martin *et al.*, 1983; Viola *et al.*, 2005) (Figure 1–3). Nappes within the NNC are divided by five major thrust faults, although previous authors disagree on criteria for differentiating nappe bounding faults from other thrust faults (Korn & Martin, 1959; Ahrendt *et al.*, 1978; Hartnady, 1978; Martin *et al.*, 1983) (Figure 1–4,1–5). The upper nappes are underlain by a basal décollement, the Naukluft Thrust, first mapped as a sedimentary unconformity overlain by dolostone, referred to as the "Unconformity Dolomite" by Korn & Martin (1959). They surmised that it facilitated gravitational sliding by acting as a lubricating layer. The "Unconformity Dolomite" was later renamed the "Sole Dolomite" and interpreted as an evaporite-sourced intrusion which lubricated nappe transport (Münch, 1978; Hartnady, 1978; Weber & Ahrendt, 1983). Viola *et al.* (2006) returned to the seismotectonic nature of the basal thrust and proposed a mechanism of earthquake cycling to

develop fault rocks on the Naukluft Thrust. It is thought that the NNC was transported over the Sole Dolomite a distance of 50 - 80 km with a southeast vergence, however the area of nappe origin is loosely constrained (Martin *et al.*, 1983).

Deformation on the Naukluft Thrust was at shallow crustal levels. Ahrendt *et al.* (1978) investigated the age and degree of metamorphism in the NNC using illite crystallinity and K-Ar ages determination. The illite crystallinity tests were carried out on slates and phyllites in the NNC and surrounding regions. Illite crystallinity suggests temperatures did not exceed 200 - 250 °. Illite crystallinity increases northward within the nappes, suggesting higher metamorphic conditions. Recrystallization of quartz and phyllosilicates as well as the occurance of biotite in phyllites showed a NNC metamorphic temperature of 350° (Ahrendt *et al.*, 1978). Low vitrinite reflectance (Rm% = 0.99, Ahrendt *et al.* (1978) Table 2) is consistent with temperatures in footwall basin rocks. However, the sample location is unknown and proximity to the NNC is unconstrained. K-Ar dating yields two dates for the NNC: 530 Ma and 495 Ma, respectively. The age of 530 ma is identical to the age found for the Nama sediments of the footwall. The age of 495 Ma corresponds to a younger cooling age and is found in the Naukluft Thrust (Ahrendt *et al.*, 1978).

The Naukluft Thrust fault rock is regionally extensive yet varies locally in fault core, damage, and alteration style. It is comprised of calc-mylonite, dolo-mylonite, a granular fault rock known as "gritty dolomite", massive dolostones, and carbonate breccias (Korn & Martin, 1959; Viola *et al.*, 2005; Rowe *et al.*, 2012a). Other features and structures present around the fault include fractures, color alteration, and dolomitization (Viola *et al.*, 2005), although some structures, such as fault rock injectites, are so large ($\sim$50 - 70 m normal to the fault surface) that they cannot be defined to fit into an orderly "damage zone" classification scheme. The gritty dolomite rocks including injectites show a lack of metamorphic overprinting (Rowe *et al.*, 2012a,b) which rules out interpreting them as "early" soft-sediment deformation features. Additionally, injectites crosscut minor thrusts and folds in nappes,

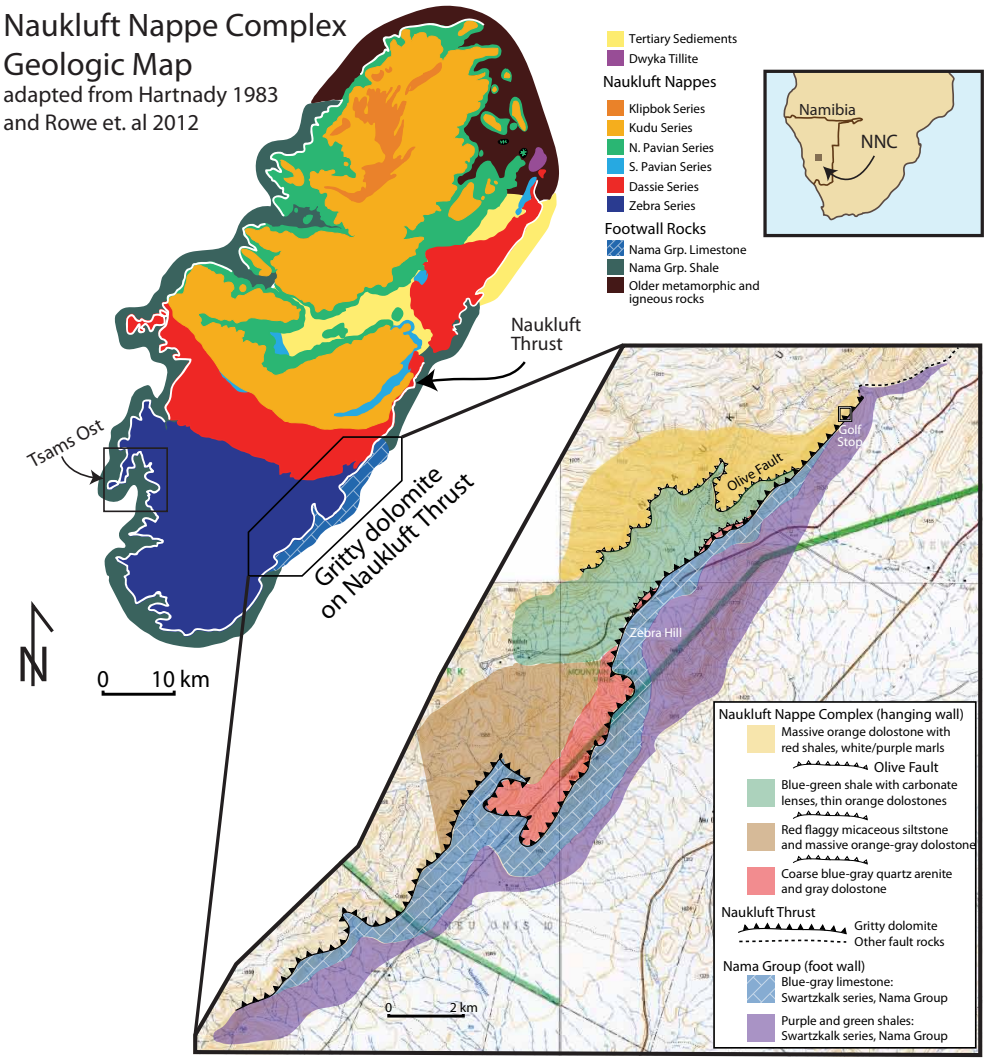

Figure 1–3: Simplified geologic map of the Naukluft Nappe Complex. Adapted from Rowe *et al.* (2012a) and Hartnady (1978).

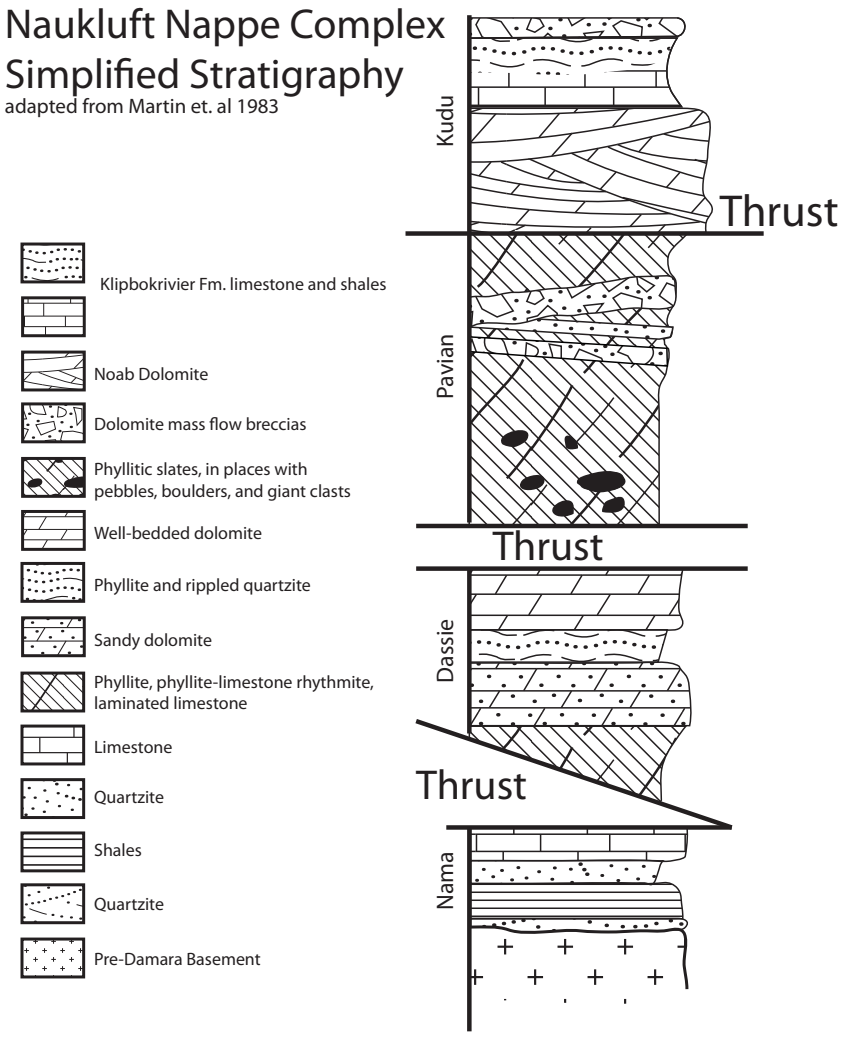

Figure 1–4: Simplified stratigraphic column of the Naukluft Nappe Complex. Adapted from Martin *et al.* (1983).

clearly supporting the hypothesis that they are late-post emplacement features and post-date peak metamorphism.

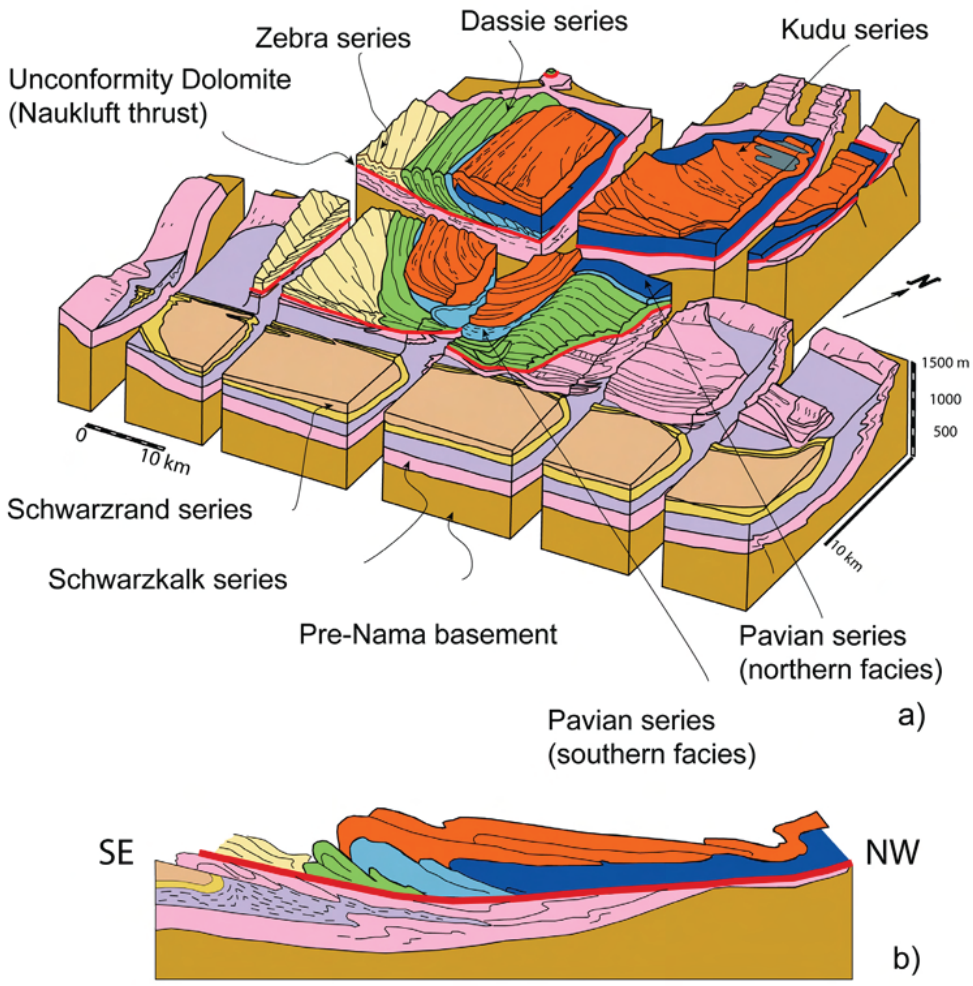

Figure 1–5: Naukluft Nappe Complex cross section from Viola *et al.* (2006) modified from Korn & Martin (1959).

CHAPTER 2
Methods

Fault Surface Models

The Naukluft-9 and Tsams Ost localities were GPS mapped using a two handheld Trimble GEO-XH units. In total over 30 km of fault trace was mapped for the two localities. A differential correction was applied to the GPS files using Trimble Pathfinder software bringing the accuracy of the data to a range of centimeters to meters. A Natural Neighbor Surface Interpolation was performed using the ArcGIS 3D Analysis toolbox to generate topographic representations of the fault surfaces. Natural Neighbor was selected as the interpolation method because it considers data points that are local (surrounding) the grid node in question and does not infer trends that would create artificial valleys and ridges where no data is present (Sibson, 1981; Watson, 1992). This approach generates smooth surfaces across gaps between data points and allows for shorter wavelength roughness where the data requires it. A consequence of this method is that it is highly effective in revealing fault geometry where data points are densely populated, i.e. along the edges of a narrow river valley. Where data is sparsely spaced, such as across a broad valley, the fault surface is modeled as smooth. It is therefore necessary to compare the modeled surfaces with field observations and measurements to confirm that the model is indeed representative of the fault.

Other interpolation methods were attempted in ArcGIS that produced modeled surfaces that did not match field observations. A surface TIN (Triangulated Irregular Network) produced sharp, unnatural intersections along triangle sides. Other statistical methods such as IDW (Inverse Distance Weighting), Spline, and Kriging were attempted in ArcGIS. These

methods were rejected because they produced unnatural fault surface topographies that contained divots and sharp peaks that decayed in sequence away from data point clusters.

Mapping Injectites

The surface trace of injectites were mapped using GPS. Injectite height above the fault plane was determined by subtracting the elevation at the top of the base of the injectite from the elevation at the top of the injectite. The geometry of injectites is assumed to be generally tabular and is a filled elastic opening-mode crack (Rowe *et al.*, 2012a) starting at the fault surface. Field observations and mapped extents of well-exposed injectite walls and geometries support this assumption (see Figures 1–2 and 4–2).

Static Tensile Stress Change Models

The geometric influence on static stress change from motion on the fault was investigated using USGS Coulomb 3 software. Coulomb 3 (version 3.3) maps a modeled static stress change field relative to a specified fault geometry and slip (Lin & Stein, 2004; Toda *et al.*, 2005). King *et al.* (1994) compared static stress change maps with aftershock distributions to show that static stress changes loaded adjacent faults and triggered aftershocks associated with the Homestead Valley Earthquake. The Coulomb stress change ($\Delta\sigma_C$) is defined as the change in stress parallel to the fault (shear stress change, $\Delta\tau$) plus a friction coefficient (μ) multiplied by the change in stress perpendicular to the walls of the fault (normal stress change, $\Delta\sigma_n$) (Stein, 2005):

$$\Delta\sigma_C = \Delta\tau + (\mu \times \Delta\sigma_n) \tag{2.1}$$

The focus of this investigation is how tensile structures correlate with clamping (positive $\Delta\sigma_n$) and unclamping (negative $\Delta\sigma_n$). From here normal stress change is referred to as tensile stress change (normal to the fault) because we are looking for evidence of fault dilation to move past the thrust ramp. Using the 3D interpolated fault surface, I extracted 2D cross

sections parallel to the hanging wall transport direction (southeast). This produced a 2D profile of the fault geometry, which served as the geometric input into Coulomb 3. The cross sections were modeled in Coulomb 3 as a right lateral strike-slip fault which corresponds to top to the right motion on the thrust sheet. Rupture opening was not modeled due to Coulomb 3 only allowing fault (Kode 100) slip and Mode 1 opening (Kode 200) on the same fault (Stein, 2005).

Static stress change model input parameters for elastic properties and failure criterion were sensitivity tested over a range of values derived from laboratory mechanical tests on rocks of similar lithology to those on the Naukluft Thrust. Dolostone has an unconfined tensile strength of 7 MPa **??**, although this number is variable for specific rocks. The model color scale saturation limits was set at 7 MPa to test static stress change against wall rock tensile strength. The Poisson's ratio of Naukluft rocks may have varied depending on fluid saturation levels. Values ranging from 0.25 - 0.35 were tested and did not impact model results, so drained conditions were assumed and a value of 0.25 was used for the models. A Young's Modulus of 800,000 bar was used because the dolostone wallrock hosting the injectites is crystalline and fractures are generally healed, so the wallrock was assumed to be strong at the time of injection. The models were sensitivity tested for a Young's Modulus of 200,000 bar for weak wallrock conditions, which decreased the magnitude of static stress changes. Fault tips influence the model by focusing stress change lobes. To test this influence, fault tips were extended $\pm$10 km which removes lobes from the model. The models were ran without artificial tip extension to preserve original geometry. Fault slip along the fault was set at a uniform 10 cm. A model with tapered slip towards the tips was tested, which produced unnatural stress change bumps at the intersections between fault segments in the model. The spatial locations of the fault rock injectites and fault plane dilation were compared with the cross section static normal stress change models. The location of injectites that did not intersect cross sections due to erosion were traced along injectite strike to the cross sections.

This is reasonable because for this locality the fault plane was exposed by a narrow valley. Any injectite that would have formed above the mapped valley would have been eroded away during valley incision. The models investigated stress changes parallel to the fault, specifically normal stress change which is perpendicular to the fault strand.

Injectite intrusion can potentially affect the stress field. Several Coulomb 3 models were made to investigate the influence of an injectite opening on hanging wall tensile stress change along the fault. The injectite was modeled as a 60 m tall subvertical injectite (using the Coulomb 3 conventions for dikes as they are similar in tabular shape and opening-mode displacement) located at the base of the fault ramp. These models were sensitivity tested for injectite openings of 0.1 m, 1 m, and 1 m at the base tapering to 0.1 m at the tip. Static tensile stress change was modeled both normal to the dike and normal to the fault. The same elastic properties as outlined above (Poisson's Ratio 0.25 and Young's Modulus 800,000 bar) were applied and a color saturation of 7 MPa.

Additionally, a schematic model thrust ramp was constructed to test the influence of lithostatic pressures on the cross section models. The thrust fault has an initial dip of 20° which increases to 30° at the ramp and shoals back to 20°. Elastic properties are the same as the models above and a uniform slip of 10 cm was applied to the model.

See Appendix for input files.

Deciphering Paleoearthquake Magnitude From Injectite Aperture Opening

My approach to estimating paleo-earthquake magnitude relies on a model of formation of carbonate granular fault rock by coseismic decarbonation (described by Rowe *et al.*, 2012a). In this model, hot CO_2 is expelled from an earthquake slip surface and pressurizes the granular rock already present in the fault. This pressurized slurry flows into the wall rock fractures to form the injectites. By estimating the volume and pressure of pore gas required to fill the observed injectites, I estimate the slip area of the paleo-earthquake, and relate this to magnitude. The suspected CO_2 source rock is a dolomylonite layer with an approximate

thickness = 5 cm, which underlies fault plane gritty dolomite and has slickensides on the top surface.

Field observations of fault rock injectites provide a lower-bound constraint on the volumes of fluid derived from the fault plane. The injectite volume is related to theoretical fluid volumes with varying mole fraction combinations of CO_2 and H_2O at temperature and pressure. It is inferred that fluid volumes vary with the volume of dissociated dolomite host rock. Frictional heating via coseismic slip is the assumed source of temperature increase required to dissociate dolomite. This model tests the volume of dolomite dissociated as it scales with the earthquake slip patch area. This model makes no assumptions about the state of and spatial variability of friction during coseismic slip, it simply relies on total heat production of the earthquake.

Dissociation Model

The volume of the injectite can be related back to a starting volume of CO_2. First, dolomite of a known volume (1 m^3) and known density, assuming complete dissociation, decomposes into its constitutive parts via the reaction:

$$CaMg(CO_3)_2 \rightarrow CaCO_3 + MgCO_3 \rightarrow CaO(s) + MgO(s) + 2CO_2(g) \tag{2.2}$$

where (s) and (g) denote solid and gas particles, respectively. The MgO and CaO solids facilitate fault slip through nanoparticle lubrication (Han *et al.*, 2007). Using the molar mass of dolomite the molar volume of generated CO_2 was calculated. Thermal dissociation experiments on Naukluft Thrust and gritty dolomite samples show CO_2 dissociation at 700-800 °C (Unpublished data from Mike Heap). Following Holland & Powell (1998)'s thermodynamic model molar volumes were calculated for various mole fractions of $CO_2 - H_2O$ mixtures ranging from 10% to 100% CO_2 at 800°C and 50 MPa using Perple_X Fluids software. This model was selected because it includes both thermal expansion and fluid compressibility,

and is well calibrated at temperatures and pressures estimated for the Naukluft Thrust. The volumes obtained from Perple_X were multiplied with the number of mols CO_2 derived from 1 m^3 $CaMg(CO_3)_2$ which yielded volumes of $CO_2 - H_2O$ mixtures for various mole fractions. The fluidization of grains into a slurry requires a threshold porosity, ϕ, of approximately $\phi = 50\%$ (Leva, 1959), although the threshold porosity is influenced by other factors such as particle grainsize and grain cohesion (Patwardhan & Tien, 1985; Nichols *et al.*, 1994).

Injectite volume and Paleoearthquake Magnitude

Injectite geometry and source rock volume

The injectite is modeled as an elastic opening mode crack (Rowe *et al.*, 2012b) (Figure 1–2) with a volume equivalent to half an ellipsoid following Equation 2.3 with half observed length, L, and width, W:

$$V_{Inj} = \frac{(2/3) * \pi * H * ((L * W)/2)}{2} \tag{2.3}$$

To find the volume of earthquake slip patch, V_{patch} that generated the injectite volume, V_Inj is related to the idealized volume of gritty dolomite,V_{gritty} derived from 1 m^3.

$$V_{patch} = (\frac{V_{Inj}}{V_{gritty}}) * 1m^3 \tag{2.4}$$

The slip patch area, A_{patch} is calculated by dividing the V_{patch} by the thickness of the source rock layer. Assuming a square slip patch, the length, L_{patch} where $A_{patch} = L^2_{patch}$. The model was also sensitivity tested for a circular slip patch where $L_{c-patch} = 2\sqrt{\frac{3A_{patch}}{4\pi}}$.

Paleoearthquake magnitude

Following earthquake slip scaling relationships (Kanamori & Brodsky, 2004) the displacement, D was calculated for both L_{patch} and $L_{c-patch}$ where $D = \frac{L_{patch}}{10000}$. The seismic

moment, M_o is defined by Equation 2.5:

$$M_o = G * D * A_{patch} \tag{2.5}$$

where G is the crustal shear modulus at 30 GPa (Kanamori & Anderson, 1975; Kanamori & Brodsky, 2001, 2004). The moment magnitude, M_w is then calculated using Equation 2.6:

$$M_w = (2/3)log(M_o) - 6.07 \tag{2.6}$$

This allows us to compare the earthquake that produced the injectites with events of similar magnitude.

CHAPTER 3
Naukluft Thrust Rocks and Morphology

The Naukluft Thrust crops out over a large extent of the Naukluft Mountains. Over the entire length of exposure there are observed differences in footwall lithology, hanging wall structures, fault rock alteration and damage, and fault geometry or shape. The differences imply variabilities in the processes and mechanisms at work as well as the accommodation of deformation. To better understand the differences along the Naukluft Thrust two "type localities" were selected for investigation: Naukluft-9 and Tsams Ost (Figure 1–1).

Located in the southwestern Naukluft Mountains, Tsams Ost is a broad shallow valley with an area of $\sim$10 km^2. Here the Naukluft Thrust is easily recognizable as a band of orange dolomite ringing the sides of the valley like a coffee stain on a mug (Figure 3–1A). Approximately 11 km of the fault trace was mapped with GPS.

The Naukluft-9 locality has a different shape from Tsams Ost. Sitting in the southeastern side of the Naukluft Mountains, this represents the distal deformation associated with the Damara Orogen (Korn & Martin, 1959). Here the Naukluft Thrust dips steeply northwest and is recognized in the mountain and cliff sides by the sharp contrasting colors between footwall and hanging wall lithologies (Figure 3–4A). The Naukluft Thrust in Naukluft-9 is host to a number of fault features including local flat-ramp geometries and impressive fault rock damage structures. At Naukluft-9 the basal thrust was mapped over an area of approximately 10 km^2 for a total trace length of 20 km thanks to sharp river and valley incision that exposes the fault plane.

Defining Characteristics of Tsams Ost

The Naukluft Thrust at Tsams Ost is oriented at 009/09E. Field observations indicate that the fault is nearly planar across the mapped area and lacks ramp structures.

Lithology and Structures

Fault core rocks are poorly developed in Tsams Ost valley. Slip vergence is inferred from synthetic faults and folds in the hanging wall. The Tsams Ost footwall is dominated by meta-shale with some folded limestones, and calc-mylonites present (Figure 3–1B,D). Limestone footwall is found only in the south margin of the field area and is black in outcrop. Limestone beds are observed to be folded into parallel with the fault plane (Korn & Martin, 1959). The limestone at this location overlies the shales observed elsewhere in the field area. The shales are chlorite rich with a blue-green color. In outcrop they are have an intense wavy cleavage, and have experienced lower greenschist facies metamorphism (Ahrendt *et al.*, 1978). Shale fabric dips at a mean orientation of 260/24N, but a variation of 298/61W to 150/34E demonstrates the wavy nature of the fabric. Fold hinges are folded (Korn & Martin, 1959). The Naukluft Thrust décollement sharply cuts the shales. Lenses of calc-mylonite are occasionally present in the footwall. The lenses may be up to 3-5 m thick. Calc-mylonite foliation is typically fault parallel which suggests that they are tectonic slivers of fault core. At some locations calc-mylonite is asymmetrically folded with the shales which suggests either an origin as limestone interbeds or that folding occurred during fault slip, after mylonitization.

The hanging wall lithology consists of a 3 m thick, layered, grey dolo-micrite breccia (Korn & Martin, 1959). At the fault plane there is an orange alteration, but this sometimes grades to grey upsection. Minor fractures are abundant and filled with calcite or quartz veins. Minor thrust faults repeat dolomicrite layers. Above the dolomicrite sits a series of quartzite beds and interbedded shales (Figure 3–1C). The quartzite beds are typically 2

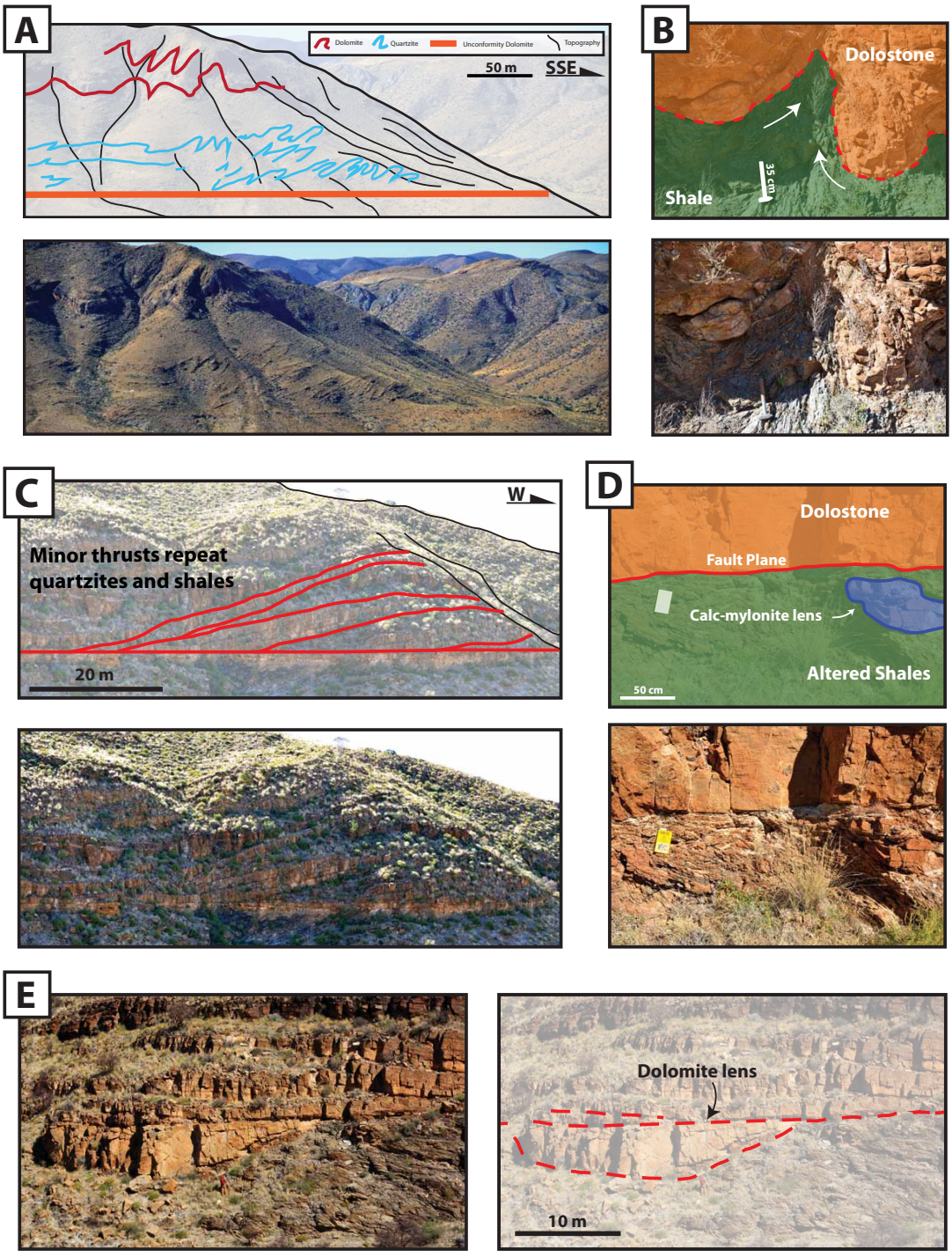

Figure 3–1: A. Tsams Ost stratigraphy shows intense folding in the hanging wall. B. Footwall shale in a hanging wall fracture. C. Repeating quartzite beds in the hanging wall. D. Fault core featuring orange-ocre alteration near the fault plane and calc-mylonite lens. E. Hanging wall dolostone with planar fault above and abandoned fault strand below.

meters in thickness. Minor thrust faults repeat quartzite and shale beds. On the east side of the valley the same quartzite beds are tightly deformed (Figure 3–1A). Overlying the folded quartzite beds is a section of thick folded dolomite beds with a wavelength of ∼100 m. Observations of these folds in both the hanging wall and footwall were first made by Korn & Martin (1959). Folds in the hanging wall have a southeast vergence. Fold shape can be highly variable from open folds to tight isoclinal folds (Figure 3–1A; see also Figure 6 in Korn & Martin (1959)).

The units of Tsams Ost have experienced prehnite-pumpellyite facies metamorphism (Ahrendt *et al.*, 1978), but structures both in the hanging wall and footwall accommodate a large amount of deformation through folds and thrust faults.

Fault Zone

The Naukluft Thrust fault plane at Tsams Ost is clearly recognized by the sharp lithologic change from footwall shales, limestones, and calc-mylonites to hanging wall dolomicrite (Figure 3–1D,E). Although this change is sharply defined, the surrounding rock ∼2 - 5 m up and down section shows a irregular zone of yellow-orange dolomitic alteration. At one locality footwall shale filled a fracture in hanging wall dolomicrite (Figure 3–1B). This feature is ∼1 m wide at the base and the entire structure is ∼1 m in height with a sharp taper towards the tip. Preserved shale cleavage emplaced into the fracture with an upside-down "U" shape (Figure 3–1B). Another feature which deviated from the typical planar nature of the fault was the presence of ∼5 m thick, ∼20 m wide, massive dolomite lenses (Figure 3–1E) of hanging wall rock below the fault. This suggests a transfer of fault slip to higher structura levels and the abandonment of slivers of hanging wall rock. We term this process"downplating". The lenses are identical in lithology to the hanging wall dolomicrite, and the fault and accompanying alteration was observed both above and below, anastomosing around the lenses. Figure 3–2 shows a schematic model of hanging wall material incorporated into the footwall

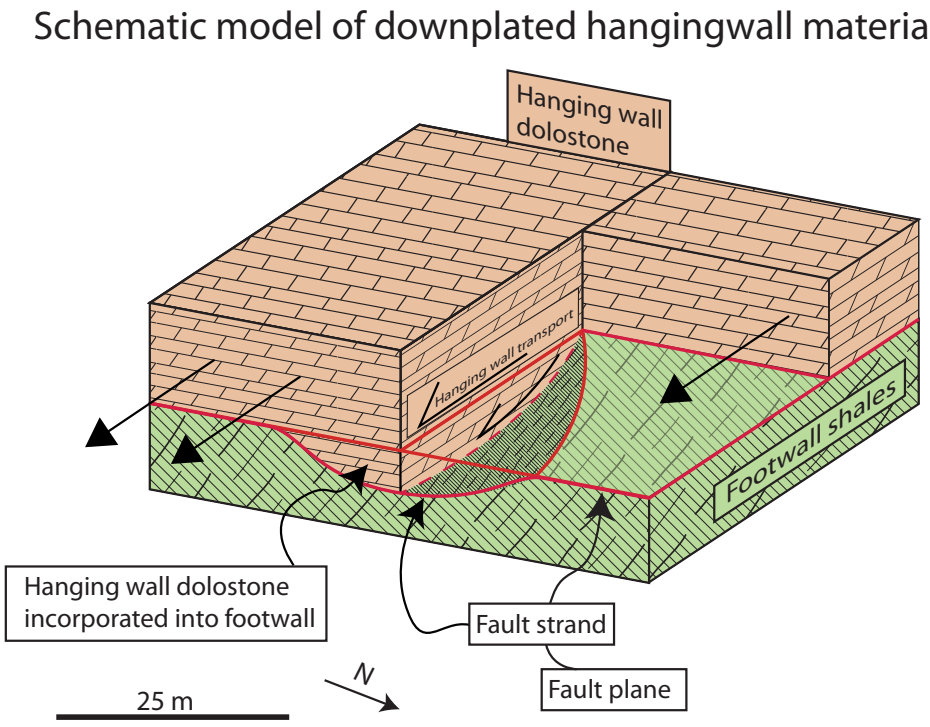

Figure 3–2: Schematic block model of downplating. Hanging wall material is incorporated into the footwall and cut by the primary fault plane.

below the primary thrust plane. This observation differs from previous work on stacked thrust sheets by Boyer & Elliott (1982) and Butler (1982) where stacked thrust sheets are never below the basal décollment. Korn & Martin (1959) mapped the "Rietoog Nappe" below the Naukluft Thrust, but is composed of footwal Nama sediments which suggests that forward / downcutting is occurring on a regional scale.

A discontinuous ∼10 cm thick zone of breccia is observed at one location ∼1 m above the fault plane. The matrix is powder white and the rock is poorly consolidated. Clasts are composed of a pink limestone, are angular, and 0.5 - 3 cm in diameter. Larger clast margins are sharp whereas smaller clast margins have a spongey, smeared texture. The breccia is matrix supported. There are also small 1- 2 mm diameter iron oxide "blebs".

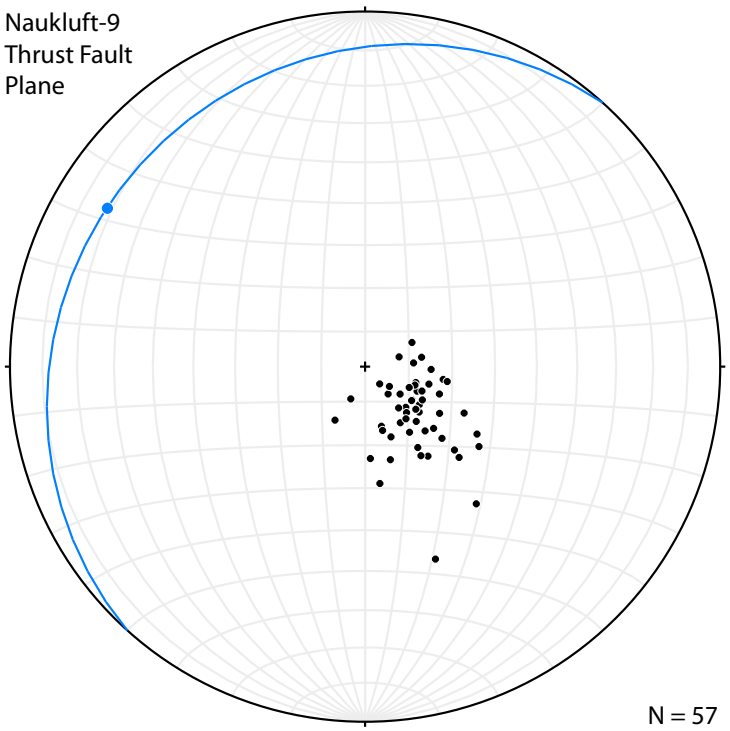

Figure 3–3: Stereonet showing Naukluft-9 poles to fault plane orientations across the locality field area. Variablility includes Zebra Hill ramp, but also includes other changes in fault orientation in the field area. Blue great circle and dot show "Type Locality" fault plane and slickenline orientation.

Defining Characteristics of Naukluft-9

Driving East into the Naukluft-Zebra Park, the Naukluft Thrust is easily recognized by the remarkable contrasting colors of the bright blue footwall carbonate and the orange-grey hanging wall rocks (Figure 3–4A). The Naukluft Thrust in Naukluft-9 Park has an average dip of ∼15 - 25° NW (Figure 3–3). Fault dip varies from 10°-40° NW depending on location, most notably at the Zebra Hill thrust ramp.

Lithology and Structures

Carbonates and shales make up the footwall lithology and hosts less deformation structures compared to the hanging wall. Blue limestone (Figure 3–4A) is thick-bedded, massive,

fine grained, and lack fossils. Underlying the footwall limestones are red shale and quartzite sequences. Although the limestone is the dominate footwall rock at Naukluft-9, to the northeast along the Naukluft Thrust the limestone is interfingered and overlain with shales. Extensional calcite veins are common in the limestone, especially near the fault surface (Fagereng *et al.*, 2014). Mylonitization of limestone bedding occurs near the fault plane with bedding dragged parallel to the fault plane.

The hanging wall is composed of metasediments and hosts a variety of structures. Lithologies include grey dolomites, grey cross bedded quartzites, and brown, purple, and green shales with some localized conglomerate lenses. The grey dolostone is a sedimentary mosaic breccia composed of a fine matrix of similar composition to the clasts. Grey dolostone thickness varies, but at most is 10s of meters thick. Secondary calcite, quartz, and dolomite veins are present (Fagereng *et al.*, 2014). The shales are fine grained, thin bedded, have undergone lower greenschist facies metamorphism, and are tightly folded. Quartzites found in the hanging wall are coarse grained, well sorted, well indurated, and cross bedded. Upsection, dolomite and quartzite beds are folded (Figure 3–4A), and are cut by the overlying nappe. Hanging wall nappes are limited in strike length, and to the southwest and northeast, the hanging wall rocks are part of other nappes. Details of hanging wall stratigraphy, structures and overlying nappes are described and discussed in Korn & Martin (1959) and Hartnady (1978). A synthetic fault (Figure 3–5) was observed upsection from the Naukluft Thrust with fault-core slickensides at an orientation of 051/76N/80E. The slickensided surface is surrounded by a chaotic breccia with a matrix composed of a fine, tan-yellow dolomite. Breccia clasts are angular grey dolomicrite and range in size from 2 mm to 2 cm. Fagereng *et al.* (2014) examined calcite, dolomite, and quartz filled veins, as well as the gritty dolomite filled injections, which are the focus of this paper, around the thrust ramp on Zebra Hill and concluded that they are the result of multiple failure events due to cyclical transient

stress changes and suggested the ramp as a focal point for earthquake rupture nucleation. Limestone bedding is a possible control on ramp geometry (Fagereng *et al.*, 2014).

In summary, The Naukluft Thrust ramps at an area known as Zebra Hill (Figure 3–6). At the ramp, the fault dip increases to ∼40°NW for a distance of 200 m before shoaling back to the original dip of 15° (Fagereng *et al.*, 2014). Incised valleys allowed for detailed mapping of the fault plane around the thrust ramp. This mapping revealed subtle geometries of a second, smaller ramp structure southeast of the main ramp (Figure 4–2). At this second ramp fault dip increase to ∼25° for ∼100 m.

Fault Zone

A coarse granular fault rock called "Gritty Dolomite" dominates the fault zone at Naukluft-9. Gritty dolomite is composed largely of coarse, rounded dolomite grains (Figure 3–7). Euhedral neocrystalized magnetites are present, as are euhedral neocrystalized quartz (up to 4 cm), and euhedral akali feldspars. Entrained wall rock clasts are typically of local dolomites, quartzites, shales, and limestones. Additionally, a rare, basement gneiss clast (2 cm diameter) is present. Size of entrained clasts varies from ∼2 cm to ∼45 cm and are angular to subrounded. A fine (<5 μm) dolomite (Rowe *et al.*, 2012a) matrix cements the rock. Gritty dolomite is either massive or laminated. Laminae are recognized by grainsize sorting or color variation in matrix (Rowe *et al.*, 2012a). Laminae always parallel other laminae and are typically parallel to the walls of the fault plane. Folded laminae are common, resembling flow banding (Figure 3–4C, nappe transport direction is towards viewer). Laminae always wrap around entrained wallrock clasts (Figure 3–4D). Microfault offsets are recognized in the gritty dolomite due to presence of offset laminae (Figure 3–8). A discrete secondary overgrowth cement is formed by a brown, well indurated, spongy-porous silica which always traces laminae. At some locations the margins of quartzite inclusions are disrupted, wavy, and mixed with brown silica, suggesting quartzite as a possible brown silica protolith.

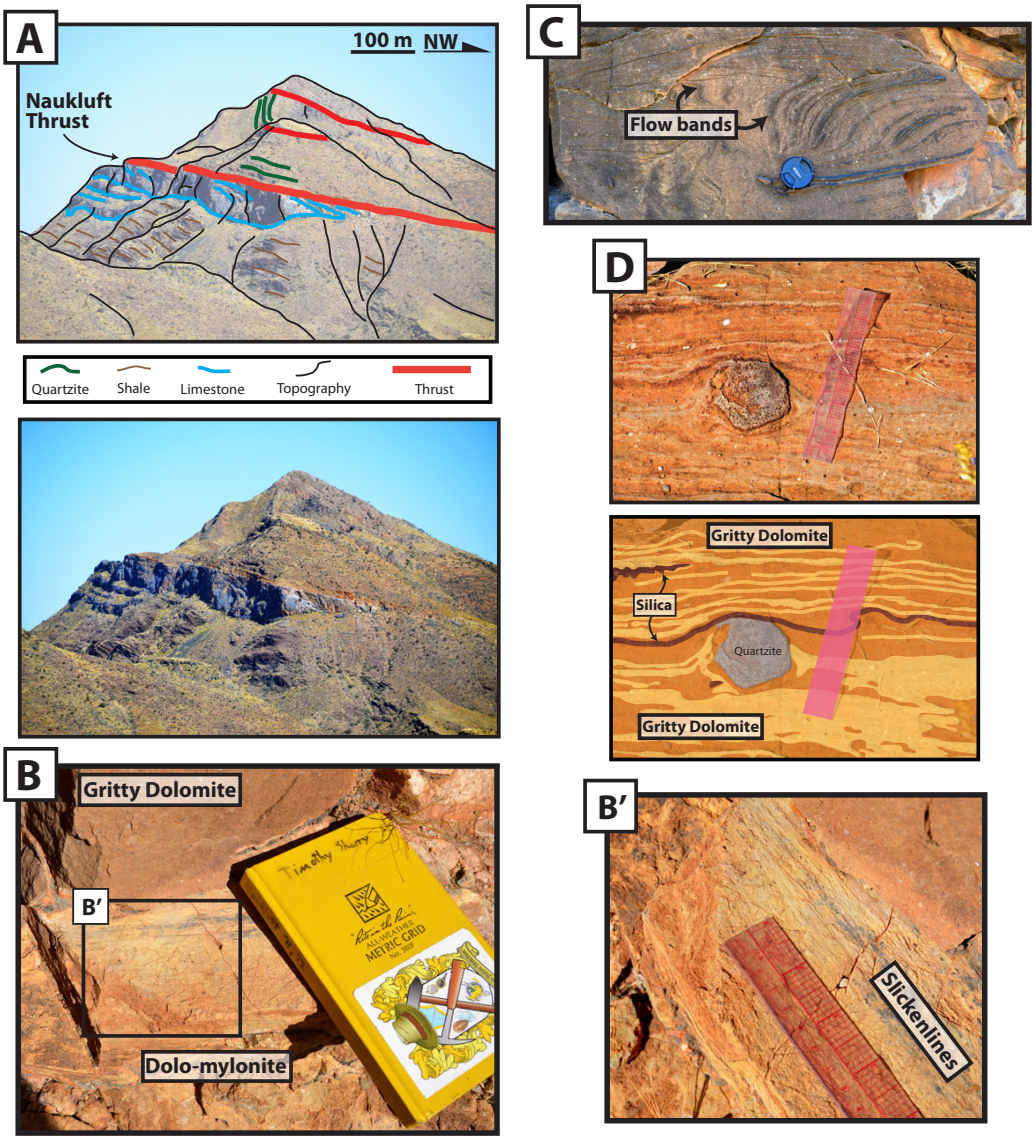

Figure 3–4: A. Naukluft-9 stratigraphy with prominent Naukluft Thrust fault zone. B. Dolo-mylonite layer with slickenlines. C. Flow-folded laminae in Gritty Dolomite. D. Gritty dolomite laminae wrapping around a quartzite inclusion.

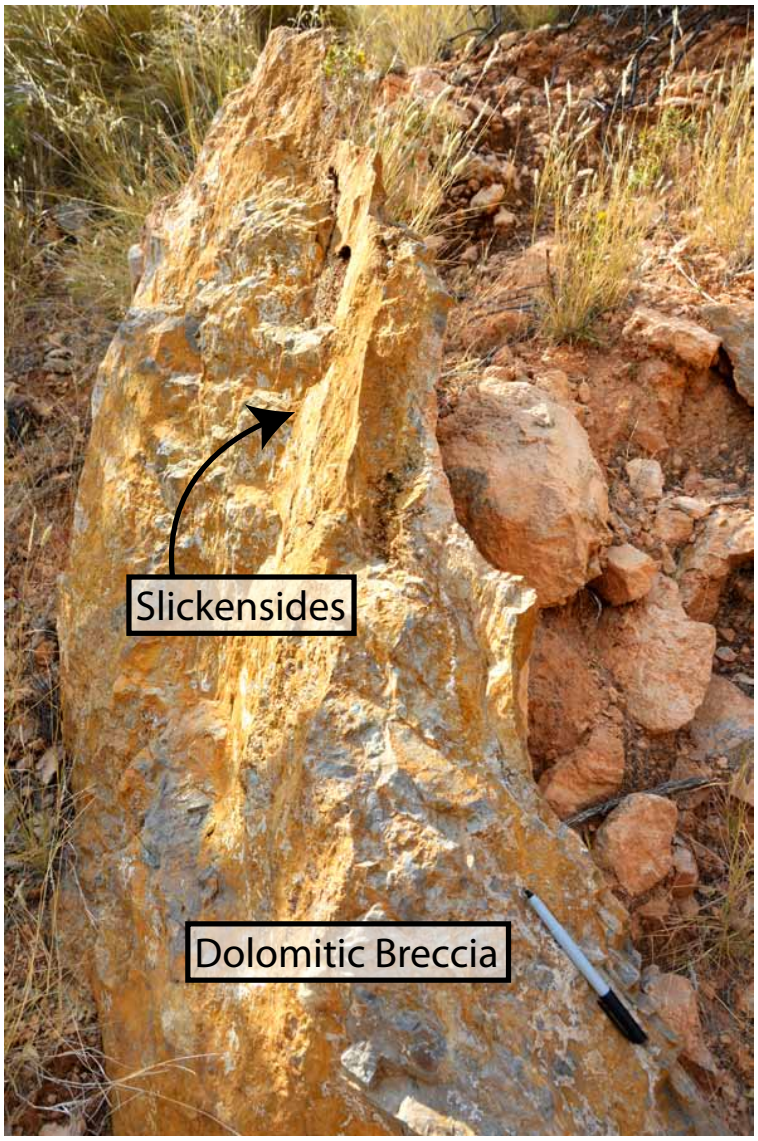

Figure 3–5: Possible dolomitic breccia injectite or backthrust in the Naukluft Thrust hanging wall. Slickenlines observed have an orientation of 051/76N/80E. The breccia is cemented with a fine, yellow-tan dolomite. Breccia clasts are grey dolomicrite, similar to dolomicrite wall rock found downsection above the fault plane.

Figure 3–6: The Naukluft Thrust increases in dip entering the ramp and shoals to original dip exiting the ramp. Photo is looking West from park entrance road.

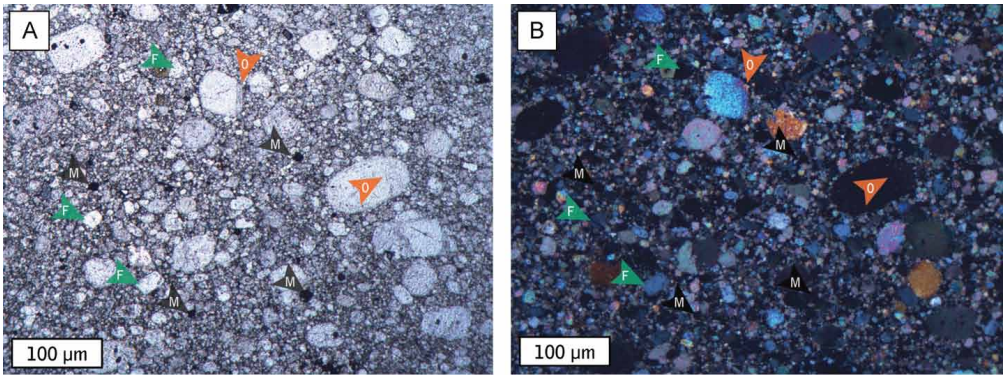

Figure 3–7: Photomicrograph of gritty dolomite from Rowe *et al.* (2012a) shows magnetite, "M", dolomite overgrowth or grain coating, "O", and feldspar, "F" grains. A. Plane polarized light. B. Cross polarized light.

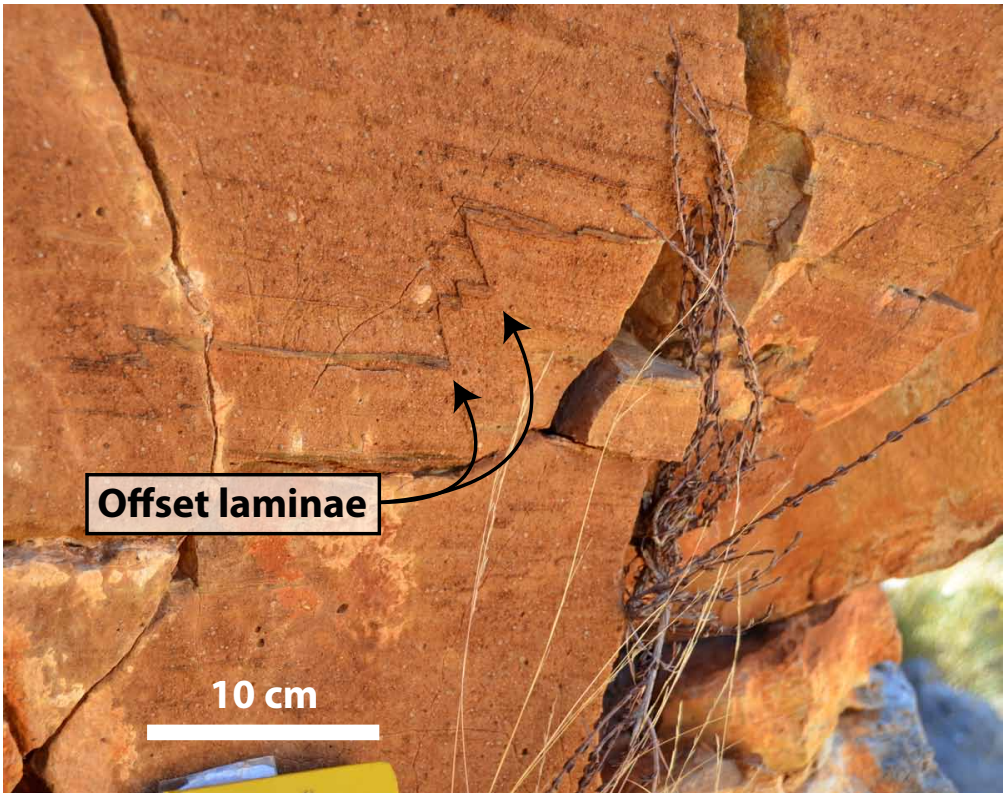

Figure 3–8: Microfaults in gritty dolomite are recognized through offset laminae.

The cross cutting relationships between gritty dolomite and other fault rocks varies. Gritty dolomite typically cuts other fault rocks, yet in some instances fine dolomite fault rock was observed cutting gritty dolomite (Figure 3–9). Gritty dolomite cuts previous generations of gritty dolomite-supported breccia (Figure 3–10) which suggests multiple events occurred in this field area. In all instances gritty dolomite is an unusual fault rock with a complex history.

The thickness of the gritty dolomite layer varies across the field area. Typically the gritty dolomite is 2 -3 m thick. In select locations, specifically near the thrust ramp on Zebra Hill, the thickness increases to >5 m.

Underlying the gritty dolomite layer is a cream-yellow mylonitized dolomite. This layer is fine grained, crystalline, and typically $\sim$ 5 to 15 cm thick. Slickenlines with an orientation of 16°/222° (Figure 3–3) are found on the top surface which contacts the overlying gritty

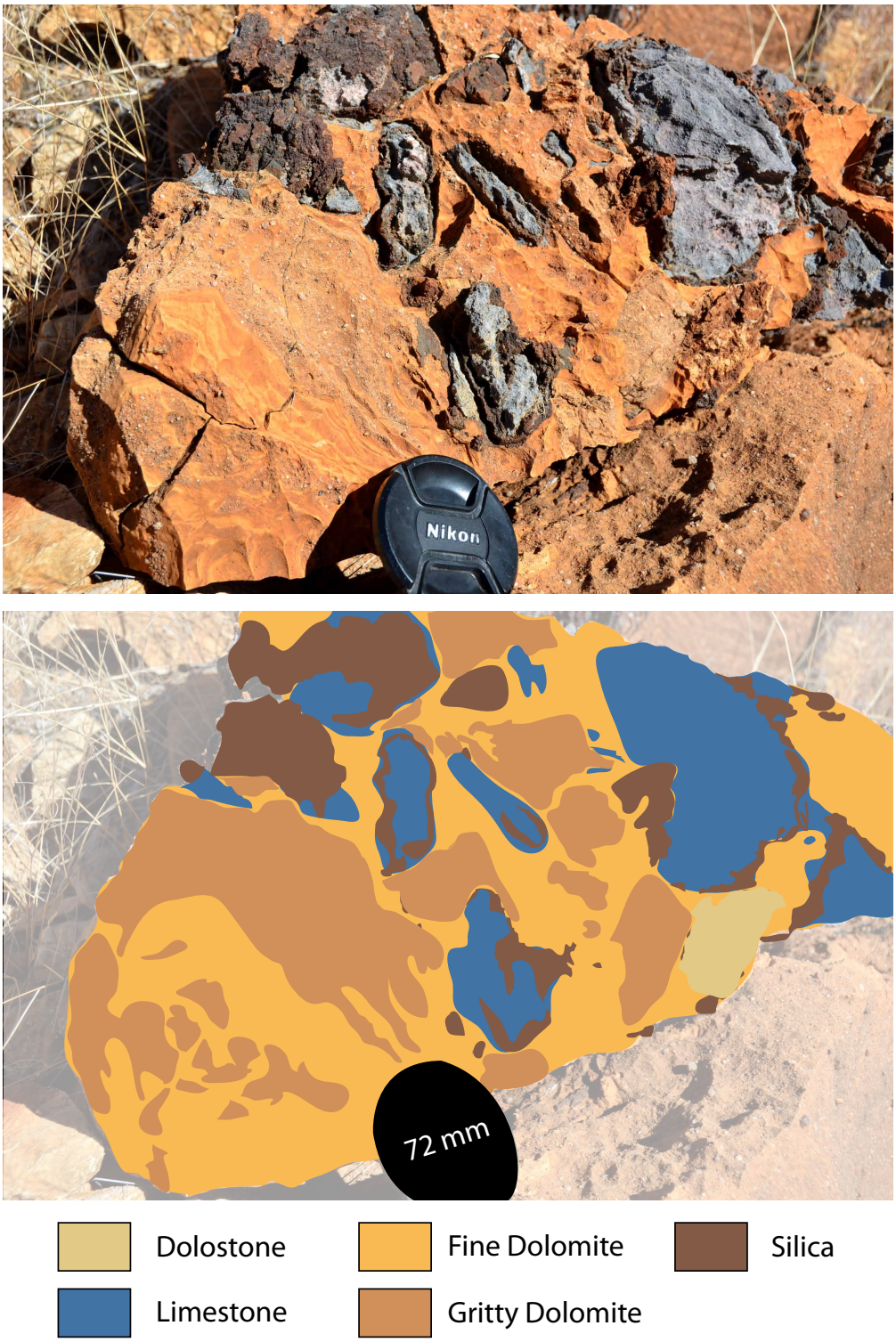

Figure 3–9: Complex gritty dolomite breccia hosts footwall limestone clasts with a brown silica cortex. Gritty dolomite is broken by finer dolomite matrix.

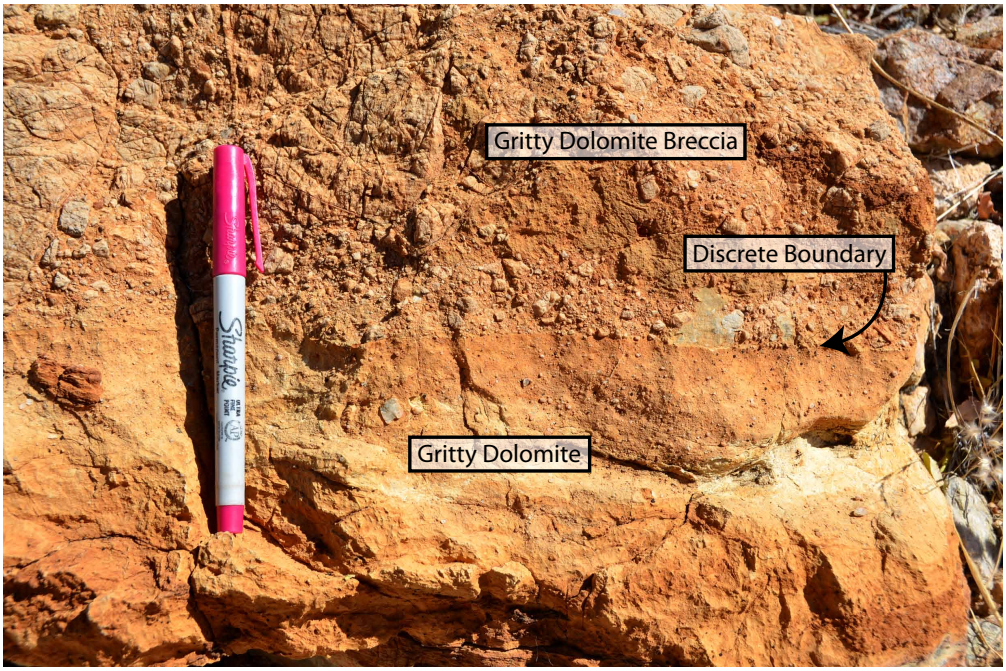

Figure 3–10: Top: Gritty Dolomite breccia with dolostone clasts. Bottom: Gritty Dolomite. A discrete boundary cuts clasts in the breccia and is evidence for multiple events on the Naukluft Thrust.

dolomite at an orientation of 038/16NW (Figure 3–4B,B'). Below the dolo-mylonite is a section of blue, white, and pink calc-mylonite. The intensity of mylonitization is strongest at the fault plane and grades away downsection into blue footwall limestone. Foliations and bedding in the limestone are pulled parallel with the fault at the fault plane. Calcite veining is prevalent and cuts both footwall and hanging wall rocks (Fagereng *et al.*, 2014).

Previous workers in the Naukluft Nappe Complex drew different conclusions on the origins of the basal faultrock. It was first classified as an "unconformity dolomite" of sedimentological origin (Korn & Martin, 1959), as an evaporite sourced intrustion (Hartnady, 1978), and as a paleoseismic fault Viola *et al.* (2006). All previous authors recognized the tectonic significance of the rock as a "lubricating layer" that facilitated nappe transport. Viola *et al.* (2006) identified a tectonostratigraphy within the fault plane consisting of a 1) massive yellow-orange dolomite, 2) "gritty dolomite", 3) foliated calc-mylonites, 4) yellow

dolo-mylonite, and 5) a discrete brittle fault which may occur anywhere in the sequence. Breccias are also found in the fault plane, but are not spatially continuous. Our fieldwork identified hydrofracture breccias *sensu* Swanson (1990) which contained clasts of either footwall or hanging wall lithologies, but a mixed breccia was not observed. Breccia matrix is most often gritty dolomite. However, gritty dolomite is sometimes observed as the clasts within a finer dolomite matrix.

Injectites

The Zebra Hill Injectites are large-scale gritty dolomite-filled fault rock injections sourced from the fault plane (Rowe *et al.*, 2012a; Fagereng *et al.*, 2014) (Figure 1–2). Three large injectites were identified in the exposed hillside and their extents were mapped with GPS (Figure 4–2B). The injectites intruded upsection into the hanging wall and are subvertical. Injectites are generally tabular in shape with a width of 8 - 10 m at the base and a slight taper upsection 3 - 4 m from the tip. The largest injectite (Injectite 1) had a vertical height of 70 m, true vertical extent is unknown due to erosion and must be >70 m. The complete vertical extent of Injectite 2 was ∼50 m. At the injectite tip small veins (∼1 cm wide) filled with neocrystalized dolomite intruded wall rock parallel injectite strike. The injectites have an average strike of ∼030° and a strike-parallel extent of 188 - 220 m, respectively for Injectites 2 and 1. Injectite 3 has a much smaller extent than the other Zebra Hill Injectites due to erosion. Injectite 3 is divided into two segments separated by valley erosion and has a total length of ∼250 m. This injectite dips ∼45°SE. Gritty dolomite laminae found within injectites are typically sub-parallel to the injectite walls, but may be folded, and will wrap around any entrained clasts. Laminae in the zone of fault dilation on Zebra Hill are oriented vertically.

Additional gritty dolomite injectites are present at the North corner of Naukluft-9 locality. The Golf Stop Injectites features another geometrical end member which contrasts

Figure 3–11: Fault rock breccia at Golf Stop contains gritty dolomite, dolomicrite and shale wall rock clasts, and brown silica cements.

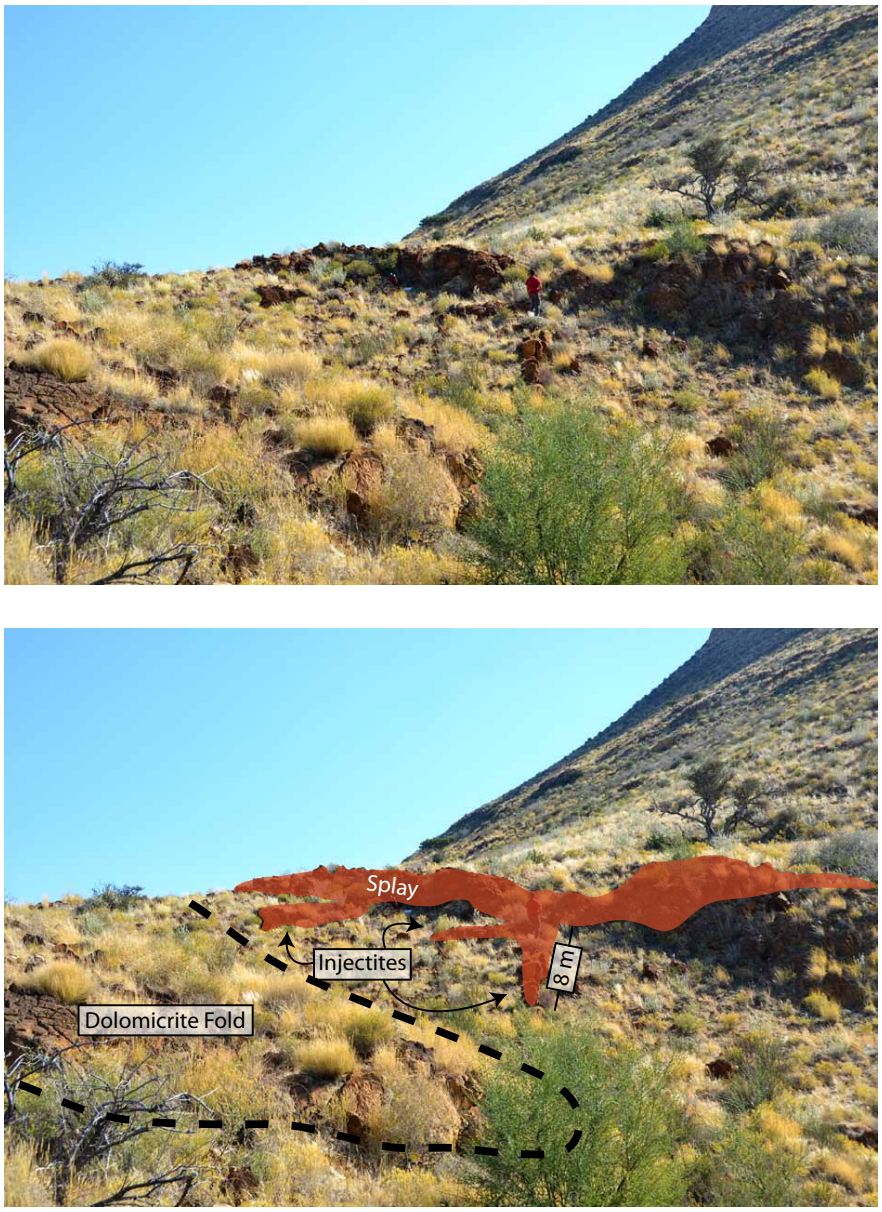

Figure 3–12: Golf Stop Injectites emplace downward from the splay fault.

Figure 3–13: Gritty dolomite following shale horizontal shale cleavage.

with the Zebra Hill Injectites. At this locality gritty dolomite injectites are sourced from a Naukluft Thrust splay which is ∼30 m upsection from the mainthrust (Figure 3–12). The wall rock lithology is more complex at this locality with discontinuous, broken and folded dolomicrite blocks and meta-shales hosting the gritty dolomite. Dolomicrite is folded in Class 1C folds (Ramsay, 1967). Golf Stop gritty dolomite is courser than other areas in Naukluft-9, deep red in color, and contains pockets of doubly-terminating neocrystalized quartz (Figure 3–11). The three injectites here intrude down section at high angle to the source rock for lengths of ∼3.5 - 8.5 m and are ∼40 cm wide with a taper towards the tip.

Northeast from Golf Stop, the gritty dolomite injectites take on a dike-sill geometry with injected gritty dolomite forming a network of tabular bodies along (sills) and across (dikes) the local foliation. Gritty dolomite sills formed along bedding in shales and range in thickness from 4 cm to 1 - 2 meters (Figure 3–13). Gritty dolomite dikes are at high angle to sills and have a similar range of thicknesses. Smaller (10 cm thick) sills exhibited an anastamosing pattern in the shales and the trace of gritty dolomite is at times discontinuous.

Farther northeast the dip of the Naukluft Thrust increases to ∼35° NW.

Naukluft Thust localities key feature summary

Tsams Ost

- The Naukluft Thrust at Tsams Ost is planar and dips ∼9° to the East.
- Fault contact is sharp, but sometimes wavy. The fault zone is dolomizited, with an orange alteration color.
- Off-fault deformation is recorded in hanging wall thrust faults and folds, as well as in footwall folding.
- Lenses of hanging wall dolomicrite are emplaced into the footwall as fault slip migrates to a structurally higher strand, abandoning the sliver of hanging wall rock into the footwall below the basal décollment, a process we refer to as downplating.

Naukluft-9

- Naukluft Thrust is has a ramp-flat geometry, striking ∼45° and dipping at 15° - 40°.
- The dominant fault rock "Gritty dolomite" deformed via granular flow supported by a super critical CO_2 slurry (Rowe *et al.*, 2012a).
- Brittle fault damage is pervasive in this locaility including breccias and injectites.
- Zebra Hill gritty dolomite injectites emplaced subvertically up to 70 m upsection off the fault plane into the hanging wall.
- Golf Stop injectites intruded downsection into dolomicrite and into multiple shale bedding planes forming a dike - sill complex.

‘

CHAPTER 4
Interpolated Fault Geometry

Tsams Ost

Tsams Ost interpolated fault geometry is generally flat and has a consistent shallow dip to the East across the broad valley (Figure 4–1) consistent with field observations. Irregularities in the modeled fault surface correspond both to the sometimes wavy contact between the hanging wall and footwall. Other variations are due to the mapping of "downplated" lenses of hanging wall material (Figure 3–1E,3–2) which were incorporated emplaced below the basal décollment into the footwall. The models reveal that although the fault is near planar, variations occur on wavelengths of 100s meters. These second order geometries are present particularly on the southeast and northwest margins.

Naukluft-9

The Naukluft-9 interpolated geometry dips to the northwest (Figure 4–2A) and has a second order geometry consisting of ramps and flats. Ramp and flat geometry is associated with hanging wall structures such as injectites in the area known as Zebra Hill (Figure 4–2B) Here the focus is on the geometry of Zebra Hill where a ramp-flat is well-constrained due to close spacing of the data points. Ramp strike ranges from perpendicular to oblique relative to hanging wall transport direction. Two ramps are revealed by the model. Ramp 1 and Ramp 2 are $\sim$100 m and $\sim$150 m long, respectively. Ramps strike is perpendicular to oblique to nappe transport direction and spatially discontinuous which suggests that the hanging wall deformed obliquely during transport. Variations in footwall limestone bedding

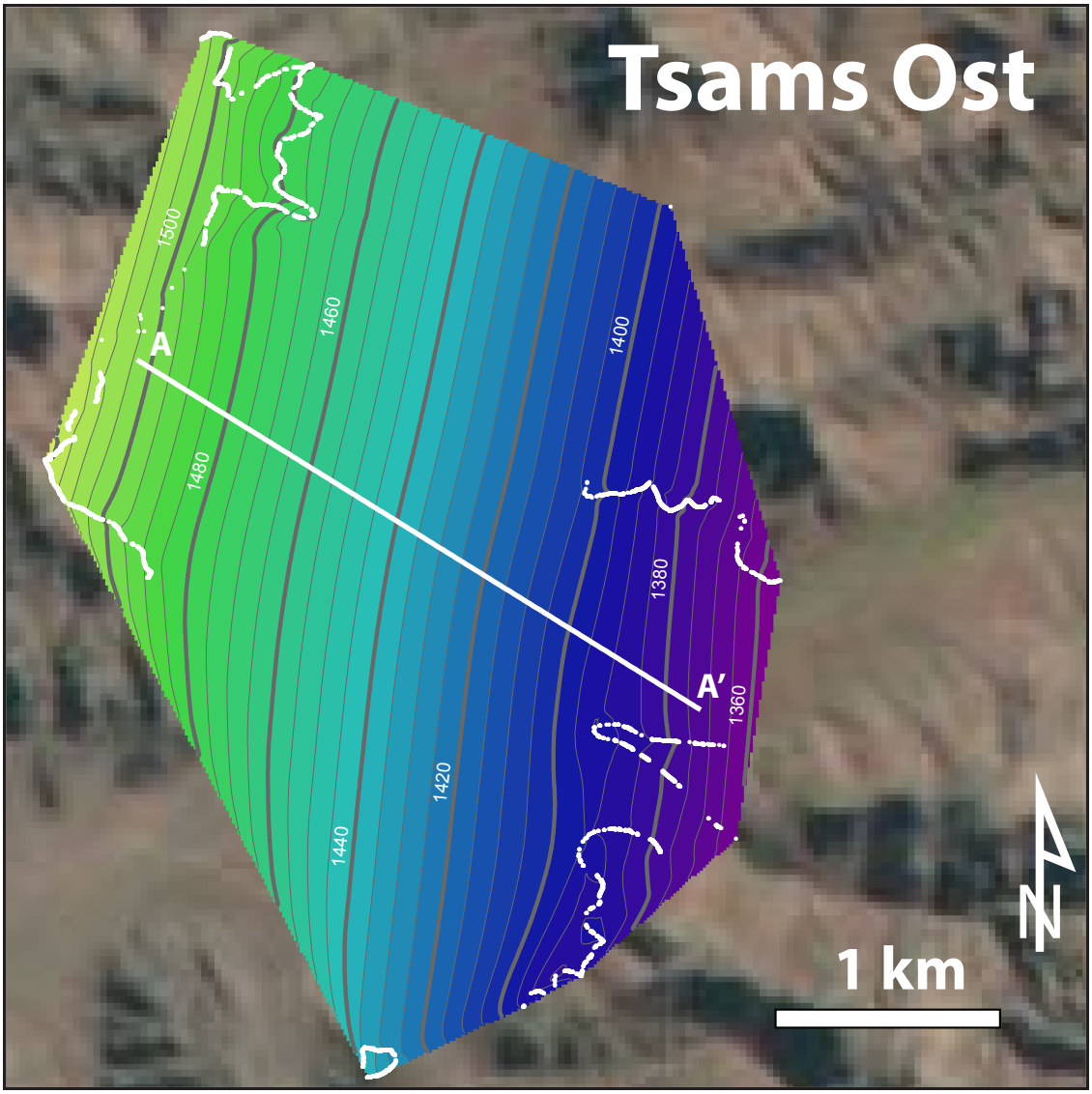

Figure 4–1: Natural Neighbor interpolation of Naukluft Thrust fault surface at Tsams Ost. The fault surface is generally planar and dips ∼10°E.

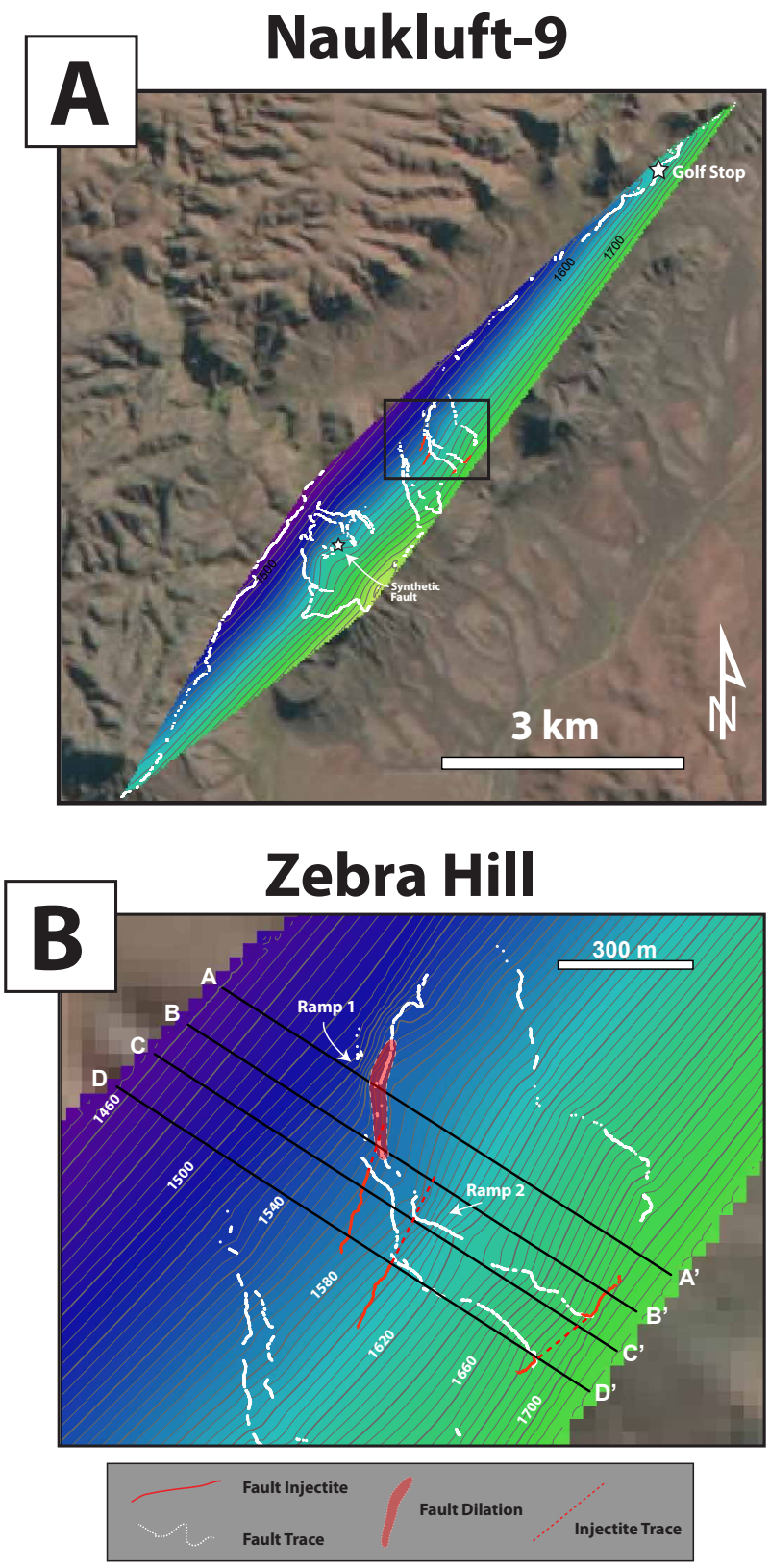

Figure 4–2: A. Natural Neighbor interpolation of Naukluft Thrust fault surface at Naukluft-9. B. Mapped extent of Zebra Hill Injectites and fault zone dilation relative to thrust ramps.

thickness are likely responsible for Naukluft Thrust ramp geometry (Fagereng *et al.*, 2014).

CHAPTER 5
Tensile Stress Models and Injectite Locations

I modeled the tensile static stress change along various cross sections of the Naukluft Thrust, for a uniform fault slip of 10 cm (approximately equivalent to a magnitude 4 - 5 magnitude earthquake. The stress regime (compressional vs tensile) changes across an inflection point in a fault and static stress changes concentrate at inflection points. Static stress changes are symmetrical on both sides of an idealized symmetric fault, and the sharper the bend of the inflection point, the stronger the static stress change (Kilsdonk & Fletcher, 1989). During slip across a thrust ramp, where the hanging wall enters a thrust ramp, static compressive stress increases at the downthrust half of the inflection. The inflection's upthrust half and the along the ramp will show an increase in static tensile stress as the hanging wall deforms over the ramp. Exiting the ramp is a shoaling of the fault dip. Here the upthrust half of the inflection is compressive. Static tensile stress changes decrease away from the inflection as the fault returns to original dip. My models input the cross section geometry as a right-lateral strike slip fault, which is equivalent to top to the right motion on the thrust. A schematic thrust ramp model was made to test the sensitivity of the models to lithostatic load, where lithostatic loads reduced the magnitude of static stress changes from 7 MPa to 2 MPa, but does not affect the spatial distribution of stress changes.

Although, the cross sections along which static stress changes were modeled are not perfectly symmetric, the models displayed expected spatial distribution of static stress changes (Figure 5–1) which are also confirmed by the schematic thrust ramp model which accounts for lithostatic pressures (Figure 5–3). The ramp is located at ∼400 m on cross section A-A'.

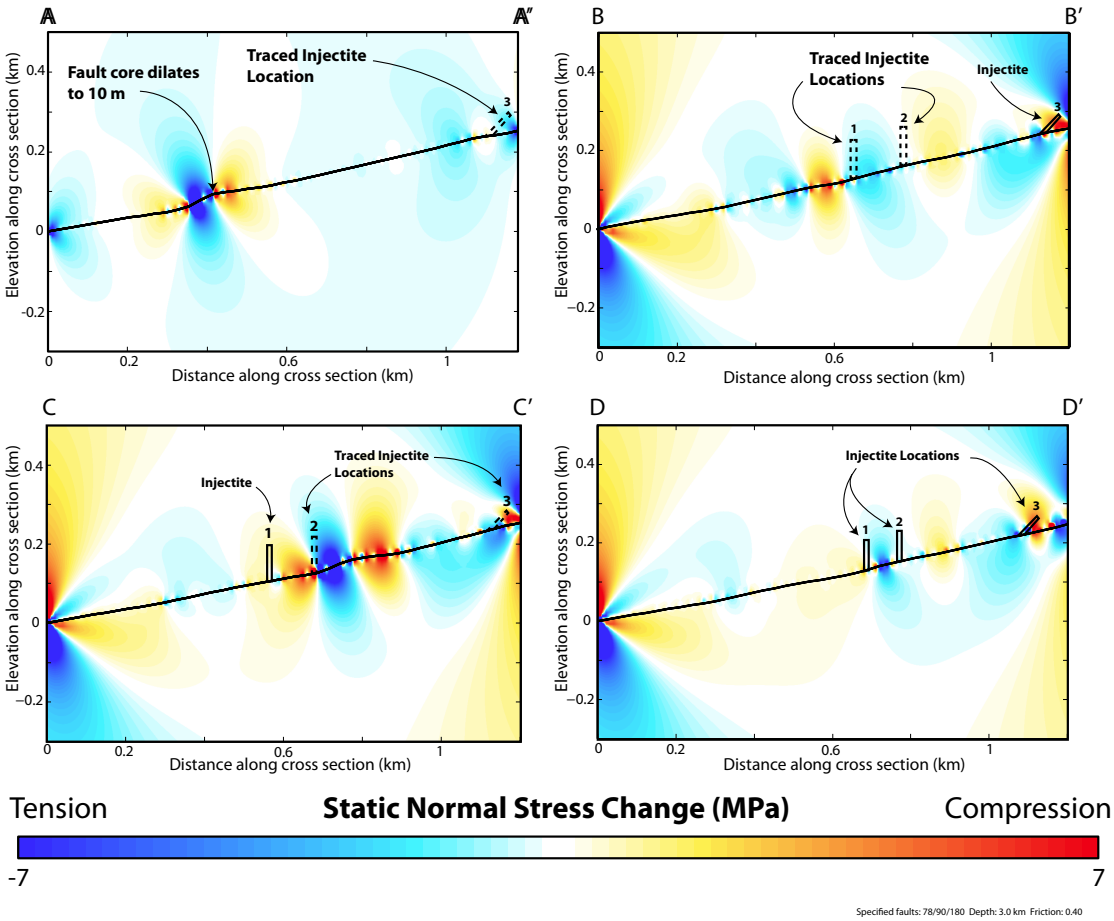

Figure 5–1: Static tensile stress change along cross sections shown in Figure 4–2B with spatial location of injectites. A-A'. The Naukluft Thrust fault core dilates to 5 m at the sharp transition from tensile to compressional stress associated with shoaling of the fault ramp to a flat. B-B'. The Injectite 1 trace at ∼600 m and Injectite 2 trace at ∼800 m. C-C'. Injectite 1 is located at ∼600 m. Trace location of Injectite 2 is located at ∼700 m, at a sharp transition from compressional to tensile stress where the thrust enters a ramp. D-D'. Injectite 1 and 2 are located at ∼700 m and 800 m, respectively. These cross sections demonstrate the complex geometry of the fault ramp in this area and shows evidence for two ramps on Zebra Hill. Stress field around Injectite 3 are dominated by model edge effects.

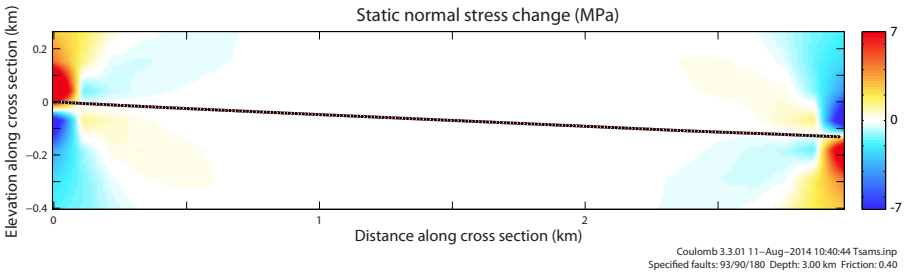

Figure 5–2: Modeled tensile stress change along a geometrically flat cross section at Tsams Ost. Large stress change lobes at left and right of the figure are due to model fault tips. The flat geometry does not influence tensile stress change.

Static normal stress changes are in tension along the length of the ramp and become compressive as the fault shoals (Figure 5–1A-A'). Cross section B-B' features only a subtle ramp geometry, which illustrates the limited along-strike extent of the ramps. The static tensile stresses are much weaker at ∼400 - 500 m (Figure 5–1B-B'), which corresponds to the stress fields on A-A'. Cross section C-C' has a ramp located at ∼650-700 m. Static tensile stresses are in tension along the ramp and is flanked by compressive stresses (Figure 5–1C-C'). Cross section D-D' has a subtle ramp located at ∼650 m, with a small tensile static stress change along it (Figure 5–1D-D').

The static tensile stress model for Tsams Ost is shows no stress change. The model is dominated by stress change lobes caused by model fault tips (Figure 5–2). Planar geometries do not produce local static tensile stress changes.

The spatial locations of the Zebra Hill Injectites were compared with static tensile stress change modeled in Coulomb 3 (Figure 5–1). Exposure of Injectite 1 intersects cross sections C-C' and D-D'. Injectite 2 intersects cross section D-D'. Injecite 3 intersects B-B' and D-D'. Injectite locations were inferred on some cross sections by tracing injectite strike across the eroded valley. The models were designed to test against a rock tensile strength of 7 MPa (Duncan, 1969), where a value of -7 MPa fractures the wall rock. On cross section A-A' the area of fault dilation shown in Figure 4–2B is located at ∼400 m, where the fault shoals.

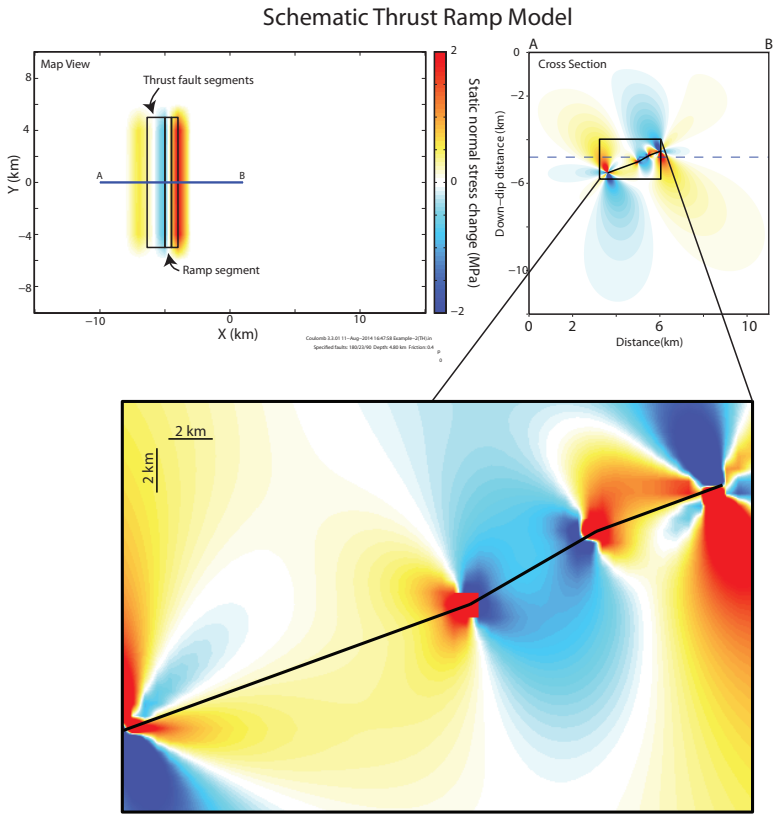

Figure 5–3: Schematic model of static normal stress change on a thrust ramp to test sensitivity of the models to lithostatic pressure. Note saturation of colorbar is set to 2 MPa. Tensile stresses are concentrated along the length of the ramp.

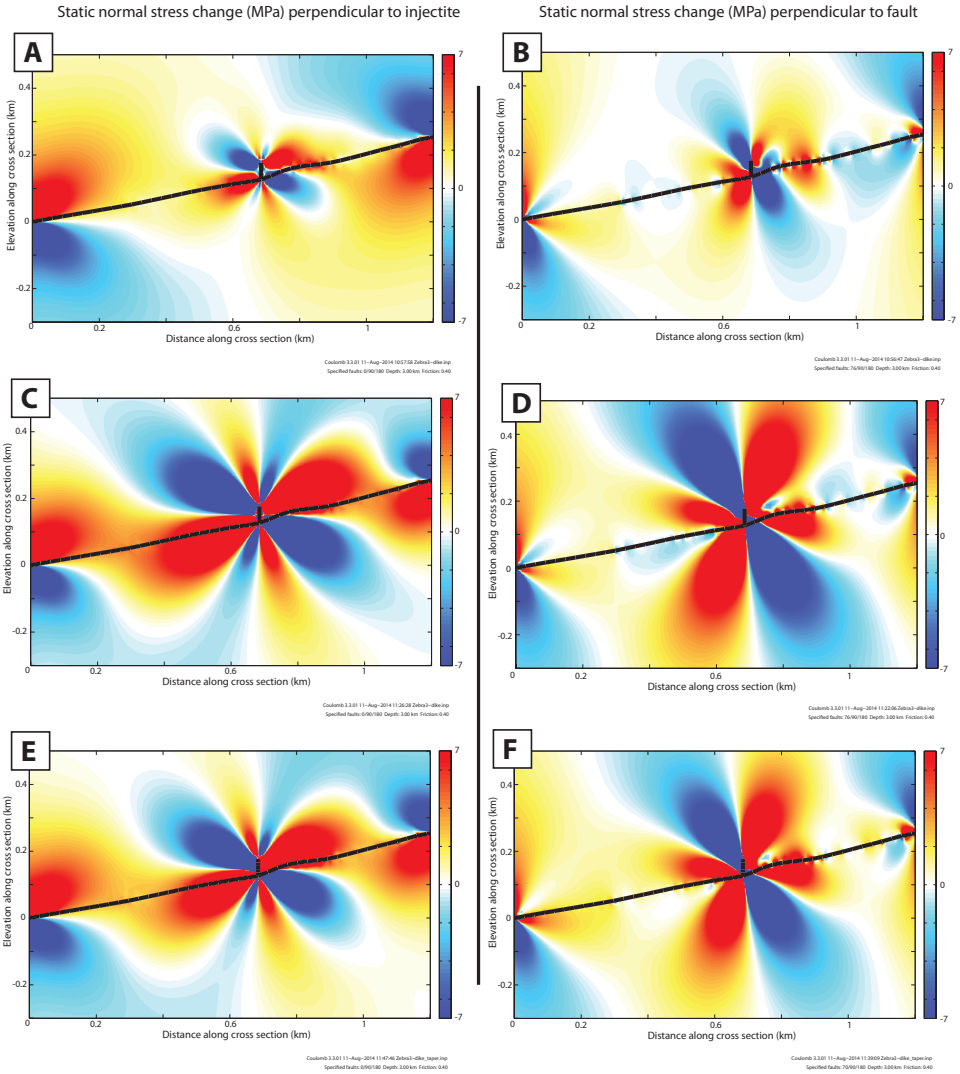

Figure 5–4: Static tensile stress change for vertical intrusions were modeled for orientations parallel to the injectite and parallel to the fault. A) Injectite opening 10 cm, stress change perpendicular to injectite. Stress change lobes due to injectite tips dominate model. B) Injectite opening 10 cm, stress change perpendicular to fault. Stress change lobes from injectite dominate model, but influence of thrust ramp still visible. C) 1 m injectite opening, stress change perpendicular to injectite. Injectite stress change lobes dominate model. D) 1 m injectite opening, stress change perpendicular to fault. Stress change lobes dominate model, asymmetry is caused by stress change due to thrust ramp. E) Tapered 1 m injectite opening for stress change perpendicular to injectite. Stress change lobes dominate model, but are slightly less in magnitude than untapered model. F) Tapered 1 m injectite opening for stress change perpendicular to fault. Asymmetry caused by the thrust ramp is present. The lobes are slightly less in magnitude compared to that untapered model.

This corresponds to an area of sharp static stress gradients between tension and compression (Figure 5–1A-A'). Injectite locations traced onto cross section B-B' place Injectite 1 at ∼600 m in a weak tension field and Injectite 2 at ∼800 m on the margin of the same weak field (Figure 5–1B-B') Injectite 3 intersects at ∼1100 m in a field of compression, which is due to a model edge artifact. Cross section C-C' intersects Injectite 1 at ∼600 m (Figure 5–1C-C'). The trace of Injectite 2 is at ∼700 m and corresponds with a sharp stress gradient between areas of tension and compression. The trace of Injectite 3 is located at ∼1100 m and correlates with an area of tensile stress change. Cross section D-D' is the only model that intersects all three observed injectites (Figure 5–1D-D'). Injectite 1 is located at ∼700 m in an area of tensile stress change. Injectite 2 is located at ∼800 m in an area of very weak compression and Injectite 3 is locaed at ∼1100 m in an area of weak compression, an edge artifact caused by the boundary of the model.

Static normal stress change was modeled for a 60 m injectite at the base of the ramp (Figure 5–4). Stress change was investigated for both perpendicular to the injectite and the fault (same orientation as previous models). Strong static normal stress change lobes dominate the models with static stress change perpendicular to the injectite (Figure 5–4A,C,E). Injectite opening of 1 m produces stress change magnitudes much greater than the 10 cm opening model (Figure 5–4A,C). Tapered 1 m opening (Figure 5–4C) produces slightly smaller stress change lobes compared to uptapered opening (Figure 5–4E). The models with stress change perpendicular to the fault produced slightly more asymmetrical results (Figure 5–4B,D,F). This is due to the influence of the thrust ramp. Injectite opening of 10 cm had the smallest stress change lobes (Figure 5–4B). Injectite opening of 1 m produced the largest stress change lobes (Figure 5–4D), and a tapered 1 m opening had slightly smaller stress change lobes (Figure 5–4F).

The models may be influenced by changes in parameters (Figure 5–5). Several sensitivity tests were modeled to determine how elastic parameters influence the end result of

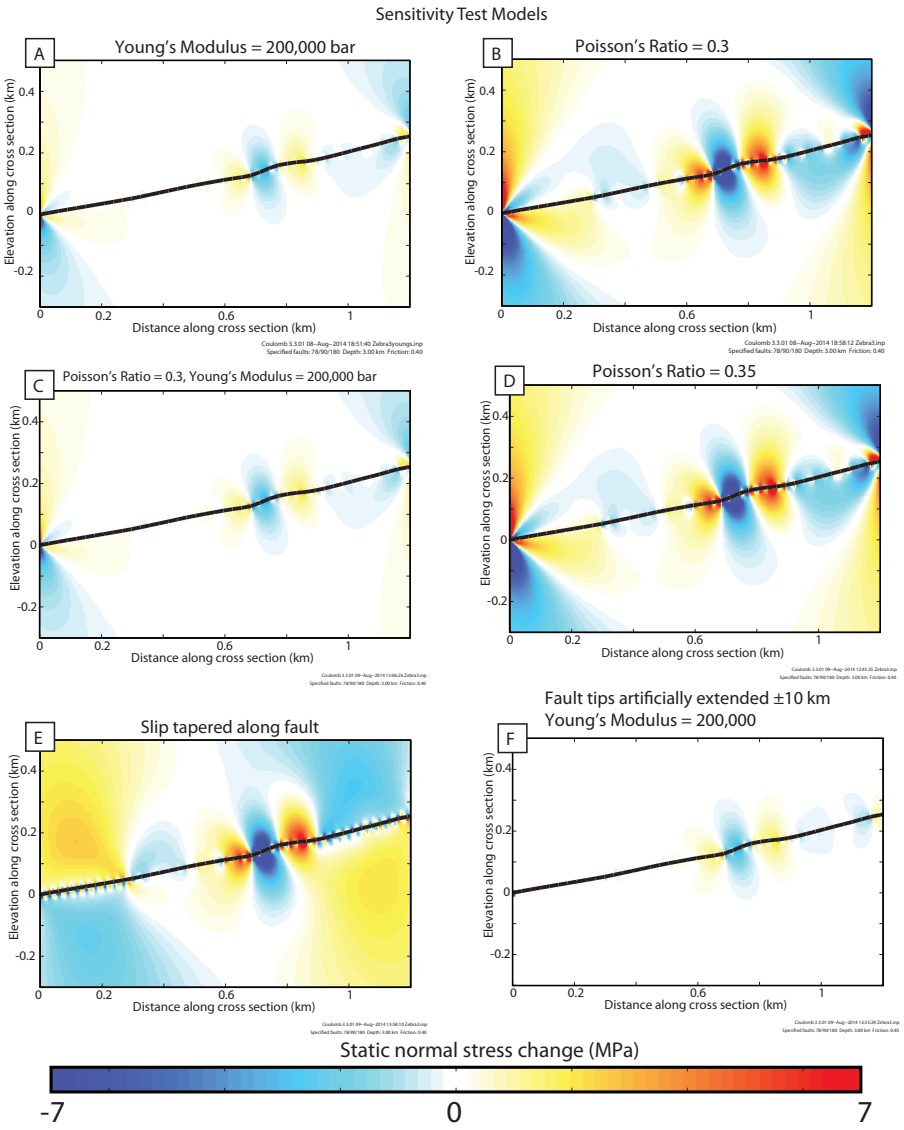

Figure 5–5: Sensitivity test models. A) Young's Modulus = 200,000 bar. This dramatically decreases the magnitude of stress changes compared to 800,000 bar models. B) Poisson's Ratio = 0.3. No noticeable change in stress change magnitudes. C) Poisson's Ratio = 0.3, Young's Modulus = 200,000 bar. Significant decrease in stress change magnitude. D) Poisson's Ratio = 0.35. No noticeable change in stress change magnitudes. E) Slip tapered along fault. Tapering the slip towards the tips of the fault generates bumps of static stress change where fault segments meet. F) Fault tips artificially extended ±10 km and Young's Modulus = 200,000 bar. The stress change lobes due to tip effects are removed.

the model. The sensitivity of the model to fault taper and fault tips were also tested. A decrease in the Young's Modulus from 800,000 bar (strong wallrock, crystalline dolomite) to 200,000 bar (weak wall rock, shales or highly fractured limestone) significantly reduced the magnitude of static normal stress change (Figure 5–5A). This is due to the Young's Modulus controlling the rigidity of the model wallrocks. A stiffer rigidity produces greater magnitude static stress changes. Changes in Poisson's ratio did not affect stress changes magnitudes (Figure 5–5B,D). Tapering slip along the fault from 0 to 10 cm slip produced stress change bumps in the model between linking fault segments that form the geometry of the cross section (Figure 5–5E). Artificially extending the fault tips ±10 km beyond the cross section removed the stress change lobes concentrated at fault tips from the model view, this sensitivity model also applied a Young's Modulus of 200,000 bar and shows stress magnitudes that are smaller compared to Young's Modulus = 800,000 bar models (Figure 5–5F).

Paleoearthquake Magnitude

Paleoearthquake magnitude was modeled for various concentrations of CO_2 and H_2O to test the sensitivity of the system to water compressibility. Following CO_2-H_2O volumes from Holland & Powell (1998) Perple_X calculations and using observed injectite dimensions and observed source rock thicknesses of 5 cm and 10 cm, the earthquake slip patch area was estimated at 180 - 230 km^2 and 94 - 116 km^2, respectively. The source rock thickness is somewhat poorly constrained as field observations are of remnant, undissociated dolomite. The dissociation calculations do not account for volume lost by the source rock dolomite. Models were ran for both 10 cm and 5 cm source rock thicknesses. Additionally this is an idealized system of pure CO_2-H_2O and assumed 50% fluidization porosity that does not account for lithic wall rock clasts and the specific volumes of dissociated solids. Accounting for those volumes would reduce the slip patch area. From the slip patch area calculations the displacement is calculated following Kanamori & Brodsky (2004) earthquake scaling laws with $D = \frac{L}{10^4}$. Comparing slip patch area with earthquake scaling relationships outlined by Kanamori & Brodsky (2004)'s Figure 11 should result in a M_w∼6. Our paleomagnitude estimates are from M_w∼3.52 - 3.62 for a square slip patch and 5 cm source rock thickness, M_w∼3.42 - 3.52 for a square slip patch and 10 cm source rock thickness, and M_w∼3.52 - 3.61 for a circular slip patch and 5 cm source rock thickness (Figure 5–6). Kanamori & Brodsky (2004)'s scaling relationships use a rupture length scale that is the square root of the rupture area. It should be noted that different faults have different aspect ratios of rupture areas (Kanamori & Brodsky, 2004) and the rupture length and width will influence the behavior the scaling law. A fault with a high length to width aspect ratio will scale for a longer slip, D, compared to a more square fault aspect ratio. The increased D for the high aspect ratio fault will increase the calculated seismic moment, M_o, and thus the moment magnitude, M_w. To apply this relationship to our models, the source rock thickness represents an important control on the slip patch area, and thus on the slip patch length.

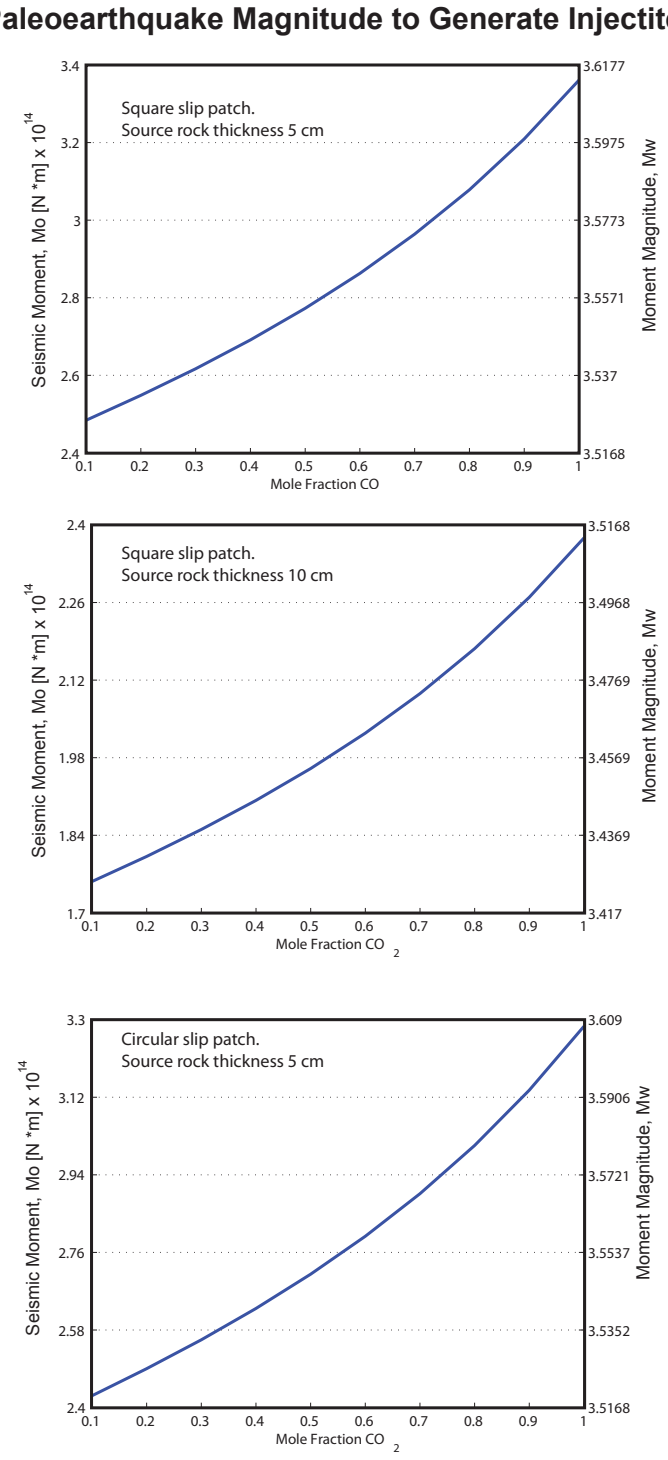

Figure 5–6: The influence of water on estimates of Seismic Moment (M_o) and Moment Magnitude (M_w). The water content will offset the volume of CO_2 from the total volume. With increasing CO_2 fraction more dolomite must be dissociated to generate that volume, requiring a larger earthquake slip patch and a larger amount of energy.

CHAPTER 6
Discussion

Fault Geometry

Comparison of the lithologic, geometric, and deformation features between the Tsams Ost and Naukluft-9 localities show that accommodation of hanging wall displacement was achieved through different processes along the Naukluft Thrust. At Tsams Ost local fault asperities were bypassed and abandoned through the development of planar faults above the lenticular hanging wall rock (Figure 3–1E). Asperity abandonment downplated the hanging wall lens into the foot wall below the basal décollment. In Tsams Ost fault geometry does not have a large influence on the development of fault rock because the fault prefers to cut and abandon asperities, rather than deform around them. Other factors such as lithology and fluid pressure play a greater role in fault evolution. The presence of calc-mylonite lenses in the footwall show that there was at least local ductile deformation occurring at some point in the fault's history. The fold and thrust structures and stratigraphy of the hanging wall combined with the lack of complex brittle features at the fault surface shows that motion of the hanging wall was accommodated through a broad (100s m) zone of deformation. The basal décollement acted as a planar sliding surface similar to the models put forth by Korn & Martin (1959). The flatness and low angle of the Naukluft Thrust is reminiscent of Hubbert & Rubey (1959)'s invocation of elevated fluid pressure at the footwall - hanging wall interface to reduce the effective normal stress and facilitate low angle displacements. This requires a low-permeability fault core to confine fluid pressure at the interface.

At Tsams Ost there was a rheological constrast between footwall and hanging wall rocks. Footwall shales emplaced into the a fracture in the hanging wall dolomite (Figure

3–1B) could be an example of large scale boudinaging of a strong hanging wall with weaker footwall shales filling in the gaps consistent with the mechanics of boudinage theory (Wegmann, 1932; Cloos, 1947; Ramberg, 1955). Cleavage in the shales form an upside-down "U" shape in the fracture leading to the conclusion that the shales are analogous to a viscous flow experiencing frictional drag (*sensu* Ramberg, 1955) during fracture of the competent dolomite, similar to fault gouge injections observed by Rowe *et al.* (2012a) as opposed to a turbulent, chaotic flow which would have destroyed shale cleavage. It is also possible that the calc-mylonite lenses observed at various locations in Tsams Ost are boudins derived from the same limestone bed as opposed to limestone lenses that are spatially constrained, depositional in origin, and were dragged, maintaining their original positions relative to the shales around them.

Modeled Tensile Stress and Fault Rock Injectites

Modeled static tensile stress changes show that fault geometry is a major control on the spatial distribution of stresses (Kilsdonk & Fletcher, 1989) and will influence fault related damage such as fractures (Kirkpatrick *et al.*, 2008). At Zebra Hill in Naukluft-9 the spatial correlation between fault ramps and fault dilation and injection demonstrates a geometric control on the development of these structures (Figure 4–2B). The modeled static tensile stress change, which isolates the variable of geometry, shows that an increase in tensile stress at ramp inflections is great enough to exceed wall rock tensile stress (estimated at 7 MPa for dolomite (Duncan, 1969)). The injectites are thought to form as elastic opening mode fractures (Rowe *et al.*, 2012a) and any fluid present fills fracture space. The slurry that fills the injectites was pressurized at time of formation due to volume increase in CO_2 and thermal pressurization of H_2O. Fault inflections may drive the transport of fluids, where areas of compressive stress change squeeze fluids towards areas of tensile stress change. The direction (up or down) of injection is controlled by rheologic characteristics of footwall and

hanging wall rocks and the overall stress regime. To inject downwards into the footwall, fluid pressure must be greater than the positive buoyancy of the fluids. Zebra Hill Injectites are found only in the hanging wall which demonstrates that the local stresses and tensile cracking favored upward vertical injection. In contrast, the Golf Stop Injectites emplaced down-section, indicating that the local tensile stress was greater than buoyancy of the slurry.

The injectites are tensile fractures filled with granular fault rock material. Static stress change models show sharp gradients between compressive and tensile stresses in the wallrock where the injectites branch from the fault surface. It is likely that these locally different stress regimes worked together to emplace the injectites. As the wall rock is fractured, fluid pressure drives the slurry into the fracture. Adjacent compressive stress areas may locally squeeze the slurry towards tensile fractures, which increases total fluid pressure in the injectite. The area of fault dilation was observed along cross section A-A' and intersects the trace of Injectite 1 (Figure 4–2) which poses the question: are they related? There are three possibilities. 1) The area of fault dilation is an eroded portion of Injectite 1 and the two features are separated by valley erosion. The hanging wall is eroded at the area of dilation, exposing the top of the fault core on the surface. 2) Dilation of the fault core is a mechanism for the hanging wall to deform over the ramp. The injectite emplaced obliquely into the hanging wall from the dilation zone. 3) The features are unrelated. A dilation of the fault surface requires a different stress regime than one for injection. In two dimensions the maximum principal stress axis, σ_1, is parallel the thrust ramp and the minimum principal stress axis, σ_3 is normal to the ramp. The injectite scenario requires σ_1 at the fracture tip and σ_3 normal to the fracture. Therefore locally variable stresses are required for oblique emplacement. The fault dilation is most likely an eroded injectite because gritty dolomite laminae on top of the dilation zone are oriented vertically, similarly to laminae found in the vertical injectites. A fourth possibility is that the injectites are formed through many small events. This assumes that once an injectite is formed, future injectites will localize at the same location. Why then

would an injectite form at a different location as observed instead of continuing to exploit the same wall rock weakness as the first injectite?

Fault geometry plays an important role in localizing damage. The geometrically-controlled high static normal stress gradients augment coseismic dynamic stresses such as thermal pressurization. Stress and fluid pressure are focused at ramp inflections, which focuses hanging wall strain. The injectites are emplaced through this combination of static and dynamic stresses.

The Golf Stop Injectite Complex shows that lithology plays a key control on injectite morphology. Where the injectite is emplacing into a strong, cohesive wall rock, one large injectite forms. If the wall rock is soft, or has many bedding or cleavage planes, such as in the case of the shale North of Golf Stop, the injectite will exploit the weak bedding and cleavage planes, forming a complex network of dikes and sills. Here dynamic stresses are likely more important than static stresses. Mechanisms such as thermal pressurization during coseismic slip would increase the fluid pressure of the slurry which exploits bedding and cleavage weaknesses in the weak shales.

Paleoearthquake Magnitude from Injectite Opening Aperture

Paleoearthquake magnitudes were modeled for varying percents CO_2 and H_2O content. The model estimated moderate sized events of $M_w \sim 4.2$. This is a fraction of the total earthquake energy because the energy estimated is only the energy required to generate the size of one injectite (there are three total on Zebra Hill) and our estimated energy does not include seismic energy dissipated into the surrounding region, frictional heating which dissociated the CO_2 from carbonate wallrock, nor does it include energy consumed during fracturing fault rock to produce the breccias and gouges observed.

Water is expected to influence the model in a number of ways. Thermal pressurization of water molecules along a fault lowers dynamic friction on a fault (Rice, 2006). Water

compressibility is another factor which will influence the density of the water, and thus the density of the slurry. At low fractions of CO_2, the compressibility of water produces a lower fluid volume compared to high fractions CO_2 fluids (Holland & Powell, 1998). Exploring the influence of different mole-fractions of CO_2 and H_2O combinations reveals that water plays a minor role on estimates of earthquake magnitude (Figure 5–6). Even in a system of 90% H_2O - 10% CO_2 the compressibility effect of water is a minor factor.

The presence of multiple injectites at various locations relative to the ramps must lead to the discussion of their original formation locations. Three possibilities exist: 1) injectites formed in situ during last phase of deformation on the Naukluft Thrust and did not experience later transport, or 2) Injectites formed at the base of the ramp or elsewhere and have since been transported with the hanging wall during subsequent events, or 3) once an injectite has intruded into the wallrock, that area local wallrock is weak and prevents future large intrusions until the injectite has been adequately transported away from the bending site. Because the distance between injectites is relatively great ($\sim$100 m) and it implausible that 100 m slip occurred in a single event, either interseismic transport of the hanging wall had to occur, or small events that did not generate injectites are needed to transport the injectites in the hanging wall.

CHAPTER 7
Conclusion

The Cambrian basal forland décollement, the Naukluft Thrust, in central Namibia exhibits different fault dip and style of fault core over a distances of 100s km. GPS mapping of the the fault at two localities revealed a nearly planar geometry at Tsams Ost and a steep ramp-flat geometry at Naukluft-9 localities, respectively. Different footwall lithologies dominate each locality with metashales as the predominate footwall at Tsams Ost and limestone as the predominate footwall at Naukluft-9. The planar fault at Tsams Ost has a sharp, but sometimes wavy alteration zone at the footwall hanging wall contact. Deformation was primarily accommodated through large scale folding and and minor thrust faults in the hanging wall as well as folding in the footwall. Lenses of hanging wall blocks are incorporated into the footwall by stratigraphically higher splay faults. At Naukluft-9 the primary fault rock is granular "Gritty Dolomite" which was fluidized in a supercritical slurry and deformed via granular flow mechanisms during coseismic slip (Rowe *et al.*, 2012a). Intrusions of gritty dolomite are emplaced upwards in the hanging wall from the fault plane in the proximity of a thrust ramp at "Zebra Hill" (Rowe *et al.*, 2012b; Fagereng *et al.*, 2014). The injectites are about 70 m in height from the fault plane to their mapped vertical extent. A topographic model of the fault surface revealed two thrust ramps in the area of the injectites.

Static tensile stress change models of fault surface cross sections exhibit tension across thrust ramps. The spatial distribution of injectites and fault zone dilation were correlated with the stress change models. An observed area of fault dilation correlates with modeled dilation on the thrust ramp. Gritty dolomite injectites and their along strike traces correlate with sharp transitions between compressive and tensile stress. These areas of stress change

are targets for wall rock fracturing during deformation. The static stress changes from ramp geometry along with dynamic coseismic stresses and the fluid pressure of the gritty dolomite slurry emplaced the fault rock injectites. In contrast to the Zebra Hill Injectites, the "Golf Stop" injectites emplaced downward from a Naukluft Thrust spaly fault. This suggests that local stresses and fluid pressures exceeded the natural buoyancy force of the injecting material. Northeast of Golf Stop the wall rock lithology changes to a metashale. Gritty dolomite forms an anastomosing dike and sill complex, exploiting weaknesses in shale bedding and cleavage planes. This highlights an important lithology control on injectite morphology. Strong, homogeneous wall rock will fracture and a single, large intrusion of fault rock is emplaced. Where wall rock has many weak points, the fluid pressure of the intruding material will drive the material along the weak planes.

The dimensions of Zebra Hill Injectites were used to create a simplified model volumes of material generated during coseismic slip for combinations of CO_2 - H_2O. These volumes were used to calculate the slip patch area of an earthquake and estimate paleoearthquake magnitudes. This model produced moderate size events of $M_w \sim 4.2$. The compressibility of water was not a major control in the volumes calculated, and thus did not greatly influence the magnitude. As far as we know this method of using fault rock injectite aperture opening to estimate earthquake energy along carbonate faults is novel.

References

Ahrendt, H., Hunziker, J. C., & Weber, K. (1978). Age and degree of metamorphism and time of nappe emplacement along the southern margin of the Damara Orogen/Namibia (SW-Africa). *Geologische Rundschau*, *67*(2), 719–742.

Apotria, T. G. (1995). Thrust sheet rotation and out-of-plane strains associated with oblique ramps: An example from the wyoming salient usa. *Journal of Structural Geology*, *17*(5), 647–662.

Bartlett, S. F. & Youd, T. L. (1992). *Empirical analysis of horizontal ground displacement generated by liquefaction-induced lateral spreads*. National Center for earthquake engineering research Buffalo, NY.

Behrmann, J. H. (1991). Conditions for hydrofracture and the fluid permeability of accretionary wedges. *Earth and Planetary Science Letters*, *107*(3), 550–558.

Billi, A., Salvini, F., & Storti, F. (2003). The damage zone-fault core transition in carbonate rocks: implications for fault growth, structure and permeability. *Journal of Structural Geology*, *25*(11), 1779–1794.

Boehm, A. & Moore, J. C. (2002). Fluidized sandstone intrusions as an indicator of paleostress orientation, Santa Cruz, California. *Geofluids*, *2*, 147–161.

Bonilla, M. G., Mark, R. K., & Lienkaemper, J. J. (1984). Statistical relations among earthquake magnitude, surface rupture length, and surface fault displacement. *Bulletin of the Seismological Society of America*, *74*(6), 2379–2411.

Boyer, S. E. & Elliott, D. (1982). Thrust systems. *AAPG Bulletin*, *66*(9), 1196–1230.

Briggs, S. E., Davies, R. J., Cartwright, J. A., & Morgan, R. (2006). Multiple detachment levels and their control on fold styles in the compressional domain of the deepwater west

niger delta. *Basin Research*, *18*(4), 435–450.

Brown, K. M., Bekins, B., Clennell, B., Dewhurst, D., & Westbrook, G. (1994). Heterogeneous hydrofracture development and accretionary fault dynamics. *Geology*, *22*(3), 259–262.

Butler, R. W. (1982). The terminology of structures in thrust belts. *Journal of structural geology*, *4*(3), 239–245.

Cartwright, J. (2010). Regionally extensive emplacement of sandstone intrusions: a brief review. *Basin Research*, *22*, 502–516.

Chester, F. & Chester, J. (1998). Ultracataclasite structure and friction processes of the punchbowl fault, san andreas system, california. *Tectonophysics*, *295*(1), 199–221.

Cloos, E. (1947). Boudinage. *Transactions, American Geophysical Union*, *28*, 626–632.

Cosgrove, J. W. (2001). Hydraulic fracturing during the formation and deformation of a basin: A factor in the dewatering of low-permeability sediments. *AAPG Bulletin*, *85*(4), 737–748.

Dieterich, J. H. & Smith, D. E. (2009). Nonplanar faults: Mechanics of slip and off-fault damage. *Pure and Applied Geophysics*, *166*(10/11), 1799–1815. doi: 10.1007/ss00024-009-0517-y.

Duncan, N. (1969). Engineering geology and rock mechanics. vols. 1 and 2.

Fagereng, Å., Smith, Z., Rowe, C. D., Makhubu, B., & Sylvester, F. Y. (2014). Stress, strain, and fault behavior at a thrust ramp: Insights from the naukluft thrust, namibia. *Journal of Structural Geology*, *58*, 95–107.

Fitz-Diaz, E., Hudleston, P., Siebenaller, L., Kirschner, D., Camprubí, A., Tolson, G., & Puig, T. P. (2011). Insights into fluid flow and water-rock interaction during deformation of carbonate sequences in the mexican fold-thrust belt. *Journal of Structural Geology*, *33*(8), 1237–1253.

Ge, S. & Garven, G. (1994). A theoretical model for thrust-induced deep groundwater expulsion with application to the canadian rocky mountains. *Journal of Geophysical Research: Solid Earth (1978–2012)*, *99*(B7), 13851–13868.

Han, R., Shimamoto, T., Hirose, T., Ree, J.-H., & Ando, J.-i. (2007). Ultralow friction of carbonate faults caused by thermal decomposition. *Science*, *316*. doi: 10.1126/science.1139763.

Hartnady, C. J. H. (1978). The stratigraphy and structure of the Naukluft Nappe Complex. In *Precambrian Research Unit Annual*, University of Cape Town Department of Geology. 163–170.

Holland, T. & Powell, R. (1998). An internally consistent thermodynamic data set for phases of petrological interest. *Journal of metamorphic Geology*, *16*(3), 309–343.

Hubbert, M. K. & Rubey, W. W. (1959). Role of fluid pressure in mechanics of overthrust faulting: I. mechanics of fluid-filled porous solids and its application to overthrust faulting. *Geological Society of America Bulletin*, *70*, 115–166. doi: 10.1130/0016-7606.

Huuse, M., Jackson, C. A.-L., van Rensbergen, P., Davies, R. J., Flemings, P. B., & Dixon, R. J. (2010). Subsurface sediment remobilization and fluid flow in sedimentary basins: an overview. *Basin Research*, *22*, 342–360. doi: 10.1111/j.1365-2117.2010.00488.x.

Kanamori, H. (1977). The energy release in great earthquakes. *Journal of Geophysical Research*, *82*(20), 2981–2987.

Kanamori, H. & Anderson, D. L. (1975). Theoretical basis of some empirical relations in seismology. *Bulletin of the Seismological Society of America*, *65*(5), 1073–1095.

Kanamori, H. & Brodsky, E. (2001). The physics of earthquakes. *Physics today*, *54*, 34.

Kanamori, H. & Brodsky, E. (2004). The physics of earthquakes. *Reports on Progress in Physics*, *67*(8), 1429.

Kilsdonk, B. & Fletcher, R. C. (1989). An analytical model of hanging-wall and footwall deformation at ramps on normal and thrust faults. *Tectonophysics*, *163*(1), 153–168.

Kim, Y.-S., Peacock, D. C. P., & Sanderson, D. J. (2004). Fault damage zones. *Journal of Structural Geology*, *26*, 503–517.

King, G. C., Stein, R. S., & Lin, J. (1994). Static stress changes and the triggering of earthquakes. *Bulletin of the Seismological Society of America*, *84*(3), 935–953.

Kirkpatrick, J. D., Shipton, Z. K., Evans, J. P., Micklethwaite, S., Lim, S. J., & McKillop, P. (2008). Strike-slip fault terminations at seismogenic depths; the structure and kinematics of the Glacier Lakes fault, Sierra Nevada, USA. *Journal of Geophysical Research*, *113*(B4). doi: 10.1029/2007JB005311.

Kirschner, D., Masson, H., & Sharp, Z. (1999). Fluid migration through thrust faults in the helvetic nappes (western swiss alps). *Contributions to Mineralogy and Petrology*, *136*(1-2), 169–183.

Kirschner, D. L. & Kennedy, L. A. (2001). Limited syntectonic fluid flow in carbonate-hosted thrust faults of the front ranges, canadian rockies, inferred from stable isotope data and structures. *Journal of Geophysical Research: Solid Earth (1978–2012)*, *106*(B5), 8827–8840.

Korn, H. & Martin, H. (1959). Gravity tectonics in the Naukluft Mountains of South West Africa. *Geological Society of America Bulletin*, *70*, 1047–1078.

Lallemant, S. J., Henry, P., Le Pichon, X., & Foucher, J. P. (1990). Detailed structure and possible fluid paths at the toe of the barbados accretionary wedge (odp leg 110 area). *Geology*, *18*(9), 854–857.

Law, K. T., Cao, Y., & He, G. (1990). An energy approach for assessing seismic liquefaction potential. *Canadian Geotechnical Journal*, *27*(3), 320–329.

Leva, M. (1959). *Fluidization*. McGraw-Hill Book Company, Inc.

Lin, J. & Stein, R. S. (2004). Stress triggering in thrust and subduction earthquakes and stress interaction between the southern san andreas and nearby thrust and strike-slip faults. *Journal of Geophysical Research: Solid Earth (1978–2012)*, *109*(B2).

Martin, H., Porada, H., & Wittig, R. (1983). The root zone of the naukluft nappe complex: geodynamic implications, 679–698.

Mavko, G., Mukerji, T., & Dvorkin, J. (2009). *The rock physics handbook: Tools for seismic analysis of porous media*. Cambridge University Press.

McCalpin, J. (1996). *Paleoseismology*, vol. 62. Academic press.

Micklethwaite, S., Sheldon, H. A., & Baker, T. (2010). Active fault and shear processes and their implications for mineral deposit formation and discovery. *Journal of Structural Geology*, *32*(2), 151–165.

Moore, J. C., Brown, K. M., Horath, F., Cochrane, G., MacKay, M., & Moore, G. (1991). Plumbing accretionary prisms: Effects of permeability variations. *Philosophical Transactions of the Royal Society of London. Series A: Physical and Engineering Sciences*, *335*(1638), 275–288.

Moore, J. C., Orange, D., & Kulm, L. D. (1990). Interrelationship of fluid venting and structural evolution: Alvin observations from the frontal accretionary prism, oregon. *Journal of Geophysical Research: Solid Earth (1978–2012)*, *95*(B6), 8795–8808.

Münch, H.-G. (1978). Das Schmiermittel an der Basis der Naukluft-Decke, Südwestafrika: The sliding layer at the base of the Naukluft Nappe, South-west Africa. *Zeitschrift. der Deutschen Geologishen Gesellsschaft*, *129*, 7–31.

Neves, F. A., Zahrani, M. S., & Bremkamp, S. W. (2004). Detection of potential fractures and small faults using seismic attributes. *The Leading Edge*, *23*(9), 903–906.

Nichols, R., Sparks, R., & Wilson, C. (1994). Experimental studies of the fluidization of layered sediments and the formation of fluid escape structures. *Sedimentology*, *41*(2), 233–253.

Obermeier, S., Weems, R., Jacobson, R., & Gohn, G. (1989). Liquefaction evidence for repeated holocene earthquakes in the coastal region of south carolinaa. *Annals of the New York Academy of Sciences*, *558*(1), 183–195.

Patwardhan, V. & Tien, C. (1985). Sedimentation and liquid fluidization of solid particles of different sizes and densities. *Chemical Engineering Science*, *40*(7), 1051–1060.

Platt, J. P. (1990). Thrust mechanics in highly overpressured accretionary wedges. *Journal of Geophysical Research*, *95*(B6), 9025–9034.

Ramberg, H. (1955). Natural and experimental boudinage and pinch-and-swell structures. *The Journal of Geology*, 512–526.

Ramsay, J. (1967). *Folding and Fracturing of Rocks*. International series in the earth and planetary sciences. Blackburn Press. URL `http://books.google.ca/books?id=KcAaAAAACAAJ`.

Rice, J. R. (2006). Heating and weakening of faults during earthquake slip. *Journal of Geophysical Research*, *111*(B5), B05311.

Rice, J. R. & Dunham, E. M. (2009). Thermo- and hydro-mechanical processes along faults during rapid slip. *Engineering*, *85*(1978), 3–16.

Ross, J. A., Peakall, J., & Keevil, G. M. (2014). Facies and flow regimes of sandstone-hosted columnar intrusions: Insights from the pipes of kodachrome basin state park. *Sedimentology*.

Rowe, C., Fagereng, Å., Miller, J., & Mapani, B. (2012a). Signature of coseismic decarbonation in dolomitic fault rocks of the naukluft thrust, namibia. *Earth and Planetary Science Letters*, *333*, 200–210.

Rowe, C., Kirkpatrick, J., & Brodsky, E. (2012b). Fault rock injections record paleoearthquakes. *Earth and Planetary Science Letters*, *335*, 154–166.

Sanderson, D. J. (1982). Models of strain variation in nappes and thrust sheets: a review. *Tectonophysics*, *88*(3), 201–233.

Scholz, C. (1988). The brittle-plastic transition and the depth of seismic faulting. *Geologische Rundschau*, *77*(1), 319–328.

Scott, A., Vigorito, M., & Hurst, A. (2009). The process of sand injection: internal structures and relationships with host strata (Yellowbank Creek Injectite Complex, California, USA). *Journal of Sedimentary Research*, *79*(8), 568–583.

Seed, H. B., Idriss, I., & Arango, I. (1983). Evaluation of liquefaction potential using field performance data. *Journal of Geotechnical Engineering*, *109*(3), 458–482.

Sheldon, H. & Ord, A. (2005). Evolution of porosity, permeability and fluid pressure in dilatant faults post-failure: implications for fluid flow and mineralization. *Geofluids*, *5*(4), 272–288.

Sherry, T. J., Rowe, C. D., Kirkpatrick, J. D., & Brodsky, E. E. (2012). Emplacement and dewatering of the world's largest exposed sand injectite complex. *Geochemistry, Geophysics, Geosystems*, *13*(8). URL `http://dx.doi.org/10.1029/2012GC004157`.

Shipley, T. H., Stoffa, P. L., & Dean, D. F. (1990). Underthrust sediments, fluid migration paths, and mud volcanoes associated with the accretionary wedge off costa rica: Middle america trench. *Journal of Geophysical Research*, *95*(B6), 8743–8752.

Sibson, R. (1981). A brief description of natural neighbour interpolation. *Interpreting multivariate data*, *21*.

Sibson, R. (2003). Thickness of the seismic slip zone. *Bulletin of the Seismological Society of America*, *93*(3), 1169–1178.

Sibson, R. H. (1986). Brecciation processes in fault zones: Inferences from earthquake rupturing. *Pure and Applied Geophysics*, *124*(1/2), 159–175.

Sibson, R. H. (1992). Implications of fault-valve behaviour for rupture nucleation and recurrence. *Tectonophysics*, *211*, 283–293.

Srivastava, D. C. & Engelder, T. (1990). Crack-propagation sequence and pore-fluid conditions during fault-bend folding in the appalachian valley and ridge, central pennsylvania. *Geological Society of America Bulletin*, *102*(1), 116–128.

Stein, R. S. (2005). Earthquake conversations. *Scientific American*, *15*(2), 82–89.

Stockmal, G. S., Beaumont, C., Nguyen, M., & Lee, B. (2007). Mechanics of thin-skinned fold-and-thrust belts: Insights from numerical models. *Geological Society of America Special Papers*, *433*, 63–98.

Suppe, J. (1983). Geometry and kinematics of fault-bend folding. *American Journal of science*, *283*(7), 684–721.

Swanson, M. T. (1990). Extensional duplexing in the york cliffs strike-slip fault system, southern coastal maine. *Journal of structural geology*, *12*(4), 499–512.

Thompson, B. J., Garrison, R. E., & Moore, J. C. (2007). A reservoir-scale Miocene injectite near Santa Cruz, California. In *Sand Injectites: Implications for hydrocarbon exploration and production*, AAPG Memoir 87. 151–162.

Toda, S., Stein, R. S., Richards-Dinger, K., & Bozkurt, S. B. (2005). Forecasting the evolution of seismicity in southern california: Animations built on earthquake stress transfer. *Journal of Geophysical Research: Solid Earth (1978–2012)*, *110*(B5).

Travé, A., Labaume, P., & Vergés, J. (2007). Fluid systems in foreland fold-and-thrust belts: an overview from the southern pyrenees. In *Thrust Belts and Foreland Basins*, Springer. 93–115.

Twiss, R. & Moores, E. (2006). *Structural Geology*. W. H. Freeman. URL `http://books.google.ca/books?id=aXvmQwAACAAJ`.

Viola, G., Andreoli, M., Ben-Avraham, Z., Stengel, I., & Reshef, M. (2005). Offshore mud volcanoes and onland faulting in southwestern Africa: neotectonic implications and constraints on the regional stress field. *Earth and Planetary Science Letters*, *231*, 147–160.

Viola, G., Mancktelow, N. S., & Miller, J. A. (2006). Cyclic frictional-viscous slip oscillations along the base of an advancing nappe complex: Insights into brittle-ductile nappe emplacement mechanisms from the Naukluft Nappe Complex, central Namibia. *Tectonics*, *25*. Doi: 10.1029/2005TC001939.

Watson, D. F. (1992). *Contouring*. Pergamon Press.

Weber, K. & Ahrendt, H. (1983). Mechanisms of nappe emplacement at the southern margin of the Damara Orogen (Namibia). *Tectonophysics*, *92*, 253–274.

Wegmann, C. (1932). Note sur le boudinage. *Bull. soc. géol. Fr*, *5*, 477–489.

Wells, D. L. & Coppersmith, K. J. (1994). New empirical relationships among magnitude, rupture length, rupture width, rupture area, and surface displacement. *Bulletin of the Seismological Society of America*, *84*(4), 974–1002.

Youd, T. L. & Perkins, D. M. (1987). Mapping of liquefaction severity index. *Journal of Geotechnical Engineering*, *113*(11), 1374–1392.

CHAPTER 8
Appendix

Coulomb 3

Model parameters

Parameter	Value	Relevant Rock Type	Model sensitivity
Poisson's Ratio	0.25	Shales and anhydrites	No effect on models
	0.3	Limestone, Dolostone, and potentially fluid saturated media	No effect on models
	0.35	Limestone, Dolostone, and potentially fluid saturated media	No effect on models
Young's Modulus	80 GPa	Calcite	Model rigidity. It should be noted that rocks such as limestone have a range of Young's Moduli of ∼97-280 GPa (Duncan, 1969)
	20 GPa	Shales	Model rigidity, lower stress magnitudes.

Coulomb 3 input files

```
A-A' cross section
header line 2
#reg1=  0  #reg2=  0  #fixed=  71  sym=  1
 PR1=       0.250     PR2=       0.250   DEPTH=      3
  E1=     0.80000e+006   E2=     0.80000e+006
XSYM=       .000     YSYM=       .000
FRIC=          0.400
S1DR=         90.0000 S1DP=          0.0000  S1IN=        100.000  S1GD=          0.000
S2DR=         89.9999  S2DP=         90.0000   S2IN=         20.000  S2GD=          0.000
S3DR=        179.9000  S3DP=          0.0000  S3IN=          0.000  S3GD=          0.000

  #  X-start   Y-start       X-fin       Y-fin   Kode   rt.lat  reverse   dip angle     top       bot
xxx   xxxxxxxxxx xxxxxxxxx   xxxxxxxxxxxx xxxxxxxxx xxx   xxxxxxx xxxxxxxxxx xxxxxxxxX   xxxxxxxx  xxxxxxxx
1 0.000000 0.000000 0.029642 0.006173 100 0.1000 0.000000 90.000000 1.000000 5.000000
1 0.029642 0.006173 0.059283 0.011549 100 0.1000 0.000000 90.000000 1.000000 5.000000
1 0.059283 0.011549 0.088925 0.016772 100 0.1000 0.000000 90.000000 1.000000 5.000000
1 0.088925 0.016772 0.118566 0.021837 100 0.1000 0.000000 90.000000 1.000000 5.000000
1 0.118566 0.021837 0.148208 0.026715 100 0.1000 0.000000 90.000000 1.000000 5.000000
1 0.148208 0.026715 0.177849 0.031572 100 0.1000 0.000000 90.000000 1.000000 5.000000
1 0.177849 0.031572 0.207491 0.036453 100 0.1000 0.000000 90.000000 1.000000 5.000000
```

```
1 0.207491 0.036453 0.237133 0.041317 100 0.1000 0.000000 90.000000 1.000000 5.000000
1 0.237133 0.041317 0.266774 0.046150 100 0.1000 0.000000 90.000000 1.000000 5.000000
1 0.266774 0.046150 0.296416 0.051115 100 0.1000 0.000000 90.000000 1.000000 5.000000
1 0.296416 0.051115 0.326057 0.056712 100 0.1000 0.000000 90.000000 1.000000 5.000000
1 0.326057 0.056712 0.355699 0.063098 100 0.1000 0.000000 90.000000 1.000000 5.000000
1 0.355699 0.063098 0.385341 0.069569 100 0.1000 0.000000 90.000000 1.000000 5.000000
1 0.385341 0.069569 0.414982 0.076420 100 0.1000 0.000000 90.000000 1.000000 5.000000
1 0.414982 0.076420 0.444623 0.083451 100 0.1000 0.000000 90.000000 1.000000 5.000000
1 0.444623 0.083451 0.474265 0.090181 100 0.1000 0.000000 90.000000 1.000000 5.000000
1 0.474265 0.090181 0.503907 0.097745 100 0.1000 0.000000 90.000000 1.000000 5.000000
1 0.503907 0.097745 0.533549 0.104410 100 0.1000 0.000000 90.000000 1.000000 5.000000
1 0.533549 0.104410 0.563189 0.109391 100 0.1000 0.000000 90.000000 1.000000 5.000000
1 0.563189 0.109391 0.592830 0.113773 100 0.1000 0.000000 90.000000 1.000000 5.000000
1 0.592830 0.113773 0.622474 0.119379 100 0.1000 0.000000 90.000000 1.000000 5.000000
1 0.622474 0.119379 0.652114 0.126609 100 0.1000 0.000000 90.000000 1.000000 5.000000
1 0.652114 0.126609 0.681757 0.134704 100 0.1000 0.000000 90.000000 1.000000 5.000000
1 0.681757 0.134704 0.711396 0.143066 100 0.1000 0.000000 90.000000 1.000000 5.000000
1 0.711396 0.143066 0.741039 0.150969 100 0.1000 0.000000 90.000000 1.000000 5.000000
1 0.741039 0.150969 0.770682 0.158376 100 0.1000 0.000000 90.000000 1.000000 5.000000
1 0.770682 0.158376 0.800323 0.165340 100 0.1000 0.000000 90.000000 1.000000 5.000000
1 0.800323 0.165340 0.829961 0.171767 100 0.1000 0.000000 90.000000 1.000000 5.000000
1 0.829961 0.171767 0.859606 0.177625 100 0.1000 0.000000 90.000000 1.000000 5.000000
1 0.859606 0.177625 0.889248 0.183327 100 0.1000 0.000000 90.000000 1.000000 5.000000
1 0.889248 0.183327 0.918888 0.189232 100 0.1000 0.000000 90.000000 1.000000 5.000000
1 0.918888 0.189232 0.948528 0.195704 100 0.1000 0.000000 90.000000 1.000000 5.000000
1 0.948528 0.195704 0.978173 0.202764 100 0.1000 0.000000 90.000000 1.000000 5.000000
1 0.978173 0.202764 1.007814 0.210501 100 0.1000 0.000000 90.000000 1.000000 5.000000
1 1.007814 0.210501 1.037454 0.218535 100 0.1000 0.000000 90.000000 1.000000 5.000000
1 1.037454 0.218535 1.067098 0.226353 100 0.1000 0.000000 90.000000 1.000000 5.000000
1 1.067098 0.226353 1.096736 0.233717 100 0.1000 0.000000 90.000000 1.000000 5.000000
1 1.096736 0.233717 1.126379 0.241690 100 0.1000 0.000000 90.000000 1.000000 5.000000
1 1.126379 0.241690 1.156022 0.247974 100 0.1000 0.000000 90.000000 1.000000 5.000000
1 1.156022 0.247974 1.185664 0.253067 100 0.1000 0.000000 90.000000 1.000000 5.000000
1 1.185664 0.253067 1.215300 0.258439 100 0.1000 0.000000 90.000000 1.000000 5.000000

    Grid Parameters
  1  ---------------------------  Start-x =          0.000000
  2  ---------------------------  Start-y =         -0.300000
  3  --------------------------   Finish-x =         1.2000000
  4  --------------------------   Finish-y =          0.500000
  5  ------------------------  x-increment =          0.010000
  6  ------------------------  y-increment =          0.010000
     Size Parameters
  1  --------------------------  Plot size =        0.50000
  2  --------------  Shade/Color increment =        0.2000000
  3  ------  Exaggeration for disp.& dist. =    10000.0000000

     Cross section default
  1  ---------------------------  Start-x =       16.8000000
  2  ---------------------------  Start-y =       23.6000000
  3  --------------------------   Finish-x =       16.8000000
  4  --------------------------   Finish-y =       25.2000000
  5  ------------------  Distant-increment =        1.0000000
  6  ---------------------------  Z-depth =      -30.0000000
  7  ------------------------  Z-increment =        1.0000000

B-B'
header line 2
#reg1=  0  #reg2=  0  #fixed=  42  sym=  1
 PR1=       0.250     PR2=       0.250   DEPTH=      10
  E1=     0.441264e+006   E2=     0.80000e+006
XSYM=       .000     YSYM=       .000
FRIC=          0.600
S1DR=         90.0000 S1DP=          0.0000  S1IN=        100.000  S1GD=          0.000
S2DR=         89.9999  S2DP=         90.0000   S2IN=         20.000  S2GD=          0.000
```

```
S3DR=        179.9000  S3DP=          0.0000  S3IN=          0.000  S3GD=          0.000

  #  X-start   Y-start       X-fin       Y-fin   Kode   rt.lat  reverse   dip angle     top       bot
xxx   xxxxxxxxxx xxxxxxxxx   xxxxxxxxxxxx xxxxxxxxx xxx   xxxxxxx xxxxxxxxxx xxxxxxxxX   xxxxxxxx  xxxxxxxx
1 -10.0000 0.000000 0.000000 0.000000 100 0.1000 0.000000 90.000000 0.000000 5.000000
1 0.000000 0.000000 0.029577 0.005936 100 0.1000 0.000000 90.000000 0.000000 5.000000
1 0.029577 0.005936 0.059155 0.011257 100 0.1000 0.000000 90.000000 0.000000 5.000000
1 0.059155 0.011257 0.088732 0.016430 100 0.1000 0.000000 90.000000 0.000000 5.000000
1 0.088732 0.016430 0.118309 0.021392 100 0.1000 0.000000 90.000000 0.000000 5.000000
1 0.118309 0.021392 0.147887 0.026111 100 0.1000 0.000000 90.000000 0.000000 5.000000
1 0.147887 0.026111 0.177464 0.030781 100 0.1000 0.000000 90.000000 0.000000 5.000000
1 0.177464 0.030781 0.207042 0.035405 100 0.1000 0.000000 90.000000 0.000000 5.000000
1 0.207042 0.035405 0.236619 0.039905 100 0.1000 0.000000 90.000000 0.000000 5.000000
1 0.236619 0.039905 0.266196 0.044309 100 0.1000 0.000000 90.000000 0.000000 5.000000
1 0.266196 0.044309 0.295774 0.048922 100 0.1000 0.000000 90.000000 0.000000 5.000000
1 0.295774 0.048922 0.325351 0.054981 100 0.1000 0.000000 90.000000 0.000000 5.000000
1 0.325351 0.054981 0.354928 0.062683 100 0.1000 0.000000 90.000000 0.000000 5.000000
1 0.354928 0.062683 0.384506 0.081098 100 0.1000 0.000000 90.000000 0.000000 5.000000
1 0.384506 0.081098 0.414083 0.093733 100 0.1000 0.000000 90.000000 0.000000 5.000000
1 0.414083 0.093733 0.443660 0.099467 100 0.1000 0.000000 90.000000 0.000000 5.000000
1 0.443660 0.099467 0.473238 0.102916 100 0.1000 0.000000 90.000000 0.000000 5.000000
1 0.473238 0.102916 0.502815 0.107027 100 0.1000 0.000000 90.000000 0.000000 5.000000
1 0.502815 0.107027 0.532392 0.111535 100 0.1000 0.000000 90.000000 0.000000 5.000000
1 0.532392 0.111535 0.561970 0.116613 100 0.1000 0.000000 90.000000 0.000000 5.000000
1 0.561970 0.116613 0.591547 0.122318 100 0.1000 0.000000 90.000000 0.000000 5.000000
1 0.591547 0.122318 0.621125 0.128483 100 0.1000 0.000000 90.000000 0.000000 5.000000
1 0.621125 0.128483 0.650702 0.134975 100 0.1000 0.000000 90.000000 0.000000 5.000000
1 0.650702 0.134975 0.680279 0.141606 100 0.1000 0.000000 90.000000 0.000000 5.000000
1 0.680279 0.141606 0.709857 0.148340 100 0.1000 0.000000 90.000000 0.000000 5.000000
1 0.709857 0.148340 0.739434 0.155135 100 0.1000 0.000000 90.000000 0.000000 5.000000
1 0.739434 0.155135 0.769011 0.162035 100 0.1000 0.000000 90.000000 0.000000 5.000000
1 0.769011 0.162035 0.798589 0.169014 100 0.1000 0.000000 90.000000 0.000000 5.000000
1 0.798589 0.169014 0.828166 0.175916 100 0.1000 0.000000 90.000000 0.000000 5.000000
1 0.828166 0.175916 0.857743 0.182703 100 0.1000 0.000000 90.000000 0.000000 5.000000
1 0.857743 0.182703 0.887321 0.189402 100 0.1000 0.000000 90.000000 0.000000 5.000000
1 0.887321 0.189402 0.916898 0.196245 100 0.1000 0.000000 90.000000 0.000000 5.000000
1 0.916898 0.196245 0.946476 0.203286 100 0.1000 0.000000 90.000000 0.000000 5.000000
1 0.946476 0.203286 0.976053 0.210589 100 0.1000 0.000000 90.000000 0.000000 5.000000
1 0.976053 0.210589 1.005630 0.218175 100 0.1000 0.000000 90.000000 0.000000 5.000000
1 1.005630 0.218175 1.035208 0.225863 100 0.1000 0.000000 90.000000 0.000000 5.000000
1 1.035208 0.225863 1.064785 0.232746 100 0.1000 0.000000 90.000000 0.000000 5.000000
1 1.064785 0.232746 1.094362 0.238077 100 0.1000 0.000000 90.000000 0.000000 5.000000
1 1.094362 0.238077 1.123940 0.242890 100 0.1000 0.000000 90.000000 0.000000 5.000000
1 1.123940 0.242890 1.153517 0.247941 100 0.1000 0.000000 90.000000 0.000000 5.000000
1 1.153517 0.247941 1.183094 0.253432 100 0.1000 0.000000 90.000000 0.000000 5.000000
1 1.183094 0.253432 10.00000 0.253432 100 0.1000 0.000000 90.000000 0.000000 5.000000

    Grid Parameters
  1  ---------------------------  Start-x =          0.000000
  2  ---------------------------  Start-y =         -0.300000
  3  --------------------------   Finish-x =         1.1800000
  4  --------------------------   Finish-y =          0.500000
  5  ------------------------  x-increment =          0.010000
  6  ------------------------  y-increment =          0.010000
     Size Parameters
  1  -------------------------  Plot size =        0.50000
  2  --------------  Shade/Color increment =        0.2000000
  3  ------  Exaggeration for disp.& dist. =    10000.0000000

     Cross section default
  1  ---------------------------  Start-x =       16.8000000
  2  ---------------------------  Start-y =       23.6000000
  3  --------------------------   Finish-x =       16.8000000
  4  --------------------------   Finish-y =       25.2000000
  5  -----------------  Distant-increment =        1.0000000
```

```
  6  ----------------------------  Z-depth =      -30.0000000
  7  ------------------------  Z-increment =        1.0000000

C-C'
header line 2
#reg1=  0  #reg2=  0  #fixed=  71  sym=  1
 PR1=       0.250     PR2=       0.250   DEPTH=      3
  E1=     0.80000e+006   E2=     0.80000e+006
XSYM=       .000     YSYM=       .000
FRIC=          0.400
S1DR=         90.0000 S1DP=          0.0000  S1IN=        100.000  S1GD=          0.000
S2DR=         89.9999  S2DP=         90.0000   S2IN=         20.000  S2GD=          0.000
S3DR=        179.9000  S3DP=          0.0000  S3IN=          0.000  S3GD=          0.000

  #  X-start   Y-start       X-fin       Y-fin   Kode   rt.lat  reverse   dip angle     top       bot
xxx   xxxxxxxxxx xxxxxxxxx   xxxxxxxxxxx xxxxxxxxx xxx   xxxxxxx xxxxxxxxxx xxxxxxxxX   xxxxxxxx  xxxxxxxx
1 0.000000 0.000000 0.029768 0.005698 100 0.1000 0.000000 90.000000 0.000000 5.000000
1 0.029768 0.005698 0.059535 0.010997 100 0.1000 0.000000 90.000000 0.000000 5.000000
1 0.059535 0.010997 0.089303 0.016205 100 0.1000 0.000000 90.000000 0.000000 5.000000
1 0.089303 0.016205 0.119070 0.021255 100 0.1000 0.000000 90.000000 0.000000 5.000000
1 0.119070 0.021255 0.148838 0.026252 100 0.1000 0.000000 90.000000 0.000000 5.000000
1 0.148838 0.026252 0.178605 0.031290 100 0.1000 0.000000 90.000000 0.000000 5.000000
1 0.178605 0.031290 0.208373 0.036376 100 0.1000 0.000000 90.000000 0.000000 5.000000
1 0.208373 0.036376 0.238141 0.041480 100 0.1000 0.000000 90.000000 0.000000 5.000000
1 0.238141 0.041480 0.267908 0.046663 100 0.1000 0.000000 90.000000 0.000000 5.000000
1 0.267908 0.046663 0.297676 0.052026 100 0.1000 0.000000 90.000000 0.000000 5.000000
1 0.297676 0.052026 0.327443 0.058053 100 0.1000 0.000000 90.000000 0.000000 5.000000
1 0.327443 0.058053 0.357211 0.064450 100 0.1000 0.000000 90.000000 0.000000 5.000000
1 0.357211 0.064450 0.386978 0.070777 100 0.1000 0.000000 90.000000 0.000000 5.000000
1 0.386978 0.070777 0.416746 0.077184 100 0.1000 0.000000 90.000000 0.000000 5.000000
1 0.416746 0.077184 0.446513 0.083633 100 0.1000 0.000000 90.000000 0.000000 5.000000
1 0.446513 0.083633 0.476281 0.089982 100 0.1000 0.000000 90.000000 0.000000 5.000000
1 0.476281 0.089982 0.506049 0.095902 100 0.1000 0.000000 90.000000 0.000000 5.000000
1 0.506049 0.095902 0.535816 0.101326 100 0.1000 0.000000 90.000000 0.000000 5.000000
1 0.535816 0.101326 0.565584 0.106620 100 0.1000 0.000000 90.000000 0.000000 5.000000
1 0.565584 0.106620 0.595351 0.112132 100 0.1000 0.000000 90.000000 0.000000 5.000000
1 0.595351 0.112132 0.625119 0.116726 100 0.1000 0.000000 90.000000 0.000000 5.000000
1 0.625119 0.116726 0.654886 0.121121 100 0.1000 0.000000 90.000000 0.000000 5.000000
1 0.654886 0.121121 0.684654 0.126773 100 0.1000 0.000000 90.000000 0.000000 5.000000
1 0.684654 0.126773 0.714422 0.137700 100 0.1000 0.000000 90.000000 0.000000 5.000000
1 0.714422 0.137700 0.744189 0.150680 100 0.1000 0.000000 90.000000 0.000000 5.000000
1 0.744189 0.150680 0.773957 0.160004 100 0.1000 0.000000 90.000000 0.000000 5.000000
1 0.773957 0.160004 0.803724 0.165826 100 0.1000 0.000000 90.000000 0.000000 5.000000
1 0.803724 0.165826 0.833492 0.169836 100 0.1000 0.000000 90.000000 0.000000 5.000000
1 0.833492 0.169836 0.863259 0.172857 100 0.1000 0.000000 90.000000 0.000000 5.000000
1 0.863259 0.172857 0.893027 0.177442 100 0.1000 0.000000 90.000000 0.000000 5.000000
1 0.893027 0.177442 0.922794 0.183781 100 0.1000 0.000000 90.000000 0.000000 5.000000
1 0.922794 0.183781 0.952562 0.191222 100 0.1000 0.000000 90.000000 0.000000 5.000000
1 0.952562 0.191222 0.982330 0.198765 100 0.1000 0.000000 90.000000 0.000000 5.000000
1 0.982330 0.198765 1.012097 0.206762 100 0.1000 0.000000 90.000000 0.000000 5.000000
1 1.012097 0.206762 1.041865 0.214675 100 0.1000 0.000000 90.000000 0.000000 5.000000
1 1.041865 0.214675 1.071632 0.222169 100 0.1000 0.000000 90.000000 0.000000 5.000000
1 1.071632 0.222169 1.101400 0.229931 100 0.1000 0.000000 90.000000 0.000000 5.000000
1 1.101400 0.229931 1.131167 0.238352 100 0.1000 0.000000 90.000000 0.000000 5.000000
1 1.131167 0.238352 1.160935 0.246558 100 0.1000 0.000000 90.000000 0.000000 5.000000
1 1.160935 0.246558 1.190703 0.252197 100 0.1000 0.000000 90.000000 0.000000 5.000000
1 1.190703 0.252197 1.220470 0.257474 100 0.1000 0.000000 90.000000 0.000000 5.000000

    Grid Parameters
  1  ----------------------------  Start-x =          0.000000
  2  ----------------------------  Start-y =         -0.300000
  3  --------------------------   Finish-x =         1.2000000
  4  --------------------------   Finish-y =          0.500000
  5  ------------------------  x-increment =          0.010000
  6  ------------------------  y-increment =          0.010000
```

```
     Size Parameters
  1  -------------------------  Plot size =        0.50000
  2  -------------  Shade/Color increment =        0.2000000
  3  ------  Exaggeration for disp.& dist. =    10000.0000000

     Cross section default
  1  ---------------------------  Start-x =       16.8000000
  2  ---------------------------  Start-y =       23.6000000
  3  -------------------------   Finish-x =       16.8000000
  4  -------------------------   Finish-y =       25.2000000
  5  -----------------  Distant-increment =        1.0000000
  6  ---------------------------  Z-depth =      -30.0000000
  7  ----------------------  Z-increment =        1.0000000

D-D'
header line 2
#reg1=  0  #reg2=  0  #fixed=  71  sym=  1
 PR1=       0.250     PR2=       0.250   DEPTH=      10
  E1=     0.80000e+006   E2=     0.80000e+006
XSYM=       .000     YSYM=       .000
FRIC=          0.600
S1DR=         90.0000 S1DP=          0.0000  S1IN=        100.000  S1GD=          0.000
S2DR=         89.9999  S2DP=         90.0000   S2IN=         20.000  S2GD=          0.000
S3DR=        179.9000  S3DP=          0.0000  S3IN=          0.000  S3GD=          0.000

  #  X-start   Y-start       X-fin       Y-fin   Kode   rt.lat  reverse   dip angle     top       bot
xxx   xxxxxxxxxx xxxxxxxxx   xxxxxxxxxxx xxxxxxxxx xxx   xxxxxxx xxxxxxxxxx xxxxxxxxX   xxxxxxxx  xxxxxxxx
1 0.000000 0.000000 0.029768 0.005770 100 0.1000 0.000000 90.000000 0.000000 5.000000
1 0.029768 0.005770 0.059535 0.011084 100 0.1000 0.000000 90.000000 0.000000 5.000000
1 0.059535 0.011084 0.089303 0.016308 100 0.1000 0.000000 90.000000 0.000000 5.000000
1 0.089303 0.016308 0.119070 0.021420 100 0.1000 0.000000 90.000000 0.000000 5.000000
1 0.119070 0.021420 0.148838 0.026503 100 0.1000 0.000000 90.000000 0.000000 5.000000
1 0.148838 0.026503 0.178605 0.031657 100 0.1000 0.000000 90.000000 0.000000 5.000000
1 0.178605 0.031657 0.208373 0.036897 100 0.1000 0.000000 90.000000 0.000000 5.000000
1 0.208373 0.036897 0.238140 0.042215 100 0.1000 0.000000 90.000000 0.000000 5.000000
1 0.238140 0.042215 0.267908 0.047646 100 0.1000 0.000000 90.000000 0.000000 5.000000
1 0.267908 0.047646 0.297676 0.053317 100 0.1000 0.000000 90.000000 0.000000 5.000000
1 0.297676 0.053317 0.327443 0.059375 100 0.1000 0.000000 90.000000 0.000000 5.000000
1 0.327443 0.059375 0.357211 0.065702 100 0.1000 0.000000 90.000000 0.000000 5.000000
1 0.357211 0.065702 0.386978 0.071859 100 0.1000 0.000000 90.000000 0.000000 5.000000
1 0.386978 0.071859 0.416746 0.077742 100 0.1000 0.000000 90.000000 0.000000 5.000000
1 0.416746 0.077742 0.446513 0.083660 100 0.1000 0.000000 90.000000 0.000000 5.000000
1 0.446513 0.083660 0.476281 0.089373 100 0.1000 0.000000 90.000000 0.000000 5.000000
1 0.476281 0.089373 0.506048 0.094995 100 0.1000 0.000000 90.000000 0.000000 5.000000
1 0.506048 0.094995 0.535816 0.100533 100 0.1000 0.000000 90.000000 0.000000 5.000000
1 0.535816 0.100533 0.565584 0.106108 100 0.1000 0.000000 90.000000 0.000000 5.000000
1 0.565584 0.106108 0.595351 0.111778 100 0.1000 0.000000 90.000000 0.000000 5.000000
1 0.595351 0.111778 0.625119 0.117521 100 0.1000 0.000000 90.000000 0.000000 5.000000
1 0.625119 0.117521 0.654886 0.123392 100 0.1000 0.000000 90.000000 0.000000 5.000000
1 0.654886 0.123392 0.684654 0.129473 100 0.1000 0.000000 90.000000 0.000000 5.000000
1 0.684654 0.129473 0.714421 0.136405 100 0.1000 0.000000 90.000000 0.000000 5.000000
1 0.714421 0.136405 0.744189 0.145095 100 0.1000 0.000000 90.000000 0.000000 5.000000
1 0.744189 0.145095 0.773956 0.152464 100 0.1000 0.000000 90.000000 0.000000 5.000000
1 0.773956 0.152464 0.803724 0.159569 100 0.1000 0.000000 90.000000 0.000000 5.000000
1 0.803724 0.159569 0.833492 0.166415 100 0.1000 0.000000 90.000000 0.000000 5.000000
1 0.833492 0.166415 0.863259 0.172613 100 0.1000 0.000000 90.000000 0.000000 5.000000
1 0.863259 0.172613 0.893027 0.178514 100 0.1000 0.000000 90.000000 0.000000 5.000000
1 0.893027 0.178514 0.922794 0.184907 100 0.1000 0.000000 90.000000 0.000000 5.000000
1 0.922794 0.184907 0.952562 0.192103 100 0.1000 0.000000 90.000000 0.000000 5.000000
1 0.952562 0.192103 0.982329 0.199510 100 0.1000 0.000000 90.000000 0.000000 5.000000
1 0.982329 0.199510 1.012097 0.207145 100 0.1000 0.000000 90.000000 0.000000 5.000000
1 1.012097 0.207145 1.041864 0.214974 100 0.1000 0.000000 90.000000 0.000000 5.000000
1 1.041864 0.214974 1.071632 0.223047 100 0.1000 0.000000 90.000000 0.000000 5.000000
1 1.071632 0.223047 1.101400 0.230010 100 0.1000 0.000000 90.000000 0.000000 5.000000
1 1.101400 0.230010 1.131167 0.234845 100 0.1000 0.000000 90.000000 0.000000 5.000000
```

```
1 1.131167 0.234845 1.160935 0.240922 100 0.1000 0.000000 90.000000 0.000000 5.000000
1 1.160935 0.240922 1.190702 0.249086 100 0.1000 0.000000 90.000000 0.000000 5.000000
1 1.190702 0.249086 1.220470 0.256258 100 0.1000 0.000000 90.000000 0.000000 5.000000
1 1.220470 0.256258 1.250237 0.261603 100 0.1000 0.000000 90.000000 0.000000 5.000000

    Grid Parameters
  1  ---------------------------  Start-x =          0.000000
  2  ---------------------------  Start-y =         -0.300000
  3  --------------------------   Finish-x =         1.2000000
  4  --------------------------   Finish-y =          0.500000
  5  ------------------------  x-increment =          0.010000
  6  ------------------------  y-increment =          0.010000
     Size Parameters
  1  -------------------------  Plot size =        0.50000
  2  -------------  Shade/Color increment =        0.2000000
  3  ------  Exaggeration for disp.& dist. =    10000.0000000

     Cross section default
  1  ---------------------------  Start-x =       16.8000000
  2  ---------------------------  Start-y =       23.6000000
  3  --------------------------   Finish-x =       16.8000000
  4  --------------------------   Finish-y =       25.2000000
  5  -----------------  Distant-increment =        1.0000000
  6  ---------------------------  Z-depth =      -30.0000000
  7  ------------------------  Z-increment =        1.0000000

Tsmas Ost A-A'
header line 2
#reg1=  0  #reg2=  0  #fixed=  226  sym=  1
 PR1=       0.250     PR2=       0.250   DEPTH=      3
  E1=     0.80000e+006   E2=     0.80000e+006
XSYM=       .000     YSYM=       .000
FRIC=          0.400
S1DR=         90.0000 S1DP=          0.0000  S1IN=        100.000  S1GD=          0.000
S2DR=         89.9999  S2DP=         90.0000   S2IN=         20.000  S2GD=          0.000
S3DR=        179.9000  S3DP=          0.0000  S3IN=          0.000  S3GD=          0.000

  # X-start   Y-start       X-fin       Y-fin   Kode   rt.lat  reverse   dip angle     top       bot
xxx xxxxxxxxxx xxxxxxxxx   xxxxxxxxxxxx xxxxxxxxx xxx   xxxxxxx xxxxxxxxxx xxxxxxxxX   xxxxxxxx  xxxxxxxx
1 2.945755 -0.131190 2.958847 -0.131764 100 0.1000 0.000000 90.000000 0.000000 5.000000
1 2.932663 -0.130624 2.945755 -0.131190 100 0.1000 0.000000 90.000000 0.000000 5.000000
1 2.919571 -0.130062 2.932663 -0.130624 100 0.1000 0.000000 90.000000 0.000000 5.000000
1 2.906478 -0.129504 2.919571 -0.130062 100 0.1000 0.000000 90.000000 0.000000 5.000000
1 2.893386 -0.128947 2.906478 -0.129504 100 0.1000 0.000000 90.000000 0.000000 5.000000
1 2.880294 -0.128393 2.893386 -0.128947 100 0.1000 0.000000 90.000000 0.000000 5.000000
1 2.867202 -0.127840 2.880294 -0.128393 100 0.1000 0.000000 90.000000 0.000000 5.000000
1 2.854109 -0.127287 2.867202 -0.127840 100 0.1000 0.000000 90.000000 0.000000 5.000000
1 2.841017 -0.126734 2.854109 -0.127287 100 0.1000 0.000000 90.000000 0.000000 5.000000
1 2.827925 -0.126180 2.841017 -0.126734 100 0.1000 0.000000 90.000000 0.000000 5.000000
1 2.814833 -0.125627 2.827925 -0.126180 100 0.1000 0.000000 90.000000 0.000000 5.000000
1 2.801740 -0.125072 2.814833 -0.125627 100 0.1000 0.000000 90.000000 0.000000 5.000000
1 2.788648 -0.124518 2.801740 -0.125072 100 0.1000 0.000000 90.000000 0.000000 5.000000
1 2.775556 -0.123963 2.788648 -0.124518 100 0.1000 0.000000 90.000000 0.000000 5.000000
1 2.762464 -0.123413 2.775556 -0.123963 100 0.1000 0.000000 90.000000 0.000000 5.000000
1 2.749371 -0.122865 2.762464 -0.123413 100 0.1000 0.000000 90.000000 0.000000 5.000000
1 2.736279 -0.122319 2.749371 -0.122865 100 0.1000 0.000000 90.000000 0.000000 5.000000
1 2.723187 -0.121779 2.736279 -0.122319 100 0.1000 0.000000 90.000000 0.000000 5.000000
1 2.710095 -0.121252 2.723187 -0.121779 100 0.1000 0.000000 90.000000 0.000000 5.000000
1 2.697002 -0.120741 2.710095 -0.121252 100 0.1000 0.000000 90.000000 0.000000 5.000000
1 2.683910 -0.120241 2.697002 -0.120741 100 0.1000 0.000000 90.000000 0.000000 5.000000
1 2.670818 -0.119752 2.683910 -0.120241 100 0.1000 0.000000 90.000000 0.000000 5.000000
1 2.657726 -0.119271 2.670818 -0.119752 100 0.1000 0.000000 90.000000 0.000000 5.000000
1 2.644633 -0.118795 2.657726 -0.119271 100 0.1000 0.000000 90.000000 0.000000 5.000000
1 2.631541 -0.118325 2.644633 -0.118795 100 0.1000 0.000000 90.000000 0.000000 5.000000
1 2.618449 -0.117860 2.631541 -0.118325 100 0.1000 0.000000 90.000000 0.000000 5.000000
```

```
1 2.605357 -0.117400 2.618449 -0.117860 100 0.1000 0.000000 90.000000 0.000000 5.000000
1 2.592264 -0.116944 2.605357 -0.117400 100 0.1000 0.000000 90.000000 0.000000 5.000000
1 2.579172 -0.116488 2.592264 -0.116944 100 0.1000 0.000000 90.000000 0.000000 5.000000
1 2.566080 -0.116030 2.579172 -0.116488 100 0.1000 0.000000 90.000000 0.000000 5.000000
1 2.552988 -0.115570 2.566080 -0.116030 100 0.1000 0.000000 90.000000 0.000000 5.000000
1 2.539895 -0.115107 2.552988 -0.115570 100 0.1000 0.000000 90.000000 0.000000 5.000000
1 2.526803 -0.114640 2.539895 -0.115107 100 0.1000 0.000000 90.000000 0.000000 5.000000
1 2.513711 -0.114168 2.526803 -0.114640 100 0.1000 0.000000 90.000000 0.000000 5.000000
1 2.500619 -0.113682 2.513711 -0.114168 100 0.1000 0.000000 90.000000 0.000000 5.000000
1 2.487526 -0.113184 2.500619 -0.113682 100 0.1000 0.000000 90.000000 0.000000 5.000000
1 2.474434 -0.112676 2.487526 -0.113184 100 0.1000 0.000000 90.000000 0.000000 5.000000
1 2.461342 -0.112160 2.474434 -0.112676 100 0.1000 0.000000 90.000000 0.000000 5.000000
1 2.448250 -0.111636 2.461342 -0.112160 100 0.1000 0.000000 90.000000 0.000000 5.000000
1 2.435158 -0.111105 2.448250 -0.111636 100 0.1000 0.000000 90.000000 0.000000 5.000000
1 2.422065 -0.110569 2.435158 -0.111105 100 0.1000 0.000000 90.000000 0.000000 5.000000
1 2.408973 -0.110028 2.422065 -0.110569 100 0.1000 0.000000 90.000000 0.000000 5.000000
1 2.395881 -0.109483 2.408973 -0.110028 100 0.1000 0.000000 90.000000 0.000000 5.000000
1 2.382789 -0.108934 2.395881 -0.109483 100 0.1000 0.000000 90.000000 0.000000 5.000000
1 2.369696 -0.108381 2.382789 -0.108934 100 0.1000 0.000000 90.000000 0.000000 5.000000
1 2.356604 -0.107824 2.369696 -0.108381 100 0.1000 0.000000 90.000000 0.000000 5.000000
1 2.343512 -0.107265 2.356604 -0.107824 100 0.1000 0.000000 90.000000 0.000000 5.000000
1 2.330420 -0.106702 2.343512 -0.107265 100 0.1000 0.000000 90.000000 0.000000 5.000000
1 2.317327 -0.106133 2.330420 -0.106702 100 0.1000 0.000000 90.000000 0.000000 5.000000
1 2.304235 -0.105558 2.317327 -0.106133 100 0.1000 0.000000 90.000000 0.000000 5.000000
1 2.291143 -0.104977 2.304235 -0.105558 100 0.1000 0.000000 90.000000 0.000000 5.000000
1 2.278051 -0.104393 2.291143 -0.104977 100 0.1000 0.000000 90.000000 0.000000 5.000000
1 2.264958 -0.103807 2.278051 -0.104393 100 0.1000 0.000000 90.000000 0.000000 5.000000
1 2.251866 -0.103218 2.264958 -0.103807 100 0.1000 0.000000 90.000000 0.000000 5.000000
1 2.238774 -0.102629 2.251866 -0.103218 100 0.1000 0.000000 90.000000 0.000000 5.000000
1 2.225682 -0.102038 2.238774 -0.102629 100 0.1000 0.000000 90.000000 0.000000 5.000000
1 2.212589 -0.101448 2.225682 -0.102038 100 0.1000 0.000000 90.000000 0.000000 5.000000
1 2.199497 -0.100857 2.212589 -0.101448 100 0.1000 0.000000 90.000000 0.000000 5.000000
1 2.186405 -0.100266 2.199497 -0.100857 100 0.1000 0.000000 90.000000 0.000000 5.000000
1 2.173313 -0.099675 2.186405 -0.100266 100 0.1000 0.000000 90.000000 0.000000 5.000000
1 2.160220 -0.099082 2.173313 -0.099675 100 0.1000 0.000000 90.000000 0.000000 5.000000
1 2.147128 -0.098490 2.160220 -0.099082 100 0.1000 0.000000 90.000000 0.000000 5.000000
1 2.134036 -0.097898 2.147128 -0.098490 100 0.1000 0.000000 90.000000 0.000000 5.000000
1 2.120944 -0.097305 2.134036 -0.097898 100 0.1000 0.000000 90.000000 0.000000 5.000000
1 2.107851 -0.096713 2.120944 -0.097305 100 0.1000 0.000000 90.000000 0.000000 5.000000
1 2.094759 -0.096121 2.107851 -0.096713 100 0.1000 0.000000 90.000000 0.000000 5.000000
1 2.081667 -0.095529 2.094759 -0.096121 100 0.1000 0.000000 90.000000 0.000000 5.000000
1 2.068575 -0.094937 2.081667 -0.095529 100 0.1000 0.000000 90.000000 0.000000 5.000000
1 2.055482 -0.094345 2.068575 -0.094937 100 0.1000 0.000000 90.000000 0.000000 5.000000
1 2.042390 -0.093756 2.055482 -0.094345 100 0.1000 0.000000 90.000000 0.000000 5.000000
1 2.029298 -0.093167 2.042390 -0.093756 100 0.1000 0.000000 90.000000 0.000000 5.000000
1 2.016206 -0.092579 2.029298 -0.093167 100 0.1000 0.000000 90.000000 0.000000 5.000000
1 2.003113 -0.091993 2.016206 -0.092579 100 0.1000 0.000000 90.000000 0.000000 5.000000
1 1.990021 -0.091409 2.003113 -0.091993 100 0.1000 0.000000 90.000000 0.000000 5.000000
1 1.976929 -0.090827 1.990021 -0.091409 100 0.1000 0.000000 90.000000 0.000000 5.000000
1 1.963837 -0.090246 1.976929 -0.090827 100 0.1000 0.000000 90.000000 0.000000 5.000000
1 1.950744 -0.089667 1.963837 -0.090246 100 0.1000 0.000000 90.000000 0.000000 5.000000
1 1.937652 -0.089089 1.950744 -0.089667 100 0.1000 0.000000 90.000000 0.000000 5.000000
1 1.924560 -0.088512 1.937652 -0.089089 100 0.1000 0.000000 90.000000 0.000000 5.000000
1 1.911468 -0.087937 1.924560 -0.088512 100 0.1000 0.000000 90.000000 0.000000 5.000000
1 1.898375 -0.087361 1.911468 -0.087937 100 0.1000 0.000000 90.000000 0.000000 5.000000
1 1.885283 -0.086786 1.898375 -0.087361 100 0.1000 0.000000 90.000000 0.000000 5.000000
1 1.872191 -0.086212 1.885283 -0.086786 100 0.1000 0.000000 90.000000 0.000000 5.000000
1 1.859099 -0.085637 1.872191 -0.086212 100 0.1000 0.000000 90.000000 0.000000 5.000000
1 1.846007 -0.085062 1.859099 -0.085637 100 0.1000 0.000000 90.000000 0.000000 5.000000
1 1.832914 -0.084488 1.846007 -0.085062 100 0.1000 0.000000 90.000000 0.000000 5.000000
1 1.819822 -0.083913 1.832914 -0.084488 100 0.1000 0.000000 90.000000 0.000000 5.000000
1 1.806730 -0.083339 1.819822 -0.083913 100 0.1000 0.000000 90.000000 0.000000 5.000000
1 1.793638 -0.082764 1.806730 -0.083339 100 0.1000 0.000000 90.000000 0.000000 5.000000
1 1.780545 -0.082189 1.793638 -0.082764 100 0.1000 0.000000 90.000000 0.000000 5.000000
1 1.767453 -0.081614 1.780545 -0.082189 100 0.1000 0.000000 90.000000 0.000000 5.000000
```

```
1 1.754361 -0.081039 1.767453 -0.081614 100 0.1000 0.000000 90.000000 0.000000 5.000000
1 1.741269 -0.080465 1.754361 -0.081039 100 0.1000 0.000000 90.000000 0.000000 5.000000
1 1.728176 -0.079890 1.741269 -0.080465 100 0.1000 0.000000 90.000000 0.000000 5.000000
1 1.715084 -0.079315 1.728176 -0.079890 100 0.1000 0.000000 90.000000 0.000000 5.000000
1 1.701992 -0.078740 1.715084 -0.079315 100 0.1000 0.000000 90.000000 0.000000 5.000000
1 1.688900 -0.078165 1.701992 -0.078740 100 0.1000 0.000000 90.000000 0.000000 5.000000
1 1.675807 -0.077590 1.688900 -0.078165 100 0.1000 0.000000 90.000000 0.000000 5.000000
1 1.662715 -0.077016 1.675807 -0.077590 100 0.1000 0.000000 90.000000 0.000000 5.000000
1 1.649623 -0.076441 1.662715 -0.077016 100 0.1000 0.000000 90.000000 0.000000 5.000000
1 1.636531 -0.075866 1.649623 -0.076441 100 0.1000 0.000000 90.000000 0.000000 5.000000
1 1.623438 -0.075292 1.636531 -0.075866 100 0.1000 0.000000 90.000000 0.000000 5.000000
1 1.610346 -0.074717 1.623438 -0.075292 100 0.1000 0.000000 90.000000 0.000000 5.000000
1 1.597254 -0.074143 1.610346 -0.074717 100 0.1000 0.000000 90.000000 0.000000 5.000000
1 1.584162 -0.073568 1.597254 -0.074143 100 0.1000 0.000000 90.000000 0.000000 5.000000
1 1.571069 -0.072994 1.584162 -0.073568 100 0.1000 0.000000 90.000000 0.000000 5.000000
1 1.557977 -0.072420 1.571069 -0.072994 100 0.1000 0.000000 90.000000 0.000000 5.000000
1 1.544885 -0.071846 1.557977 -0.072420 100 0.1000 0.000000 90.000000 0.000000 5.000000
1 1.531793 -0.071271 1.544885 -0.071846 100 0.1000 0.000000 90.000000 0.000000 5.000000
1 1.518700 -0.070697 1.531793 -0.071271 100 0.1000 0.000000 90.000000 0.000000 5.000000
1 1.505608 -0.070123 1.518700 -0.070697 100 0.1000 0.000000 90.000000 0.000000 5.000000
1 1.492516 -0.069549 1.505608 -0.070123 100 0.1000 0.000000 90.000000 0.000000 5.000000
1 1.479424 -0.068975 1.492516 -0.069549 100 0.1000 0.000000 90.000000 0.000000 5.000000
1 1.466331 -0.068401 1.479424 -0.068975 100 0.1000 0.000000 90.000000 0.000000 5.000000
1 1.453239 -0.067827 1.466331 -0.068401 100 0.1000 0.000000 90.000000 0.000000 5.000000
1 1.440147 -0.067253 1.453239 -0.067827 100 0.1000 0.000000 90.000000 0.000000 5.000000
1 1.427055 -0.066679 1.440147 -0.067253 100 0.1000 0.000000 90.000000 0.000000 5.000000
1 1.413962 -0.066104 1.427055 -0.066679 100 0.1000 0.000000 90.000000 0.000000 5.000000
1 1.400870 -0.065530 1.413962 -0.066104 100 0.1000 0.000000 90.000000 0.000000 5.000000
1 1.387778 -0.064956 1.400870 -0.065530 100 0.1000 0.000000 90.000000 0.000000 5.000000
1 1.374686 -0.064381 1.387778 -0.064956 100 0.1000 0.000000 90.000000 0.000000 5.000000
1 1.361593 -0.063807 1.374686 -0.064381 100 0.1000 0.000000 90.000000 0.000000 5.000000
1 1.348501 -0.063232 1.361593 -0.063807 100 0.1000 0.000000 90.000000 0.000000 5.000000
1 1.335409 -0.062658 1.348501 -0.063232 100 0.1000 0.000000 90.000000 0.000000 5.000000
1 1.322317 -0.062083 1.335409 -0.062658 100 0.1000 0.000000 90.000000 0.000000 5.000000
1 1.309224 -0.061508 1.322317 -0.062083 100 0.1000 0.000000 90.000000 0.000000 5.000000
1 1.296132 -0.060933 1.309224 -0.061508 100 0.1000 0.000000 90.000000 0.000000 5.000000
1 1.283040 -0.060358 1.296132 -0.060933 100 0.1000 0.000000 90.000000 0.000000 5.000000
1 1.269948 -0.059782 1.283040 -0.060358 100 0.1000 0.000000 90.000000 0.000000 5.000000
1 1.256855 -0.059207 1.269948 -0.059782 100 0.1000 0.000000 90.000000 0.000000 5.000000
1 1.243763 -0.058631 1.256855 -0.059207 100 0.1000 0.000000 90.000000 0.000000 5.000000
1 1.230671 -0.058055 1.243763 -0.058631 100 0.1000 0.000000 90.000000 0.000000 5.000000
1 1.217579 -0.057479 1.230671 -0.058055 100 0.1000 0.000000 90.000000 0.000000 5.000000
1 1.204487 -0.056903 1.217579 -0.057479 100 0.1000 0.000000 90.000000 0.000000 5.000000
1 1.191394 -0.056326 1.204487 -0.056903 100 0.1000 0.000000 90.000000 0.000000 5.000000
1 1.178302 -0.055749 1.191394 -0.056326 100 0.1000 0.000000 90.000000 0.000000 5.000000
1 1.165210 -0.055172 1.178302 -0.055749 100 0.1000 0.000000 90.000000 0.000000 5.000000
1 1.152118 -0.054594 1.165210 -0.055172 100 0.1000 0.000000 90.000000 0.000000 5.000000
1 1.139025 -0.054016 1.152118 -0.054594 100 0.1000 0.000000 90.000000 0.000000 5.000000
1 1.125933 -0.053438 1.139025 -0.054016 100 0.1000 0.000000 90.000000 0.000000 5.000000
1 1.112841 -0.052860 1.125933 -0.053438 100 0.1000 0.000000 90.000000 0.000000 5.000000
1 1.099749 -0.052281 1.112841 -0.052860 100 0.1000 0.000000 90.000000 0.000000 5.000000
1 1.086656 -0.051702 1.099749 -0.052281 100 0.1000 0.000000 90.000000 0.000000 5.000000
1 1.073564 -0.051123 1.086656 -0.051702 100 0.1000 0.000000 90.000000 0.000000 5.000000
1 1.060472 -0.050544 1.073564 -0.051123 100 0.1000 0.000000 90.000000 0.000000 5.000000
1 1.047380 -0.049964 1.060472 -0.050544 100 0.1000 0.000000 90.000000 0.000000 5.000000
1 1.034287 -0.049383 1.047380 -0.049964 100 0.1000 0.000000 90.000000 0.000000 5.000000
1 1.021195 -0.048803 1.034287 -0.049383 100 0.1000 0.000000 90.000000 0.000000 5.000000
1 1.008103 -0.048221 1.021195 -0.048803 100 0.1000 0.000000 90.000000 0.000000 5.000000
1 0.995011 -0.047640 1.008103 -0.048221 100 0.1000 0.000000 90.000000 0.000000 5.000000
1 0.981918 -0.047058 0.995011 -0.047640 100 0.1000 0.000000 90.000000 0.000000 5.000000
1 0.968826 -0.046475 0.981918 -0.047058 100 0.1000 0.000000 90.000000 0.000000 5.000000
1 0.955734 -0.045892 0.968826 -0.046475 100 0.1000 0.000000 90.000000 0.000000 5.000000
1 0.942642 -0.045309 0.955734 -0.045892 100 0.1000 0.000000 90.000000 0.000000 5.000000
1 0.929549 -0.044725 0.942642 -0.045309 100 0.1000 0.000000 90.000000 0.000000 5.000000
1 0.916457 -0.044140 0.929549 -0.044725 100 0.1000 0.000000 90.000000 0.000000 5.000000
```

```
1 0.903365 -0.043555 0.916457 -0.044140 100 0.1000 0.000000 90.000000 0.000000 5.000000
1 0.890273 -0.042970 0.903365 -0.043555 100 0.1000 0.000000 90.000000 0.000000 5.000000
1 0.877180 -0.042383 0.890273 -0.042970 100 0.1000 0.000000 90.000000 0.000000 5.000000
1 0.864088 -0.041795 0.877180 -0.042383 100 0.1000 0.000000 90.000000 0.000000 5.000000
1 0.850996 -0.041207 0.864088 -0.041795 100 0.1000 0.000000 90.000000 0.000000 5.000000
1 0.837904 -0.040618 0.850996 -0.041207 100 0.1000 0.000000 90.000000 0.000000 5.000000
1 0.824811 -0.040027 0.837904 -0.040618 100 0.1000 0.000000 90.000000 0.000000 5.000000
1 0.811719 -0.039437 0.824811 -0.040027 100 0.1000 0.000000 90.000000 0.000000 5.000000
1 0.798627 -0.038846 0.811719 -0.039437 100 0.1000 0.000000 90.000000 0.000000 5.000000
1 0.785535 -0.038254 0.798627 -0.038846 100 0.1000 0.000000 90.000000 0.000000 5.000000
1 0.772442 -0.037662 0.785535 -0.038254 100 0.1000 0.000000 90.000000 0.000000 5.000000
1 0.759350 -0.037069 0.772442 -0.037662 100 0.1000 0.000000 90.000000 0.000000 5.000000
1 0.746258 -0.036475 0.759350 -0.037069 100 0.1000 0.000000 90.000000 0.000000 5.000000
1 0.733166 -0.035881 0.746258 -0.036475 100 0.1000 0.000000 90.000000 0.000000 5.000000
1 0.720073 -0.035287 0.733166 -0.035881 100 0.1000 0.000000 90.000000 0.000000 5.000000
1 0.706981 -0.034691 0.720073 -0.035287 100 0.1000 0.000000 90.000000 0.000000 5.000000
1 0.693889 -0.034095 0.706981 -0.034691 100 0.1000 0.000000 90.000000 0.000000 5.000000
1 0.680797 -0.033497 0.693889 -0.034095 100 0.1000 0.000000 90.000000 0.000000 5.000000
1 0.667704 -0.032899 0.680797 -0.033497 100 0.1000 0.000000 90.000000 0.000000 5.000000
1 0.654612 -0.032300 0.667704 -0.032899 100 0.1000 0.000000 90.000000 0.000000 5.000000
1 0.641520 -0.031700 0.654612 -0.032300 100 0.1000 0.000000 90.000000 0.000000 5.000000
1 0.628428 -0.031099 0.641520 -0.031700 100 0.1000 0.000000 90.000000 0.000000 5.000000
1 0.615336 -0.030498 0.628428 -0.031099 100 0.1000 0.000000 90.000000 0.000000 5.000000
1 0.602243 -0.029895 0.615336 -0.030498 100 0.1000 0.000000 90.000000 0.000000 5.000000
1 0.589151 -0.029292 0.602243 -0.029895 100 0.1000 0.000000 90.000000 0.000000 5.000000
1 0.576059 -0.028688 0.589151 -0.029292 100 0.1000 0.000000 90.000000 0.000000 5.000000
1 0.562967 -0.028082 0.576059 -0.028688 100 0.1000 0.000000 90.000000 0.000000 5.000000
1 0.549874 -0.027476 0.562967 -0.028082 100 0.1000 0.000000 90.000000 0.000000 5.000000
1 0.536782 -0.026868 0.549874 -0.027476 100 0.1000 0.000000 90.000000 0.000000 5.000000
1 0.523690 -0.026259 0.536782 -0.026868 100 0.1000 0.000000 90.000000 0.000000 5.000000
1 0.510598 -0.025648 0.523690 -0.026259 100 0.1000 0.000000 90.000000 0.000000 5.000000
1 0.497505 -0.025037 0.510598 -0.025648 100 0.1000 0.000000 90.000000 0.000000 5.000000
1 0.484413 -0.024424 0.497505 -0.025037 100 0.1000 0.000000 90.000000 0.000000 5.000000
1 0.471321 -0.023809 0.484413 -0.024424 100 0.1000 0.000000 90.000000 0.000000 5.000000
1 0.458229 -0.023193 0.471321 -0.023809 100 0.1000 0.000000 90.000000 0.000000 5.000000
1 0.445136 -0.022576 0.458229 -0.023193 100 0.1000 0.000000 90.000000 0.000000 5.000000
1 0.432044 -0.021957 0.445136 -0.022576 100 0.1000 0.000000 90.000000 0.000000 5.000000
1 0.418952 -0.021337 0.432044 -0.021957 100 0.1000 0.000000 90.000000 0.000000 5.000000
1 0.405860 -0.020715 0.418952 -0.021337 100 0.1000 0.000000 90.000000 0.000000 5.000000
1 0.392767 -0.020091 0.405860 -0.020715 100 0.1000 0.000000 90.000000 0.000000 5.000000
1 0.379675 -0.019466 0.392767 -0.020091 100 0.1000 0.000000 90.000000 0.000000 5.000000
1 0.366583 -0.018840 0.379675 -0.019466 100 0.1000 0.000000 90.000000 0.000000 5.000000
1 0.353491 -0.018211 0.366583 -0.018840 100 0.1000 0.000000 90.000000 0.000000 5.000000
1 0.340398 -0.017580 0.353491 -0.018211 100 0.1000 0.000000 90.000000 0.000000 5.000000
1 0.327306 -0.016947 0.340398 -0.017580 100 0.1000 0.000000 90.000000 0.000000 5.000000
1 0.314214 -0.016313 0.327306 -0.016947 100 0.1000 0.000000 90.000000 0.000000 5.000000
1 0.301122 -0.015676 0.314214 -0.016313 100 0.1000 0.000000 90.000000 0.000000 5.000000
1 0.288029 -0.015038 0.301122 -0.015676 100 0.1000 0.000000 90.000000 0.000000 5.000000
1 0.274937 -0.014397 0.288029 -0.015038 100 0.1000 0.000000 90.000000 0.000000 5.000000
1 0.261845 -0.013753 0.274937 -0.014397 100 0.1000 0.000000 90.000000 0.000000 5.000000
1 0.248753 -0.013107 0.261845 -0.013753 100 0.1000 0.000000 90.000000 0.000000 5.000000
1 0.235660 -0.012458 0.248753 -0.013107 100 0.1000 0.000000 90.000000 0.000000 5.000000
1 0.222568 -0.011807 0.235660 -0.012458 100 0.1000 0.000000 90.000000 0.000000 5.000000
1 0.209476 -0.011152 0.222568 -0.011807 100 0.1000 0.000000 90.000000 0.000000 5.000000
1 0.196384 -0.010495 0.209476 -0.011152 100 0.1000 0.000000 90.000000 0.000000 5.000000
1 0.183291 -0.009834 0.196384 -0.010495 100 0.1000 0.000000 90.000000 0.000000 5.000000
1 0.170199 -0.009170 0.183291 -0.009834 100 0.1000 0.000000 90.000000 0.000000 5.000000
1 0.157107 -0.008503 0.170199 -0.009170 100 0.1000 0.000000 90.000000 0.000000 5.000000
1 0.144015 -0.007832 0.157107 -0.008503 100 0.1000 0.000000 90.000000 0.000000 5.000000
1 0.130922 -0.007157 0.144015 -0.007832 100 0.1000 0.000000 90.000000 0.000000 5.000000
1 0.117830 -0.006479 0.130922 -0.007157 100 0.1000 0.000000 90.000000 0.000000 5.000000
1 0.104738 -0.005797 0.117830 -0.006479 100 0.1000 0.000000 90.000000 0.000000 5.000000
1 0.091646 -0.005111 0.104738 -0.005797 100 0.1000 0.000000 90.000000 0.000000 5.000000
1 0.078553 -0.004418 0.091646 -0.005111 100 0.1000 0.000000 90.000000 0.000000 5.000000
1 0.065461 -0.003716 0.078553 -0.004418 100 0.1000 0.000000 90.000000 0.000000 5.000000
```

```
1 0.052369 -0.003004 0.065461 -0.003716 100 0.1000 0.000000 90.000000 0.000000 5.000000
1 0.039277 -0.002278 0.052369 -0.003004 100 0.1000 0.000000 90.000000 0.000000 5.000000
1 0.026184 -0.001537 0.039277 -0.002278 100 0.1000 0.000000 90.000000 0.000000 5.000000
1 0.013092 -0.000777 0.026184 -0.001537 100 0.1000 0.000000 90.000000 0.000000 5.000000
1 0.000000 0.000000 0.013092 -0.000777 100 0.1000 0.000000 90.000000 0.000000 5.000000

    Grid Parameters
  1  ---------------------------  Start-x =          0.000000
  2  ---------------------------  Start-y =         -0.400000
  3  --------------------------   Finish-x =         2.9500000
  4  --------------------------   Finish-y =          0.300000
  5  ------------------------  x-increment =          0.010000
  6  ------------------------  y-increment =          0.010000
     Size Parameters
  1  -------------------------  Plot size =        0.50000
  2  --------------  Shade/Color increment =        0.2000000
  3  ------  Exaggeration for disp.& dist. =    10000.0000000

     Cross section default
  1  ---------------------------  Start-x =       16.8000000
  2  ---------------------------  Start-y =       23.6000000
  3  --------------------------   Finish-x =       16.8000000
  4  --------------------------   Finish-y =       25.2000000
  5  -----------------  Distant-increment =        1.0000000
  6  ---------------------------  Z-depth =      -30.0000000
  7  ------------------------  Z-increment =        1.0000000

Thrust Fault schematic model with ramp
#reg1=  0  #reg2=  0   #fixed=  3  sym=  1
 PR1=       .250      PR2=       .250    DEPTH=        2.8
  E1=   0.800000E+06   E2=   0.800000E+06
XSYM=       .000     YSYM=       .000
FRIC=       .400
S1DR=    24.0001     S1DP=      0.0001    S1IN=    100.000     S1GD=   .000000
S3DR=   114.0001     S3DP=      0.0001    S3IN=     30.000     S3GD=   .000000
S2DR=    89.9999    S2DP=      -89.999   S2IN=      0.000     S2GD=   .000000

  #   X-start    Y-start     X-fin      Y-fin   Kode  rt.lat    reverse   dip angle     top      bot
xxx xxxxxxxxxx xxxxxxxxxx xxxxxxxxxx xxxxxxxxxx xxx xxxxxxxxxx xxxxxxxxxx xxxxxxxxxx xxxxxxxxxx xxxxxxxxxx
1 -5.00001 5.00000 -5.00001  -5.00000 100 0.0000 0.1000 20  3.00001 3.50000
1 -4.50001 5.00000 -4.50001  -5.00000 100 0.0000 0.1000 30  2.71132 3.00001
1 -4.00001 5.00000 -4.00001  -5.00000 100 0.0000 0.1000 20  2.52933 2.71132

    Grid Parameters
  1  ---------------------------  Start-x =    -15.00000
  2  ---------------------------  Start-y =    -10.00000
  3  --------------------------   Finish-x =     15.00000
  4  --------------------------   Finish-y =     10.00000
  5  ------------------------  x-increment =     1.000000
  6  ------------------------  y-increment =     1.000000
     Size Parameters
  1  -------------------------  Plot size =     2.000000
  2  --------------  Shade/Color increment =     1.000000
  3  ------  Exaggeration for disp.& dist. =     10000.00

Cross section default
  1  ---------------------------  Start-x =    -14.00000
  2  ---------------------------  Start-y =      0.00000
  3  --------------------------   Finish-x =     14.00000
  4  --------------------------   Finish-y =      0.00000
  5  -----------------  Distant-increment =     1.000000
  6  ---------------------------  Z-depth =     15.00000
  7  ------------------------  Z-increment =     1.000000

Injectite 1 m opening
```

```
header line 2
#reg1=  0  #reg2=  0  #fixed=  71  sym=  1
 PR1=       0.250     PR2=       0.250   DEPTH=      3
  E1=     0.80000e+006   E2=     0.80000e+006
XSYM=       .000     YSYM=       .000
FRIC=          0.400
S1DR=         90.0000 S1DP=          0.0000  S1IN=        100.000  S1GD=          0.000
S2DR=         89.9999  S2DP=         90.0000   S2IN=         20.000  S2GD=          0.000
S3DR=        179.9000  S3DP=          0.0000  S3IN=          0.000  S3GD=          0.000

  #  X-start   Y-start       X-fin       Y-fin   Kode   rt.lat  reverse   dip angle     top       bot
xxx   xxxxxxxxxx xxxxxxxxx   xxxxxxxxxxxx xxxxxxxxx xxx   xxxxxxx xxxxxxxxxx xxxxxxxxX   xxxxxxxx  xxxxxxxx
1 0.000000 0.000000 0.029768 0.005698 100 0.1000 0.000000 90.000000 0.000000 5.000000
1 0.029768 0.005698 0.059535 0.010997 100 0.1000 0.000000 90.000000 0.000000 5.000000
1 0.059535 0.010997 0.089303 0.016205 100 0.1000 0.000000 90.000000 0.000000 5.000000
1 0.089303 0.016205 0.119070 0.021255 100 0.1000 0.000000 90.000000 0.000000 5.000000
1 0.119070 0.021255 0.148838 0.026252 100 0.1000 0.000000 90.000000 0.000000 5.000000
1 0.148838 0.026252 0.178605 0.031290 100 0.1000 0.000000 90.000000 0.000000 5.000000
1 0.178605 0.031290 0.208373 0.036376 100 0.1000 0.000000 90.000000 0.000000 5.000000
1 0.208373 0.036376 0.238141 0.041480 100 0.1000 0.000000 90.000000 0.000000 5.000000
1 0.238141 0.041480 0.267908 0.046663 100 0.1000 0.000000 90.000000 0.000000 5.000000
1 0.267908 0.046663 0.297676 0.052026 100 0.1000 0.000000 90.000000 0.000000 5.000000
1 0.297676 0.052026 0.327443 0.058053 100 0.1000 0.000000 90.000000 0.000000 5.000000
1 0.327443 0.058053 0.357211 0.064450 100 0.1000 0.000000 90.000000 0.000000 5.000000
1 0.357211 0.064450 0.386978 0.070777 100 0.1000 0.000000 90.000000 0.000000 5.000000
1 0.386978 0.070777 0.416746 0.077184 100 0.1000 0.000000 90.000000 0.000000 5.000000
1 0.416746 0.077184 0.446513 0.083633 100 0.1000 0.000000 90.000000 0.000000 5.000000
1 0.446513 0.083633 0.476281 0.089982 100 0.1000 0.000000 90.000000 0.000000 5.000000
1 0.476281 0.089982 0.506049 0.095902 100 0.1000 0.000000 90.000000 0.000000 5.000000
1 0.506049 0.095902 0.535816 0.101326 100 0.1000 0.000000 90.000000 0.000000 5.000000
1 0.535816 0.101326 0.565584 0.106620 100 0.1000 0.000000 90.000000 0.000000 5.000000
1 0.565584 0.106620 0.595351 0.112132 100 0.1000 0.000000 90.000000 0.000000 5.000000
1 0.595351 0.112132 0.625119 0.116726 100 0.1000 0.000000 90.000000 0.000000 5.000000
1 0.625119 0.116726 0.654886 0.121121 100 0.1000 0.000000 90.000000 0.000000 5.000000
1 0.654886 0.121121 0.684654 0.126773 100 0.1000 0.000000 90.000000 0.000000 5.000000
1 0.684654 0.126773 0.714422 0.137700 100 0.1000 0.000000 90.000000 0.000000 5.000000
1 0.714422 0.137700 0.744189 0.150680 100 0.1000 0.000000 90.000000 0.000000 5.000000
1 0.744189 0.150680 0.773957 0.160004 100 0.1000 0.000000 90.000000 0.000000 5.000000
1 0.773957 0.160004 0.803724 0.165826 100 0.1000 0.000000 90.000000 0.000000 5.000000
1 0.803724 0.165826 0.833492 0.169836 100 0.1000 0.000000 90.000000 0.000000 5.000000
1 0.833492 0.169836 0.863259 0.172857 100 0.1000 0.000000 90.000000 0.000000 5.000000
1 0.863259 0.172857 0.893027 0.177442 100 0.1000 0.000000 90.000000 0.000000 5.000000
1 0.893027 0.177442 0.922794 0.183781 100 0.1000 0.000000 90.000000 0.000000 5.000000
1 0.922794 0.183781 0.952562 0.191222 100 0.1000 0.000000 90.000000 0.000000 5.000000
1 0.952562 0.191222 0.982330 0.198765 100 0.1000 0.000000 90.000000 0.000000 5.000000
1 0.982330 0.198765 1.012097 0.206762 100 0.1000 0.000000 90.000000 0.000000 5.000000
1 1.012097 0.206762 1.041865 0.214675 100 0.1000 0.000000 90.000000 0.000000 5.000000
1 1.041865 0.214675 1.071632 0.222169 100 0.1000 0.000000 90.000000 0.000000 5.000000
1 1.071632 0.222169 1.101400 0.229931 100 0.1000 0.000000 90.000000 0.000000 5.000000
1 1.101400 0.229931 1.131167 0.238352 100 0.1000 0.000000 90.000000 0.000000 5.000000
1 1.131167 0.238352 1.160935 0.246558 100 0.1000 0.000000 90.000000 0.000000 5.000000
1 1.160935 0.246558 1.190703 0.252197 100 0.1000 0.000000 90.000000 0.000000 5.000000
1 1.190703 0.252197 1.220470 0.257474 100 0.1000 0.000000 90.000000 0.000000 5.000000
2 0.684500 0.126500 0.684500 0.176500 200 1.0000 0.000000 90.000000 0.000000 5.000000

   Grid Parameters
  1  ---------------------------  Start-x =          0.000000
  2  ---------------------------  Start-y =         -0.300000
  3  --------------------------   Finish-x =         1.2000000
  4  --------------------------   Finish-y =          0.500000
  5  ------------------------  x-increment =          0.010000
  6  ------------------------  y-increment =          0.010000
    Size Parameters
  1  -------------------------  Plot size =        0.50000
  2  -------------  Shade/Color increment =        0.2000000
```

```
  3  ------  Exaggeration for disp.& dist. =    10000.0000000

     Cross section default
  1  ---------------------------  Start-x =       16.8000000
  2  ---------------------------  Start-y =       23.6000000
  3  --------------------------   Finish-x =       16.8000000
  4  --------------------------   Finish-y =       25.2000000
  5  ------------------  Distant-increment =        1.0000000
  6  ---------------------------  Z-depth =      -30.0000000
  7  ------------------------  Z-increment =        1.0000000

Injectite 10 cm opening
header line 2
#reg1=  0  #reg2=  0  #fixed=  71  sym=  1
 PR1=       0.250     PR2=       0.250   DEPTH=      3
  E1=     0.80000e+006   E2=     0.80000e+006
XSYM=        .000     YSYM=        .000
FRIC=          0.400
S1DR=         90.0000 S1DP=          0.0000  S1IN=        100.000  S1GD=          0.000
S2DR=         89.9999  S2DP=         90.0000   S2IN=         20.000  S2GD=          0.000
S3DR=        179.9000  S3DP=          0.0000  S3IN=          0.000  S3GD=          0.000

  #  X-start   Y-start       X-fin       Y-fin   Kode   rt.lat  reverse   dip angle     top       bot
xxx   xxxxxxxxxx xxxxxxxxx   xxxxxxxxxxxx xxxxxxxxx xxx   xxxxxxx xxxxxxxxxx xxxxxxxxX   xxxxxxxx  xxxxxxxx
1 0.000000 0.000000 0.029768 0.005698 100 0.1000 0.000000 90.000000 0.000000 5.000000
1 0.029768 0.005698 0.059535 0.010997 100 0.1000 0.000000 90.000000 0.000000 5.000000
1 0.059535 0.010997 0.089303 0.016205 100 0.1000 0.000000 90.000000 0.000000 5.000000
1 0.089303 0.016205 0.119070 0.021255 100 0.1000 0.000000 90.000000 0.000000 5.000000
1 0.119070 0.021255 0.148838 0.026252 100 0.1000 0.000000 90.000000 0.000000 5.000000
1 0.148838 0.026252 0.178605 0.031290 100 0.1000 0.000000 90.000000 0.000000 5.000000
1 0.178605 0.031290 0.208373 0.036376 100 0.1000 0.000000 90.000000 0.000000 5.000000
1 0.208373 0.036376 0.238141 0.041480 100 0.1000 0.000000 90.000000 0.000000 5.000000
1 0.238141 0.041480 0.267908 0.046663 100 0.1000 0.000000 90.000000 0.000000 5.000000
1 0.267908 0.046663 0.297676 0.052026 100 0.1000 0.000000 90.000000 0.000000 5.000000
1 0.297676 0.052026 0.327443 0.058053 100 0.1000 0.000000 90.000000 0.000000 5.000000
1 0.327443 0.058053 0.357211 0.064450 100 0.1000 0.000000 90.000000 0.000000 5.000000
1 0.357211 0.064450 0.386978 0.070777 100 0.1000 0.000000 90.000000 0.000000 5.000000
1 0.386978 0.070777 0.416746 0.077184 100 0.1000 0.000000 90.000000 0.000000 5.000000
1 0.416746 0.077184 0.446513 0.083633 100 0.1000 0.000000 90.000000 0.000000 5.000000
1 0.446513 0.083633 0.476281 0.089982 100 0.1000 0.000000 90.000000 0.000000 5.000000
1 0.476281 0.089982 0.506049 0.095902 100 0.1000 0.000000 90.000000 0.000000 5.000000
1 0.506049 0.095902 0.535816 0.101326 100 0.1000 0.000000 90.000000 0.000000 5.000000
1 0.535816 0.101326 0.565584 0.106620 100 0.1000 0.000000 90.000000 0.000000 5.000000
1 0.565584 0.106620 0.595351 0.112132 100 0.1000 0.000000 90.000000 0.000000 5.000000
1 0.595351 0.112132 0.625119 0.116726 100 0.1000 0.000000 90.000000 0.000000 5.000000
1 0.625119 0.116726 0.654886 0.121121 100 0.1000 0.000000 90.000000 0.000000 5.000000
1 0.654886 0.121121 0.684654 0.126773 100 0.1000 0.000000 90.000000 0.000000 5.000000
1 0.684654 0.126773 0.714422 0.137700 100 0.1000 0.000000 90.000000 0.000000 5.000000
1 0.714422 0.137700 0.744189 0.150680 100 0.1000 0.000000 90.000000 0.000000 5.000000
1 0.744189 0.150680 0.773957 0.160004 100 0.1000 0.000000 90.000000 0.000000 5.000000
1 0.773957 0.160004 0.803724 0.165826 100 0.1000 0.000000 90.000000 0.000000 5.000000
1 0.803724 0.165826 0.833492 0.169836 100 0.1000 0.000000 90.000000 0.000000 5.000000
1 0.833492 0.169836 0.863259 0.172857 100 0.1000 0.000000 90.000000 0.000000 5.000000
1 0.863259 0.172857 0.893027 0.177442 100 0.1000 0.000000 90.000000 0.000000 5.000000
1 0.893027 0.177442 0.922794 0.183781 100 0.1000 0.000000 90.000000 0.000000 5.000000
1 0.922794 0.183781 0.952562 0.191222 100 0.1000 0.000000 90.000000 0.000000 5.000000
1 0.952562 0.191222 0.982330 0.198765 100 0.1000 0.000000 90.000000 0.000000 5.000000
1 0.982330 0.198765 1.012097 0.206762 100 0.1000 0.000000 90.000000 0.000000 5.000000
1 1.012097 0.206762 1.041865 0.214675 100 0.1000 0.000000 90.000000 0.000000 5.000000
1 1.041865 0.214675 1.071632 0.222169 100 0.1000 0.000000 90.000000 0.000000 5.000000
1 1.071632 0.222169 1.101400 0.229931 100 0.1000 0.000000 90.000000 0.000000 5.000000
1 1.101400 0.229931 1.131167 0.238352 100 0.1000 0.000000 90.000000 0.000000 5.000000
1 1.131167 0.238352 1.160935 0.246558 100 0.1000 0.000000 90.000000 0.000000 5.000000
1 1.160935 0.246558 1.190703 0.252197 100 0.1000 0.000000 90.000000 0.000000 5.000000
1 1.190703 0.252197 1.220470 0.257474 100 0.1000 0.000000 90.000000 0.000000 5.000000
```

```
2 0.684500 0.126500 0.684500 0.176500 200 0.1000 0.000000 90.000000 0.000000 5.000000

    Grid Parameters
  1  ---------------------------  Start-x =          0.000000
  2  ---------------------------  Start-y =         -0.300000
  3  --------------------------   Finish-x =         1.2000000
  4  --------------------------   Finish-y =          0.500000
  5  ------------------------  x-increment =          0.010000
  6  ------------------------  y-increment =          0.010000
     Size Parameters
  1  --------------------------  Plot size =        0.50000
  2  --------------  Shade/Color increment =        0.2000000
  3  ------  Exaggeration for disp.& dist. =    10000.0000000

     Cross section default
  1  ----------------------------  Start-x =       16.8000000
  2  ----------------------------  Start-y =       23.6000000
  3  --------------------------   Finish-x =       16.8000000
  4  --------------------------   Finish-y =       25.2000000
  5  -----------------  Distant-increment =        1.0000000
  6  ----------------------------  Z-depth =      -30.0000000
  7  ------------------------  Z-increment =        1.0000000

Tapered Injectite
header line 2
#reg1=  0  #reg2=  0  #fixed=  71  sym=  1
 PR1=       0.250     PR2=       0.250   DEPTH=      3
  E1=     0.80000e+006   E2=     0.80000e+006
XSYM=       .000     YSYM=       .000
FRIC=          0.400
S1DR=         90.0000 S1DP=          0.0000  S1IN=        100.000  S1GD=          0.000
S2DR=         89.9999  S2DP=         90.0000   S2IN=         20.000  S2GD=          0.000
S3DR=        179.9000  S3DP=          0.0000  S3IN=          0.000  S3GD=          0.000

  #  X-start   Y-start       X-fin       Y-fin   Kode   rt.lat  reverse   dip angle     top       bot
xxx   xxxxxxxxxx xxxxxxxxx   xxxxxxxxxxx xxxxxxxxx xxx   xxxxxxx xxxxxxxxxx xxxxxxxxX   xxxxxxxx  xxxxxxxx
1 0.000000 0.000000 0.029768 0.005698 100 0.1000 0.000000 90.000000 0.000000 5.000000
1 0.029768 0.005698 0.059535 0.010997 100 0.1000 0.000000 90.000000 0.000000 5.000000
1 0.059535 0.010997 0.089303 0.016205 100 0.1000 0.000000 90.000000 0.000000 5.000000
1 0.089303 0.016205 0.119070 0.021255 100 0.1000 0.000000 90.000000 0.000000 5.000000
1 0.119070 0.021255 0.148838 0.026252 100 0.1000 0.000000 90.000000 0.000000 5.000000
1 0.148838 0.026252 0.178605 0.031290 100 0.1000 0.000000 90.000000 0.000000 5.000000
1 0.178605 0.031290 0.208373 0.036376 100 0.1000 0.000000 90.000000 0.000000 5.000000
1 0.208373 0.036376 0.238141 0.041480 100 0.1000 0.000000 90.000000 0.000000 5.000000
1 0.238141 0.041480 0.267908 0.046663 100 0.1000 0.000000 90.000000 0.000000 5.000000
1 0.267908 0.046663 0.297676 0.052026 100 0.1000 0.000000 90.000000 0.000000 5.000000
1 0.297676 0.052026 0.327443 0.058053 100 0.1000 0.000000 90.000000 0.000000 5.000000
1 0.327443 0.058053 0.357211 0.064450 100 0.1000 0.000000 90.000000 0.000000 5.000000
1 0.357211 0.064450 0.386978 0.070777 100 0.1000 0.000000 90.000000 0.000000 5.000000
1 0.386978 0.070777 0.416746 0.077184 100 0.1000 0.000000 90.000000 0.000000 5.000000
1 0.416746 0.077184 0.446513 0.083633 100 0.1000 0.000000 90.000000 0.000000 5.000000
1 0.446513 0.083633 0.476281 0.089982 100 0.1000 0.000000 90.000000 0.000000 5.000000
1 0.476281 0.089982 0.506049 0.095902 100 0.1000 0.000000 90.000000 0.000000 5.000000
1 0.506049 0.095902 0.535816 0.101326 100 0.1000 0.000000 90.000000 0.000000 5.000000
1 0.535816 0.101326 0.565584 0.106620 100 0.1000 0.000000 90.000000 0.000000 5.000000
1 0.565584 0.106620 0.595351 0.112132 100 0.1000 0.000000 90.000000 0.000000 5.000000
1 0.595351 0.112132 0.625119 0.116726 100 0.1000 0.000000 90.000000 0.000000 5.000000
1 0.625119 0.116726 0.654886 0.121121 100 0.1000 0.000000 90.000000 0.000000 5.000000
1 0.654886 0.121121 0.684654 0.126773 100 0.1000 0.000000 90.000000 0.000000 5.000000
1 0.684654 0.126773 0.714422 0.137700 100 0.1000 0.000000 90.000000 0.000000 5.000000
1 0.714422 0.137700 0.744189 0.150680 100 0.1000 0.000000 90.000000 0.000000 5.000000
1 0.744189 0.150680 0.773957 0.160004 100 0.1000 0.000000 90.000000 0.000000 5.000000
1 0.773957 0.160004 0.803724 0.165826 100 0.1000 0.000000 90.000000 0.000000 5.000000
1 0.803724 0.165826 0.833492 0.169836 100 0.1000 0.000000 90.000000 0.000000 5.000000
1 0.833492 0.169836 0.863259 0.172857 100 0.1000 0.000000 90.000000 0.000000 5.000000
```

```
1 0.863259 0.172857 0.893027 0.177442 100 0.1000 0.000000 90.000000 0.000000 5.000000
1 0.893027 0.177442 0.922794 0.183781 100 0.1000 0.000000 90.000000 0.000000 5.000000
1 0.922794 0.183781 0.952562 0.191222 100 0.1000 0.000000 90.000000 0.000000 5.000000
1 0.952562 0.191222 0.982330 0.198765 100 0.1000 0.000000 90.000000 0.000000 5.000000
1 0.982330 0.198765 1.012097 0.206762 100 0.1000 0.000000 90.000000 0.000000 5.000000
1 1.012097 0.206762 1.041865 0.214675 100 0.1000 0.000000 90.000000 0.000000 5.000000
1 1.041865 0.214675 1.071632 0.222169 100 0.1000 0.000000 90.000000 0.000000 5.000000
1 1.071632 0.222169 1.101400 0.229931 100 0.1000 0.000000 90.000000 0.000000 5.000000
1 1.101400 0.229931 1.131167 0.238352 100 0.1000 0.000000 90.000000 0.000000 5.000000
1 1.131167 0.238352 1.160935 0.246558 100 0.1000 0.000000 90.000000 0.000000 5.000000
1 1.160935 0.246558 1.190703 0.252197 100 0.1000 0.000000 90.000000 0.000000 5.000000
1 1.190703 0.252197 1.220470 0.257474 100 0.1000 0.000000 90.000000 0.000000 5.000000
2 0.684500 0.126500 0.684500 0.136500 200 1.0000 0.000000 90.000000 0.000000 5.000000
2 0.684500 0.136500 0.684500 0.146500 200 0.8000 0.000000 90.000000 0.000000 5.000000
2 0.684500 0.146500 0.684500 0.156500 200 0.6000 0.000000 90.000000 0.000000 5.000000
2 0.684500 0.156500 0.684500 0.166500 200 0.4000 0.000000 90.000000 0.000000 5.000000
2 0.684500 0.166500 0.684500 0.176500 200 0.2000 0.000000 90.000000 0.000000 5.000000

    Grid Parameters
  1  ----------------------------  Start-x =          0.000000
  2  ----------------------------  Start-y =         -0.300000
  3  --------------------------   Finish-x =         1.2000000
  4  --------------------------   Finish-y =          0.500000
  5  ------------------------  x-increment =          0.010000
  6  ------------------------  y-increment =          0.010000
     Size Parameters
  1  --------------------------  Plot size =        0.50000
  2  --------------  Shade/Color increment =        0.2000000
  3  ------  Exaggeration for disp.& dist. =    10000.0000000

     Cross section default
  1  ----------------------------  Start-x =       16.8000000
  2  ----------------------------  Start-y =       23.6000000
  3  --------------------------   Finish-x =       16.8000000
  4  --------------------------   Finish-y =       25.2000000
  5  ------------------  Distant-increment =        1.0000000
  6  ----------------------------  Z-depth =      -30.0000000
  7  ------------------------  Z-increment =        1.0000000

Fault tips artificially extened +-10 km
header line 2
#reg1=  0  #reg2=  0  #fixed=  71  sym=  1
 PR1=       0.350     PR2=       0.350   DEPTH=      3
  E1=     0.20000e+006   E2=     0.20000e+006
XSYM=       .000     YSYM=       .000
FRIC=          0.400
S1DR=         90.0000 S1DP=          0.0000  S1IN=        100.000  S1GD=          0.000
S2DR=         89.9999  S2DP=         90.0000   S2IN=          20.000  S2GD=          0.000
S3DR=        179.9000  S3DP=          0.0000  S3IN=          0.000  S3GD=          0.000

  #  X-start   Y-start       X-fin       Y-fin   Kode   rt.lat  reverse   dip angle     top       bot
xxx   xxxxxxxxxx xxxxxxxxx   xxxxxxxxxxxx xxxxxxxxx xxx   xxxxxxx xxxxxxxxxx xxxxxxxxX   xxxxxxxx  xxxxxxxx
1 -9.78147 -2.07911 0.000001 0.000001 100 0.1000 0.000000 90.000000 0.000000 5.000000
1 0.000001 0.000001 0.029768 0.005698 100 0.1000 0.000000 90.000000 0.000000 5.000000
1 0.029768 0.005698 0.059535 0.010997 100 0.1000 0.000000 90.000000 0.000000 5.000000
1 0.059535 0.010997 0.089303 0.016205 100 0.1000 0.000000 90.000000 0.000000 5.000000
1 0.089303 0.016205 0.119070 0.021255 100 0.1000 0.000000 90.000000 0.000000 5.000000
1 0.119070 0.021255 0.148838 0.026252 100 0.1000 0.000000 90.000000 0.000000 5.000000
1 0.148838 0.026252 0.178605 0.031290 100 0.1000 0.000000 90.000000 0.000000 5.000000
1 0.178605 0.031290 0.208373 0.036376 100 0.1000 0.000000 90.000000 0.000000 5.000000
1 0.208373 0.036376 0.238141 0.041480 100 0.1000 0.000000 90.000000 0.000000 5.000000
1 0.238141 0.041480 0.267908 0.046663 100 0.1000 0.000000 90.000000 0.000000 5.000000
1 0.267908 0.046663 0.297676 0.052026 100 0.1000 0.000000 90.000000 0.000000 5.000000
1 0.297676 0.052026 0.327443 0.058053 100 0.1000 0.000000 90.000000 0.000000 5.000000
1 0.327443 0.058053 0.357211 0.064450 100 0.1000 0.000000 90.000000 0.000000 5.000000
```

```
1 0.357211 0.064450 0.386978 0.070777 100 0.1000 0.000000 90.000000 0.000000 5.000000
1 0.386978 0.070777 0.416746 0.077184 100 0.1000 0.000000 90.000000 0.000000 5.000000
1 0.416746 0.077184 0.446513 0.083633 100 0.1000 0.000000 90.000000 0.000000 5.000000
1 0.446513 0.083633 0.476281 0.089982 100 0.1000 0.000000 90.000000 0.000000 5.000000
1 0.476281 0.089982 0.506049 0.095902 100 0.1000 0.000000 90.000000 0.000000 5.000000
1 0.506049 0.095902 0.535816 0.101326 100 0.1000 0.000000 90.000000 0.000000 5.000000
1 0.535816 0.101326 0.565584 0.106620 100 0.1000 0.000000 90.000000 0.000000 5.000000
1 0.565584 0.106620 0.595351 0.112132 100 0.1000 0.000000 90.000000 0.000000 5.000000
1 0.595351 0.112132 0.625119 0.116726 100 0.1000 0.000000 90.000000 0.000000 5.000000
1 0.625119 0.116726 0.654886 0.121121 100 0.1000 0.000000 90.000000 0.000000 5.000000
1 0.654886 0.121121 0.684654 0.126773 100 0.1000 0.000000 90.000000 0.000000 5.000000
1 0.684654 0.126773 0.714422 0.137700 100 0.1000 0.000000 90.000000 0.000000 5.000000
1 0.714422 0.137700 0.744189 0.150680 100 0.1000 0.000000 90.000000 0.000000 5.000000
1 0.744189 0.150680 0.773957 0.160004 100 0.1000 0.000000 90.000000 0.000000 5.000000
1 0.773957 0.160004 0.803724 0.165826 100 0.1000 0.000000 90.000000 0.000000 5.000000
1 0.803724 0.165826 0.833492 0.169836 100 0.1000 0.000000 90.000000 0.000000 5.000000
1 0.833492 0.169836 0.863259 0.172857 100 0.1000 0.000000 90.000000 0.000000 5.000000
1 0.863259 0.172857 0.893027 0.177442 100 0.1000 0.000000 90.000000 0.000000 5.000000
1 0.893027 0.177442 0.922794 0.183781 100 0.1000 0.000000 90.000000 0.000000 5.000000
1 0.922794 0.183781 0.952562 0.191222 100 0.1000 0.000000 90.000000 0.000000 5.000000
1 0.952562 0.191222 0.982330 0.198765 100 0.1000 0.000000 90.000000 0.000000 5.000000
1 0.982330 0.198765 1.012097 0.206762 100 0.1000 0.000000 90.000000 0.000000 5.000000
1 1.012097 0.206762 1.041865 0.214675 100 0.1000 0.000000 90.000000 0.000000 5.000000
1 1.041865 0.214675 1.071632 0.222169 100 0.1000 0.000000 90.000000 0.000000 5.000000
1 1.071632 0.222169 1.101400 0.229931 100 0.1000 0.000000 90.000000 0.000000 5.000000
1 1.101400 0.229931 1.131167 0.238352 100 0.1000 0.000000 90.000000 0.000000 5.000000
1 1.131167 0.238352 1.160935 0.246558 100 0.1000 0.000000 90.000000 0.000000 5.000000
1 1.160935 0.246558 1.190703 0.252197 100 0.1000 0.000000 90.000000 0.000000 5.000000
1 1.190703 0.252197 1.220470 0.257474 100 0.1000 0.000000 90.000000 0.000000 5.000000
1 1.220470 0.257474 11.00194 2.336590 100 0.1000 0.000000 90.000000 0.000000 5.000000

    Grid Parameters
  1  ----------------------------  Start-x =        -10.000000
  2  ----------------------------  Start-y =         -5.000000
  3  --------------------------   Finish-x =         14.000000
  4  --------------------------   Finish-y =          5.000000
  5  ------------------------  x-increment =          0.100000
  6  ------------------------  y-increment =          0.100000
    Size Parameters
  1  --------------------------  Plot size =        0.50000
  2  --------------  Shade/Color increment =        0.2000000
  3  ------  Exaggeration for disp.& dist. =    10000.0000000

    Cross section default
  1  ----------------------------  Start-x =       16.8000000
  2  ----------------------------  Start-y =       23.6000000
  3  --------------------------   Finish-x =       16.8000000
  4  --------------------------   Finish-y =       25.2000000
  5  -----------------  Distant-increment =        1.0000000
  6  ----------------------------  Z-depth =      -30.0000000
  7  ------------------------  Z-increment =        1.0000000

Poisson's Ratio Sensitivity Test 0.35
header line 2
#reg1=  0  #reg2=  0  #fixed=  71  sym=  1
 PR1=       0.350     PR2=       0.350   DEPTH=      3
  E1=     0.80000e+006   E2=     0.80000e+006
XSYM=        .000     YSYM=       .000
FRIC=          0.400
S1DR=         90.0000 S1DP=          0.0000  S1IN=        100.000  S1GD=          0.000
S2DR=         89.9999  S2DP=         90.0000   S2IN=         20.000  S2GD=          0.000
S3DR=        179.9000  S3DP=          0.0000  S3IN=          0.000  S3GD=          0.000

  #  X-start   Y-start       X-fin       Y-fin   Kode   rt.lat  reverse   dip angle     top       bot
xxx   xxxxxxxxxx xxxxxxxxx   xxxxxxxxxxxx xxxxxxxxx xxx   xxxxxxx xxxxxxxxxx xxxxxxxxX   xxxxxxxx  xxxxxxxx
```

```
1 0.000000 0.000000 0.029768 0.005698 100 0.1000 0.000000 90.000000 0.000000 5.000000
1 0.029768 0.005698 0.059535 0.010997 100 0.1000 0.000000 90.000000 0.000000 5.000000
1 0.059535 0.010997 0.089303 0.016205 100 0.1000 0.000000 90.000000 0.000000 5.000000
1 0.089303 0.016205 0.119070 0.021255 100 0.1000 0.000000 90.000000 0.000000 5.000000
1 0.119070 0.021255 0.148838 0.026252 100 0.1000 0.000000 90.000000 0.000000 5.000000
1 0.148838 0.026252 0.178605 0.031290 100 0.1000 0.000000 90.000000 0.000000 5.000000
1 0.178605 0.031290 0.208373 0.036376 100 0.1000 0.000000 90.000000 0.000000 5.000000
1 0.208373 0.036376 0.238141 0.041480 100 0.1000 0.000000 90.000000 0.000000 5.000000
1 0.238141 0.041480 0.267908 0.046663 100 0.1000 0.000000 90.000000 0.000000 5.000000
1 0.267908 0.046663 0.297676 0.052026 100 0.1000 0.000000 90.000000 0.000000 5.000000
1 0.297676 0.052026 0.327443 0.058053 100 0.1000 0.000000 90.000000 0.000000 5.000000
1 0.327443 0.058053 0.357211 0.064450 100 0.1000 0.000000 90.000000 0.000000 5.000000
1 0.357211 0.064450 0.386978 0.070777 100 0.1000 0.000000 90.000000 0.000000 5.000000
1 0.386978 0.070777 0.416746 0.077184 100 0.1000 0.000000 90.000000 0.000000 5.000000
1 0.416746 0.077184 0.446513 0.083633 100 0.1000 0.000000 90.000000 0.000000 5.000000
1 0.446513 0.083633 0.476281 0.089982 100 0.1000 0.000000 90.000000 0.000000 5.000000
1 0.476281 0.089982 0.506049 0.095902 100 0.1000 0.000000 90.000000 0.000000 5.000000
1 0.506049 0.095902 0.535816 0.101326 100 0.1000 0.000000 90.000000 0.000000 5.000000
1 0.535816 0.101326 0.565584 0.106620 100 0.1000 0.000000 90.000000 0.000000 5.000000
1 0.565584 0.106620 0.595351 0.112132 100 0.1000 0.000000 90.000000 0.000000 5.000000
1 0.595351 0.112132 0.625119 0.116726 100 0.1000 0.000000 90.000000 0.000000 5.000000
1 0.625119 0.116726 0.654886 0.121121 100 0.1000 0.000000 90.000000 0.000000 5.000000
1 0.654886 0.121121 0.684654 0.126773 100 0.1000 0.000000 90.000000 0.000000 5.000000
1 0.684654 0.126773 0.714422 0.137700 100 0.1000 0.000000 90.000000 0.000000 5.000000
1 0.714422 0.137700 0.744189 0.150680 100 0.1000 0.000000 90.000000 0.000000 5.000000
1 0.744189 0.150680 0.773957 0.160004 100 0.1000 0.000000 90.000000 0.000000 5.000000
1 0.773957 0.160004 0.803724 0.165826 100 0.1000 0.000000 90.000000 0.000000 5.000000
1 0.803724 0.165826 0.833492 0.169836 100 0.1000 0.000000 90.000000 0.000000 5.000000
1 0.833492 0.169836 0.863259 0.172857 100 0.1000 0.000000 90.000000 0.000000 5.000000
1 0.863259 0.172857 0.893027 0.177442 100 0.1000 0.000000 90.000000 0.000000 5.000000
1 0.893027 0.177442 0.922794 0.183781 100 0.1000 0.000000 90.000000 0.000000 5.000000
1 0.922794 0.183781 0.952562 0.191222 100 0.1000 0.000000 90.000000 0.000000 5.000000
1 0.952562 0.191222 0.982330 0.198765 100 0.1000 0.000000 90.000000 0.000000 5.000000
1 0.982330 0.198765 1.012097 0.206762 100 0.1000 0.000000 90.000000 0.000000 5.000000
1 1.012097 0.206762 1.041865 0.214675 100 0.1000 0.000000 90.000000 0.000000 5.000000
1 1.041865 0.214675 1.071632 0.222169 100 0.1000 0.000000 90.000000 0.000000 5.000000
1 1.071632 0.222169 1.101400 0.229931 100 0.1000 0.000000 90.000000 0.000000 5.000000
1 1.101400 0.229931 1.131167 0.238352 100 0.1000 0.000000 90.000000 0.000000 5.000000
1 1.131167 0.238352 1.160935 0.246558 100 0.1000 0.000000 90.000000 0.000000 5.000000
1 1.160935 0.246558 1.190703 0.252197 100 0.1000 0.000000 90.000000 0.000000 5.000000
1 1.190703 0.252197 1.220470 0.257474 100 0.1000 0.000000 90.000000 0.000000 5.000000

    Grid Parameters
  1  ----------------------------  Start-x =          0.000000
  2  ----------------------------  Start-y =         -0.300000
  3  --------------------------   Finish-x =          1.200000
  4  --------------------------   Finish-y =          0.500000
  5  ------------------------  x-increment =          0.010000
  6  ------------------------  y-increment =          0.010000
     Size Parameters
  1  --------------------------  Plot size =        0.50000
  2  --------------  Shade/Color increment =        0.2000000
  3  ------  Exaggeration for disp.& dist. =    10000.0000000

     Cross section default
  1  ----------------------------  Start-x =       16.8000000
  2  ----------------------------  Start-y =       23.6000000
  3  --------------------------   Finish-x =       16.8000000
  4  --------------------------   Finish-y =       25.2000000
  5  ------------------  Distant-increment =        1.0000000
  6  ----------------------------  Z-depth =      -30.0000000
  7  ------------------------  Z-increment =        1.0000000

Poisson's Ratio Sensitivity Test 0.3
header line 2
```

```
#reg1=  0  #reg2=  0  #fixed=  71  sym=  1
 PR1=       0.300     PR2=       0.300   DEPTH=      3
  E1=     0.80000e+006   E2=     0.80000e+006
XSYM=       .000     YSYM=       .000
FRIC=          0.400
S1DR=         90.0000 S1DP=          0.0000  S1IN=        100.000  S1GD=          0.000
S2DR=         89.9999  S2DP=         90.0000   S2IN=         20.000  S2GD=          0.000
S3DR=        179.9000  S3DP=          0.0000  S3IN=          0.000  S3GD=          0.000

  #  X-start   Y-start       X-fin       Y-fin   Kode   rt.lat  reverse   dip angle     top       bot
xxx   xxxxxxxxxx xxxxxxxxx   xxxxxxxxxxx xxxxxxxxx xxx   xxxxxxx xxxxxxxxxx xxxxxxxxX   xxxxxxxx  xxxxxxxx
1 0.000000 0.000000 0.029768 0.005698 100 0.1000 0.000000 90.000000 0.000000 5.000000
1 0.029768 0.005698 0.059535 0.010997 100 0.1000 0.000000 90.000000 0.000000 5.000000
1 0.059535 0.010997 0.089303 0.016205 100 0.1000 0.000000 90.000000 0.000000 5.000000
1 0.089303 0.016205 0.119070 0.021255 100 0.1000 0.000000 90.000000 0.000000 5.000000
1 0.119070 0.021255 0.148838 0.026252 100 0.1000 0.000000 90.000000 0.000000 5.000000
1 0.148838 0.026252 0.178605 0.031290 100 0.1000 0.000000 90.000000 0.000000 5.000000
1 0.178605 0.031290 0.208373 0.036376 100 0.1000 0.000000 90.000000 0.000000 5.000000
1 0.208373 0.036376 0.238141 0.041480 100 0.1000 0.000000 90.000000 0.000000 5.000000
1 0.238141 0.041480 0.267908 0.046663 100 0.1000 0.000000 90.000000 0.000000 5.000000
1 0.267908 0.046663 0.297676 0.052026 100 0.1000 0.000000 90.000000 0.000000 5.000000
1 0.297676 0.052026 0.327443 0.058053 100 0.1000 0.000000 90.000000 0.000000 5.000000
1 0.327443 0.058053 0.357211 0.064450 100 0.1000 0.000000 90.000000 0.000000 5.000000
1 0.357211 0.064450 0.386978 0.070777 100 0.1000 0.000000 90.000000 0.000000 5.000000
1 0.386978 0.070777 0.416746 0.077184 100 0.1000 0.000000 90.000000 0.000000 5.000000
1 0.416746 0.077184 0.446513 0.083633 100 0.1000 0.000000 90.000000 0.000000 5.000000
1 0.446513 0.083633 0.476281 0.089982 100 0.1000 0.000000 90.000000 0.000000 5.000000
1 0.476281 0.089982 0.506049 0.095902 100 0.1000 0.000000 90.000000 0.000000 5.000000
1 0.506049 0.095902 0.535816 0.101326 100 0.1000 0.000000 90.000000 0.000000 5.000000
1 0.535816 0.101326 0.565584 0.106620 100 0.1000 0.000000 90.000000 0.000000 5.000000
1 0.565584 0.106620 0.595351 0.112132 100 0.1000 0.000000 90.000000 0.000000 5.000000
1 0.595351 0.112132 0.625119 0.116726 100 0.1000 0.000000 90.000000 0.000000 5.000000
1 0.625119 0.116726 0.654886 0.121121 100 0.1000 0.000000 90.000000 0.000000 5.000000
1 0.654886 0.121121 0.684654 0.126773 100 0.1000 0.000000 90.000000 0.000000 5.000000
1 0.684654 0.126773 0.714422 0.137700 100 0.1000 0.000000 90.000000 0.000000 5.000000
1 0.714422 0.137700 0.744189 0.150680 100 0.1000 0.000000 90.000000 0.000000 5.000000
1 0.744189 0.150680 0.773957 0.160004 100 0.1000 0.000000 90.000000 0.000000 5.000000
1 0.773957 0.160004 0.803724 0.165826 100 0.1000 0.000000 90.000000 0.000000 5.000000
1 0.803724 0.165826 0.833492 0.169836 100 0.1000 0.000000 90.000000 0.000000 5.000000
1 0.833492 0.169836 0.863259 0.172857 100 0.1000 0.000000 90.000000 0.000000 5.000000
1 0.863259 0.172857 0.893027 0.177442 100 0.1000 0.000000 90.000000 0.000000 5.000000
1 0.893027 0.177442 0.922794 0.183781 100 0.1000 0.000000 90.000000 0.000000 5.000000
1 0.922794 0.183781 0.952562 0.191222 100 0.1000 0.000000 90.000000 0.000000 5.000000
1 0.952562 0.191222 0.982330 0.198765 100 0.1000 0.000000 90.000000 0.000000 5.000000
1 0.982330 0.198765 1.012097 0.206762 100 0.1000 0.000000 90.000000 0.000000 5.000000
1 1.012097 0.206762 1.041865 0.214675 100 0.1000 0.000000 90.000000 0.000000 5.000000
1 1.041865 0.214675 1.071632 0.222169 100 0.1000 0.000000 90.000000 0.000000 5.000000
1 1.071632 0.222169 1.101400 0.229931 100 0.1000 0.000000 90.000000 0.000000 5.000000
1 1.101400 0.229931 1.131167 0.238352 100 0.1000 0.000000 90.000000 0.000000 5.000000
1 1.131167 0.238352 1.160935 0.246558 100 0.1000 0.000000 90.000000 0.000000 5.000000
1 1.160935 0.246558 1.190703 0.252197 100 0.1000 0.000000 90.000000 0.000000 5.000000
1 1.190703 0.252197 1.220470 0.257474 100 0.1000 0.000000 90.000000 0.000000 5.000000

    Grid Parameters
  1  ---------------------------  Start-x =          0.000000
  2  ---------------------------  Start-y =         -0.300000
  3  --------------------------   Finish-x =         1.2000000
  4  --------------------------   Finish-y =          0.500000
  5  ------------------------  x-increment =          0.010000
  6  ------------------------  y-increment =          0.010000
     Size Parameters
  1  --------------------------  Plot size =        0.50000
  2  --------------  Shade/Color increment =        0.2000000
  3  ------  Exaggeration for disp.& dist. =    10000.0000000
```

```
    Cross section default
  1  ----------------------------  Start-x =       16.8000000
  2  ----------------------------  Start-y =       23.6000000
  3  --------------------------   Finish-x =       16.8000000
  4  --------------------------   Finish-y =       25.2000000
  5  ------------------  Distant-increment =        1.0000000
  6  ----------------------------  Z-depth =      -30.0000000
  7  ------------------------  Z-increment =        1.0000000

Tapered fault slip Test
header line 2
#reg1=  0  #reg2=  0  #fixed=  71  sym=  1
 PR1=       0.300     PR2=       0.300   DEPTH=      3
  E1=     0.80000e+006   E2=     0.80000e+006
XSYM=       .000     YSYM=       .000
FRIC=          0.400
S1DR=         90.0000 S1DP=          0.0000  S1IN=        100.000  S1GD=          0.000
S2DR=         89.9999  S2DP=         90.0000   S2IN=         20.000  S2GD=          0.000
S3DR=        179.9000  S3DP=          0.0000  S3IN=          0.000  S3GD=          0.000

  #  X-start   Y-start       X-fin       Y-fin   Kode   rt.lat  reverse   dip angle     top       bot
xxx   xxxxxxxxxx xxxxxxxxx   xxxxxxxxxxxx xxxxxxxxx xxx   xxxxxxx xxxxxxxxxx xxxxxxxxX   xxxxxxxx  xxxxxxxx
1 0.000000 0.000000 0.029768 0.005698 100 0.0100 0.000000 90.000000 0.000000 5.000000
1 0.029768 0.005698 0.059535 0.010997 100 0.0200 0.000000 90.000000 0.000000 5.000000
1 0.059535 0.010997 0.089303 0.016205 100 0.0300 0.000000 90.000000 0.000000 5.000000
1 0.089303 0.016205 0.119070 0.021255 100 0.0400 0.000000 90.000000 0.000000 5.000000
1 0.119070 0.021255 0.148838 0.026252 100 0.0500 0.000000 90.000000 0.000000 5.000000
1 0.148838 0.026252 0.178605 0.031290 100 0.0600 0.000000 90.000000 0.000000 5.000000
1 0.178605 0.031290 0.208373 0.036376 100 0.0700 0.000000 90.000000 0.000000 5.000000
1 0.208373 0.036376 0.238141 0.041480 100 0.0800 0.000000 90.000000 0.000000 5.000000
1 0.238141 0.041480 0.267908 0.046663 100 0.0900 0.000000 90.000000 0.000000 5.000000
1 0.267908 0.046663 0.297676 0.052026 100 0.1000 0.000000 90.000000 0.000000 5.000000
1 0.297676 0.052026 0.327443 0.058053 100 0.1000 0.000000 90.000000 0.000000 5.000000
1 0.327443 0.058053 0.357211 0.064450 100 0.1000 0.000000 90.000000 0.000000 5.000000
1 0.357211 0.064450 0.386978 0.070777 100 0.1000 0.000000 90.000000 0.000000 5.000000
1 0.386978 0.070777 0.416746 0.077184 100 0.1000 0.000000 90.000000 0.000000 5.000000
1 0.416746 0.077184 0.446513 0.083633 100 0.1000 0.000000 90.000000 0.000000 5.000000
1 0.446513 0.083633 0.476281 0.089982 100 0.1000 0.000000 90.000000 0.000000 5.000000
1 0.476281 0.089982 0.506049 0.095902 100 0.1000 0.000000 90.000000 0.000000 5.000000
1 0.506049 0.095902 0.535816 0.101326 100 0.1000 0.000000 90.000000 0.000000 5.000000
1 0.535816 0.101326 0.565584 0.106620 100 0.1000 0.000000 90.000000 0.000000 5.000000
1 0.565584 0.106620 0.595351 0.112132 100 0.1000 0.000000 90.000000 0.000000 5.000000
1 0.595351 0.112132 0.625119 0.116726 100 0.1000 0.000000 90.000000 0.000000 5.000000
1 0.625119 0.116726 0.654886 0.121121 100 0.1000 0.000000 90.000000 0.000000 5.000000
1 0.654886 0.121121 0.684654 0.126773 100 0.1000 0.000000 90.000000 0.000000 5.000000
1 0.684654 0.126773 0.714422 0.137700 100 0.1000 0.000000 90.000000 0.000000 5.000000
1 0.714422 0.137700 0.744189 0.150680 100 0.1000 0.000000 90.000000 0.000000 5.000000
1 0.744189 0.150680 0.773957 0.160004 100 0.1000 0.000000 90.000000 0.000000 5.000000
1 0.773957 0.160004 0.803724 0.165826 100 0.1000 0.000000 90.000000 0.000000 5.000000
1 0.803724 0.165826 0.833492 0.169836 100 0.1000 0.000000 90.000000 0.000000 5.000000
1 0.833492 0.169836 0.863259 0.172857 100 0.1000 0.000000 90.000000 0.000000 5.000000
1 0.863259 0.172857 0.893027 0.177442 100 0.1000 0.000000 90.000000 0.000000 5.000000
1 0.893027 0.177442 0.922794 0.183781 100 0.1000 0.000000 90.000000 0.000000 5.000000
1 0.922794 0.183781 0.952562 0.191222 100 0.0900 0.000000 90.000000 0.000000 5.000000
1 0.952562 0.191222 0.982330 0.198765 100 0.0800 0.000000 90.000000 0.000000 5.000000
1 0.982330 0.198765 1.012097 0.206762 100 0.0700 0.000000 90.000000 0.000000 5.000000
1 1.012097 0.206762 1.041865 0.214675 100 0.0600 0.000000 90.000000 0.000000 5.000000
1 1.041865 0.214675 1.071632 0.222169 100 0.0500 0.000000 90.000000 0.000000 5.000000
1 1.071632 0.222169 1.101400 0.229931 100 0.0400 0.000000 90.000000 0.000000 5.000000
1 1.101400 0.229931 1.131167 0.238352 100 0.0300 0.000000 90.000000 0.000000 5.000000
1 1.131167 0.238352 1.160935 0.246558 100 0.0200 0.000000 90.000000 0.000000 5.000000
1 1.160935 0.246558 1.190703 0.252197 100 0.0100 0.000000 90.000000 0.000000 5.000000
1 1.190703 0.252197 1.220470 0.257474 100 0.0000 0.000000 90.000000 0.000000 5.000000

    Grid Parameters
```

```
  1  ----------------------------  Start-x =          0.000000
  2  ----------------------------  Start-y =         -0.300000
  3  --------------------------   Finish-x =         1.2000000
  4  --------------------------   Finish-y =          0.500000
  5  ------------------------  x-increment =          0.010000
  6  ------------------------  y-increment =          0.010000
     Size Parameters
  1  --------------------------  Plot size =        0.50000
  2  --------------  Shade/Color increment =        0.2000000
  3  ------  Exaggeration for disp.& dist. =    10000.0000000

     Cross section default
  1  ----------------------------  Start-x =       16.8000000
  2  ----------------------------  Start-y =       23.6000000
  3  --------------------------   Finish-x =       16.8000000
  4  --------------------------   Finish-y =       25.2000000
  5  ------------------  Distant-increment =        1.0000000
  6  ----------------------------  Z-depth =      -30.0000000
  7  ------------------------  Z-increment =        1.0000000

Young's Modulus 200,000 bar
header line 2
#reg1=  0  #reg2=  0  #fixed=  71  sym=  1
 PR1=       0.250     PR2=       0.250   DEPTH=      3
  E1=     0.20000e+006   E2=     0.20000e+006
XSYM=        .000     YSYM=       .000
FRIC=          0.400
S1DR=         90.0000 S1DP=          0.0000  S1IN=        100.000  S1GD=          0.000
S2DR=         89.9999  S2DP=         90.0000   S2IN=         20.000  S2GD=          0.000
S3DR=        179.9000  S3DP=          0.0000  S3IN=          0.000  S3GD=          0.000

  #  X-start   Y-start       X-fin       Y-fin   Kode   rt.lat  reverse   dip angle     top       bot
xxx   xxxxxxxxxx xxxxxxxxx   xxxxxxxxxxxx xxxxxxxxx xxx   xxxxxxx xxxxxxxxxx xxxxxxxxX   xxxxxxxx  xxxxxxxx
1 0.000000 0.000000 0.029768 0.005698 100 0.1000 0.000000 90.000000 0.000000 5.000000
1 0.029768 0.005698 0.059535 0.010997 100 0.1000 0.000000 90.000000 0.000000 5.000000
1 0.059535 0.010997 0.089303 0.016205 100 0.1000 0.000000 90.000000 0.000000 5.000000
1 0.089303 0.016205 0.119070 0.021255 100 0.1000 0.000000 90.000000 0.000000 5.000000
1 0.119070 0.021255 0.148838 0.026252 100 0.1000 0.000000 90.000000 0.000000 5.000000
1 0.148838 0.026252 0.178605 0.031290 100 0.1000 0.000000 90.000000 0.000000 5.000000
1 0.178605 0.031290 0.208373 0.036376 100 0.1000 0.000000 90.000000 0.000000 5.000000
1 0.208373 0.036376 0.238141 0.041480 100 0.1000 0.000000 90.000000 0.000000 5.000000
1 0.238141 0.041480 0.267908 0.046663 100 0.1000 0.000000 90.000000 0.000000 5.000000
1 0.267908 0.046663 0.297676 0.052026 100 0.1000 0.000000 90.000000 0.000000 5.000000
1 0.297676 0.052026 0.327443 0.058053 100 0.1000 0.000000 90.000000 0.000000 5.000000
1 0.327443 0.058053 0.357211 0.064450 100 0.1000 0.000000 90.000000 0.000000 5.000000
1 0.357211 0.064450 0.386978 0.070777 100 0.1000 0.000000 90.000000 0.000000 5.000000
1 0.386978 0.070777 0.416746 0.077184 100 0.1000 0.000000 90.000000 0.000000 5.000000
1 0.416746 0.077184 0.446513 0.083633 100 0.1000 0.000000 90.000000 0.000000 5.000000
1 0.446513 0.083633 0.476281 0.089982 100 0.1000 0.000000 90.000000 0.000000 5.000000
1 0.476281 0.089982 0.506049 0.095902 100 0.1000 0.000000 90.000000 0.000000 5.000000
1 0.506049 0.095902 0.535816 0.101326 100 0.1000 0.000000 90.000000 0.000000 5.000000
1 0.535816 0.101326 0.565584 0.106620 100 0.1000 0.000000 90.000000 0.000000 5.000000
1 0.565584 0.106620 0.595351 0.112132 100 0.1000 0.000000 90.000000 0.000000 5.000000
1 0.595351 0.112132 0.625119 0.116726 100 0.1000 0.000000 90.000000 0.000000 5.000000
1 0.625119 0.116726 0.654886 0.121121 100 0.1000 0.000000 90.000000 0.000000 5.000000
1 0.654886 0.121121 0.684654 0.126773 100 0.1000 0.000000 90.000000 0.000000 5.000000
1 0.684654 0.126773 0.714422 0.137700 100 0.1000 0.000000 90.000000 0.000000 5.000000
1 0.714422 0.137700 0.744189 0.150680 100 0.1000 0.000000 90.000000 0.000000 5.000000
1 0.744189 0.150680 0.773957 0.160004 100 0.1000 0.000000 90.000000 0.000000 5.000000
1 0.773957 0.160004 0.803724 0.165826 100 0.1000 0.000000 90.000000 0.000000 5.000000
1 0.803724 0.165826 0.833492 0.169836 100 0.1000 0.000000 90.000000 0.000000 5.000000
1 0.833492 0.169836 0.863259 0.172857 100 0.1000 0.000000 90.000000 0.000000 5.000000
1 0.863259 0.172857 0.893027 0.177442 100 0.1000 0.000000 90.000000 0.000000 5.000000
1 0.893027 0.177442 0.922794 0.183781 100 0.1000 0.000000 90.000000 0.000000 5.000000
1 0.922794 0.183781 0.952562 0.191222 100 0.1000 0.000000 90.000000 0.000000 5.000000
```

```
1 0.952562 0.191222 0.982330 0.198765 100 0.1000 0.000000 90.000000 0.000000 5.000000
1 0.982330 0.198765 1.012097 0.206762 100 0.1000 0.000000 90.000000 0.000000 5.000000
1 1.012097 0.206762 1.041865 0.214675 100 0.1000 0.000000 90.000000 0.000000 5.000000
1 1.041865 0.214675 1.071632 0.222169 100 0.1000 0.000000 90.000000 0.000000 5.000000
1 1.071632 0.222169 1.101400 0.229931 100 0.1000 0.000000 90.000000 0.000000 5.000000
1 1.101400 0.229931 1.131167 0.238352 100 0.1000 0.000000 90.000000 0.000000 5.000000
1 1.131167 0.238352 1.160935 0.246558 100 0.1000 0.000000 90.000000 0.000000 5.000000
1 1.160935 0.246558 1.190703 0.252197 100 0.1000 0.000000 90.000000 0.000000 5.000000
1 1.190703 0.252197 1.220470 0.257474 100 0.1000 0.000000 90.000000 0.000000 5.000000

    Grid Parameters
  1  ---------------------------  Start-x =          0.000000
  2  ---------------------------  Start-y =         -0.300000
  3  --------------------------   Finish-x =         1.2000000
  4  --------------------------   Finish-y =          0.500000
  5  ------------------------  x-increment =          0.010000
  6  ------------------------  y-increment =          0.010000
     Size Parameters
  1  --------------------------  Plot size =        0.50000
  2  --------------  Shade/Color increment =        0.2000000
  3  ------  Exaggeration for disp.& dist. =    10000.0000000

     Cross section default
  1  ---------------------------  Start-x =       16.8000000
  2  ---------------------------  Start-y =       23.6000000
  3  --------------------------   Finish-x =       16.8000000
  4  --------------------------   Finish-y =       25.2000000
  5  ------------------  Distant-increment =        1.0000000
  6  ---------------------------  Z-depth =      -30.0000000
  7  ------------------------  Z-increment =        1.0000000

Young's Modulus 200k bar and Poisson's Ratio 0.35
header line 2
#reg1=  0  #reg2=  0  #fixed=  71  sym=  1
 PR1=       0.350     PR2=       0.350   DEPTH=      3
  E1=     0.20000e+006   E2=     0.20000e+006
XSYM=       .000     YSYM=       .000
FRIC=          0.400
S1DR=         90.0000 S1DP=          0.0000  S1IN=        100.000  S1GD=          0.000
S2DR=         89.9999  S2DP=         90.0000   S2IN=         20.000  S2GD=          0.000
S3DR=        179.9000  S3DP=          0.0000  S3IN=          0.000  S3GD=          0.000

  #  X-start   Y-start       X-fin       Y-fin   Kode   rt.lat  reverse   dip angle     top       bot
xxx   xxxxxxxxxx xxxxxxxxx   xxxxxxxxxxx xxxxxxxxx xxx   xxxxxxx xxxxxxxxxx xxxxxxxxX   xxxxxxxx  xxxxxxxx
1 0.000000 0.000000 0.029768 0.005698 100 0.1000 0.000000 90.000000 0.000000 5.000000
1 0.029768 0.005698 0.059535 0.010997 100 0.1000 0.000000 90.000000 0.000000 5.000000
1 0.059535 0.010997 0.089303 0.016205 100 0.1000 0.000000 90.000000 0.000000 5.000000
1 0.089303 0.016205 0.119070 0.021255 100 0.1000 0.000000 90.000000 0.000000 5.000000
1 0.119070 0.021255 0.148838 0.026252 100 0.1000 0.000000 90.000000 0.000000 5.000000
1 0.148838 0.026252 0.178605 0.031290 100 0.1000 0.000000 90.000000 0.000000 5.000000
1 0.178605 0.031290 0.208373 0.036376 100 0.1000 0.000000 90.000000 0.000000 5.000000
1 0.208373 0.036376 0.238141 0.041480 100 0.1000 0.000000 90.000000 0.000000 5.000000
1 0.238141 0.041480 0.267908 0.046663 100 0.1000 0.000000 90.000000 0.000000 5.000000
1 0.267908 0.046663 0.297676 0.052026 100 0.1000 0.000000 90.000000 0.000000 5.000000
1 0.297676 0.052026 0.327443 0.058053 100 0.1000 0.000000 90.000000 0.000000 5.000000
1 0.327443 0.058053 0.357211 0.064450 100 0.1000 0.000000 90.000000 0.000000 5.000000
1 0.357211 0.064450 0.386978 0.070777 100 0.1000 0.000000 90.000000 0.000000 5.000000
1 0.386978 0.070777 0.416746 0.077184 100 0.1000 0.000000 90.000000 0.000000 5.000000
1 0.416746 0.077184 0.446513 0.083633 100 0.1000 0.000000 90.000000 0.000000 5.000000
1 0.446513 0.083633 0.476281 0.089982 100 0.1000 0.000000 90.000000 0.000000 5.000000
1 0.476281 0.089982 0.506049 0.095902 100 0.1000 0.000000 90.000000 0.000000 5.000000
1 0.506049 0.095902 0.535816 0.101326 100 0.1000 0.000000 90.000000 0.000000 5.000000
1 0.535816 0.101326 0.565584 0.106620 100 0.1000 0.000000 90.000000 0.000000 5.000000
1 0.565584 0.106620 0.595351 0.112132 100 0.1000 0.000000 90.000000 0.000000 5.000000
1 0.595351 0.112132 0.625119 0.116726 100 0.1000 0.000000 90.000000 0.000000 5.000000
```

```
1 0.625119 0.116726 0.654886 0.121121 100 0.1000 0.000000 90.000000 0.000000 5.000000
1 0.654886 0.121121 0.684654 0.126773 100 0.1000 0.000000 90.000000 0.000000 5.000000
1 0.684654 0.126773 0.714422 0.137700 100 0.1000 0.000000 90.000000 0.000000 5.000000
1 0.714422 0.137700 0.744189 0.150680 100 0.1000 0.000000 90.000000 0.000000 5.000000
1 0.744189 0.150680 0.773957 0.160004 100 0.1000 0.000000 90.000000 0.000000 5.000000
1 0.773957 0.160004 0.803724 0.165826 100 0.1000 0.000000 90.000000 0.000000 5.000000
1 0.803724 0.165826 0.833492 0.169836 100 0.1000 0.000000 90.000000 0.000000 5.000000
1 0.833492 0.169836 0.863259 0.172857 100 0.1000 0.000000 90.000000 0.000000 5.000000
1 0.863259 0.172857 0.893027 0.177442 100 0.1000 0.000000 90.000000 0.000000 5.000000
1 0.893027 0.177442 0.922794 0.183781 100 0.1000 0.000000 90.000000 0.000000 5.000000
1 0.922794 0.183781 0.952562 0.191222 100 0.1000 0.000000 90.000000 0.000000 5.000000
1 0.952562 0.191222 0.982330 0.198765 100 0.1000 0.000000 90.000000 0.000000 5.000000
1 0.982330 0.198765 1.012097 0.206762 100 0.1000 0.000000 90.000000 0.000000 5.000000
1 1.012097 0.206762 1.041865 0.214675 100 0.1000 0.000000 90.000000 0.000000 5.000000
1 1.041865 0.214675 1.071632 0.222169 100 0.1000 0.000000 90.000000 0.000000 5.000000
1 1.071632 0.222169 1.101400 0.229931 100 0.1000 0.000000 90.000000 0.000000 5.000000
1 1.101400 0.229931 1.131167 0.238352 100 0.1000 0.000000 90.000000 0.000000 5.000000
1 1.131167 0.238352 1.160935 0.246558 100 0.1000 0.000000 90.000000 0.000000 5.000000
1 1.160935 0.246558 1.190703 0.252197 100 0.1000 0.000000 90.000000 0.000000 5.000000
1 1.190703 0.252197 1.220470 0.257474 100 0.1000 0.000000 90.000000 0.000000 5.000000

    Grid Parameters
  1  ---------------------------  Start-x =          0.000000
  2  ---------------------------  Start-y =         -0.300000
  3  --------------------------   Finish-x =         1.2000000
  4  --------------------------   Finish-y =          0.500000
  5  ------------------------  x-increment =          0.010000
  6  ------------------------  y-increment =          0.010000
    Size Parameters
  1  -------------------------  Plot size =        0.50000
  2  --------------  Shade/Color increment =        0.2000000
  3  ------  Exaggeration for disp.& dist. =    10000.0000000

    Cross section default
  1  ---------------------------  Start-x =       16.8000000
  2  ---------------------------  Start-y =       23.6000000
  3  --------------------------   Finish-x =       16.8000000
  4  --------------------------   Finish-y =       25.2000000
  5  -----------------  Distant-increment =        1.0000000
  6  ---------------------------  Z-depth =      -30.0000000
  7  ------------------------  Z-increment =        1.0000000
```

Dissociation Model and Paleoearthquake Magntitude Model code

Paleoearthquake magnitude

```
% CO2 dissociation model beta. Some of the code in the first half is legacy
% from calculations before Perple_X software was used calculate molar
% volumes of CO2. To run this code be sure all files are in the same folder
% and run perplexconversion.m before running the dissociation model.

%Timothy Sherry

load p500.mat

Z_hydro = p500(11);

%Pressure
rho_hydro = 1000; %kg/m^3
g = 9.81; %m/s^2
H = 5000; %m
P_hydro = rho_hydro * g * H;
```

```
%NK88
%delta_mass = 0.3; %percent change in sample mass

%Density of CO2 at 50 MPa and 800 C
R = 8.3144621; %J/mol*K
M_CO2 = 0.044; %kg/mol
R_s = R / M_CO2;
T = 1073.15; %degrees K

rho_CO2 = P_hydro / (Z_hydro * R_s * T); % CO2 kg/m^3 from compression factor

%=========== CALCITE DISSOCIATION ==========
%Start with 1 m^3 block of calcite
%==========================================

rho_cal = 2700; %kg / m^3 %Caclite Density
M_cal = 0.1; %kg / mol %Calcite molar mass
Vm_cal = rho_cal / M_cal; %Calcite Molar Volume
Mol_cal = Vm_cal; %mols

%===== CaO =====
Mol_CaO = Mol_cal; %mols
rho_CaO = 3350; %kg / m^3
M_CaO = 0.056; %kg / mol
Vm_CaO = rho_CaO / M_CaO; %Lime Molar Volume
V_CaO = Mol_CaO / Vm_CaO;% fprintf('%.3f m^3',V_CaO); %Volume of CaO produced
%===============

%===== CO2 =====
Mol_CO2 = Mol_cal; %mols
Vm_CO2 = rho_CO2 / M_CO2; %CO2 Molar Volume (mol / m^3)
V_CO2 = Mol_CO2 / Vm_CO2 %fprintf('%.3f m^3',V_CO2) display('unit'); %Volume of CO2 produced
%===============

%===== Ideal Gas Law ======
P_CO2 = (Mol_CO2 * R *T) / V_CO2 %fprintf('P_CO2 = %.3f Pa',P_CO2);
%==========================

%========== DOLOMITE DISSOCIATION ==========
%Start with 1 m^3 block of dolomite
%===========================================

rho_dol = 2840; %kg / m^3 %Dolomite Density
M_dol = 0.184; %kg / mol %Dolomite Molar Mass
Vm_dol = rho_dol / M_dol; %Dolomite Molar Volume
Mol_dol = Vm_dol; %mols

%===== CaO =====
%Same as for calcite
%===============

%===== MgO =====
Mol_MgO = Mol_dol; %mols
rho_MgO = 3580; %kg / m^3 MgO density
M_MgO = 0.040; %kg / mol MgO Molar Mass
Vm_MgO = rho_MgO / M_MgO; %MgO Molar Volume
V_MgO = Mol_MgO / Vm_MgO; %MgO volume
%===============

%===== 2CO2 =====
Mol_dCO2 = 2 * Mol_dol;

perplexconversion %Get data from perplex
V_dCO2 = Mol_dCO2 .* mVol_CO2 %Get volume of CO2 for different mole fractions of water
```

```
%Now accounting for the ~50% porosity required for fluidizaiton
V_grit = V_dCO2 .* 2
%================

%===== Ideal Gas Law =====
%P_dCO2 = (Mol_dCO2 * R * T) / V_dCO2
%=========================

%===== Slip patch =====
%V_grit volume is derived from a 5 cm x 20 m x 1 m patch of source rock
%(dolomylonite layer)

%== Injectite Dimensions ==
H = 72;% 53]; %m
W = 8; %m
%z = [1 10 50 100 150 220];%m
z = 200; %m

%V_Inj = z .* W * H; %m^3
%V_Inj = (2/3) * pi * z .* W * H; %m^3
V_Inj = (4/3) * pi * (z/2) * (W/2) * H; %m^3

%==                      ==

%Volume factor
%If V_grit from 1 m^3 then need a factor to make V_Inj of material
F_1 = [];
for j=1:length(V_grit);
    F = V_Inj / V_grit(j);
    F_1 = [F;F_1];
end

%F = V_Inj / V_grit;

%Now what is the volume of the 0.05 m patch?
V_patch = F_1; %m^3
% Therefore the slip patch has an area of V_patch
A_patch = V_patch ./ 0.05; %m^2
A_patch2 = V_patch ./ 0.1; %m^2
%Square patch of slip
L_patch = sqrt(A_patch); %m
L_patch2 = sqrt(A_patch2);%m
r_patch = 2 * sqrt(((3/4) * A_patch) / pi);
%=======================

%===== Magnitude ======
%Seismic Moment
G = 3E10; %Pa %Crustal Shear modulus


D = L_patch / (10^4);
D2 = L_patch2 / (10^4);
D3 = r_patch / (10^4);
Mo = G .* D .* A_patch;
Mo_2 = G .* D2 .* A_patch;
Mo_r = G .* D3 .* A_patch;

Mw = (log10(Mo)/1.5) - 6.07;%Kanamori and Brodsky 2004 pg 19 or pg 1446
Mw2 = (log10(Mo_2)/1.5) - 6.07;
Mw2 = (log10(Mo_r)/1.5) - 6.07;

figure

Mo2 = Mo ./ 10^15;
```

```
plot(Mf,Mo,'LineWidth',2);
xlabel('Mole Fraction CO_2')
ylabel(gca,'Seismic Moment');
ax1 = gca;
set(gca,'Box','off',...
        'YGrid','on');

axesPosition = get(gca,'Position');

ylimits = get(ax1,'Ylim');
y1inc = (ylimits(2)-ylimits(1))/5;

set(ax1,'YTick',[ylimits(1):y1inc:ylimits(2)]);
y3limits = ((log10(ylimits))/1.5)-6.07
y3inc = (y3limits(2)-y3limits(1))/5;
ax2 = axes('Position',axesPosition,...
           'Color','none',...
           'YLim',y3limits,...
           'YAxisLocation','Right',...
           'XTick',[],...
           'YTick',[y3limits(1):y3inc:y3limits(2)],...
           'Box','off');

ylabel(ax2,'Moment Magnitude');

title('Paleoearthquake Magnitude to Generate Injectites')

figure

Mo_2a = Mo_2 ./ 10^15;
plot(Mf,Mo_2,'LineWidth',2);
xlabel('Mole Fraction CO_2')
ylabel(gca,'Seismic Moment');
ax1 = gca;
set(gca,'Box','off',...
        'YGrid','on');

axesPosition = get(gca,'Position');

ylimits = get(ax1,'Ylim');
y1inc = (ylimits(2)-ylimits(1))/5;

set(ax1,'YTick',[ylimits(1):y1inc:ylimits(2)]);
y3limits = ((log10(ylimits))/1.5)-6.07
y3inc = (y3limits(2)-y3limits(1))/5;
ax2 = axes('Position',axesPosition,...
           'Color','none',...
           'YLim',y3limits,...
           'YAxisLocation','Right',...
           'XTick',[],...
           'YTick',[y3limits(1):y3inc:y3limits(2)],...
           'Box','off');

ylabel(ax2,'Moment Magnitude');

title('Paleoearthquake Magnitude to Generate Injectites')

figure

Mo_r2 = Mo_r ./ 10^15;
plot(Mf,Mo_r,'LineWidth',2);
xlabel('Mole Fraction CO_2')
ylabel(gca,'Seismic Moment');
ax1 = gca;
set(gca,'Box','off',...
```

```
        'YGrid','on');

axesPosition = get(gca,'Position');

ylimits = get(ax1,'Ylim');
y1inc = (ylimits(2)-ylimits(1))/5;

set(ax1,'YTick',[ylimits(1):y1inc:ylimits(2)]);
y3limits = ((log10(ylimits))/1.5)-6.07
y3inc = (y3limits(2)-y3limits(1))/5;
ax2 = axes('Position',axesPosition,...
           'Color','none',...
           'YLim',y3limits,...
           'YAxisLocation','Right',...
           'XTick',[],...
           'YTick',[y3limits(1):y3inc:y3limits(2)],...
           'Box','off');

ylabel(ax2,'Moment Magnitude');

title('Paleoearthquake Magnitude to Generate Injectites')
```

Conversion from Perple_X data

```
%Access Perplex fluid tables

load modeldata1.tab
Mf = modeldata1(:,1); %mole fraction X(CO2)
cmVol_CO2 = modeldata1(:,4); %Volume (cm3/mol)
mVol_CO2 = cmVol_CO2 .* 10^-6 %Convert cm3 to m3
```

Perple_X data

```
 0.1000000       500.0000       1073.000       168.1599       0.9000000       0.1000000       0.3333333E-01  0.3666667       0.60000
 0.2000000       500.0000       1073.000       173.4130       0.8000000       0.2000000       0.6666667E-01  0.4000000       0.53333
 0.3000000       500.0000       1073.000       178.3006       0.7000000       0.3000000       0.1000000      0.4333333       0.46666
 0.4000000       500.0000       1073.000       182.8636       0.6000000       0.4000000       0.1333333      0.4666667       0.40000
 0.5000000       500.0000       1073.000       187.1424       0.5000000       0.5000000       0.1666667      0.5000000       0.33333
 0.6000000       500.0000       1073.000       191.1780       0.4000000       0.6000000       0.2000000      0.5333333       0.26666
 0.7000000       500.0000       1073.000       195.0110       0.3000000       0.7000000       0.2333333      0.5666667       0.20000
 0.8000000       500.0000       1073.000       198.6822       0.2000000       0.8000000       0.2666667      0.6000000       0.13333
 0.9000000       500.0000       1073.000       202.2322       0.1000000       0.9000000       0.3000000      0.6333333       0.66666
  1.000000       500.0000       1073.000       205.7017        0.000000        1.000000       0.3333333      0.6666667        0.0000
```